DECLARATION

This is to certify that this dissertation entitled ***"Polymer Nanocomposites reinforced with modified Graphene oxide: A Promising Material for Water Filtration"*** submitted by ***Ms. Hafsa Ilyas*** , is accepted in its present form by the Department of Chemistry, Quaid-i-Azam University, Islamabad, Pakistan, as satisfying the partial requirement for the award of degree of ***Doctor of Philosophy in Physical Chemistry.***

External Examiner (I):

Dr. Riaz Ahmed Ch.
House # 1298, Road 11,
Phase-III, Bahria Town,
Rawalpindi

External Examiner (II):

Dr. Khalid Khan
Director Coordination
PAEC Head Quarter
Islamabad

Supervisor :

Prof. Dr. Muhammad Siddiq
Department of Chemistry
Quaid-i-Azam University
Islamabad.

Head of Section:

Prof. Dr. Hazrat Hussain
Department of Chemistry
Quaid-i-Azam University
Islamabad.

Chairman:

Prof. Dr. Mrs. Zareen Akhter
Department of Chemistry
Quaid-i-Azam University
Islamabad.

Certificate of Approval

This is to certify that the research work presented in this thesis, entitled **"Polymer Nanocomposites reinforced with modified Graphene oxide: A Promising Material for Water Filtration"** was conducted by **Ms. Hafsa Ilyas** under the supervision **Prof. Dr. Muhammad Siddiq**

No part of this thesis has been submitted any where else for any other degree. This thesis, is submitted to the **Department of Chemistry Quaid-i-Azam University Islamabad** in partial fulfillment of the requirements for the Doctor of Philosophy in Field of **Physical Chemistry, Department of Chemistry, Quaid-i-Azam University, Islamabad.**

Student Name	Ms. Hafsa Ilyas	Signature: hafsa
Examination Committee:		
1. External Examiner:	**Dr. Riaz Ahmed Ch.** H. No. 1298, Road 11 Phase-3, Bahria Town Rawalpindi	Signature:
2. External Examiner:	**Dr. Khalid Khan** Director Coordination PAEC Head Quarter Islamabad.	Signature:
3. Internal Examiner:	**Prof. Dr. Hazrat Hussain** Department of Chemistry Quaid-i-Azam University Islamabad.	Signature:
Supervisor	**Prof. Dr. Muhammad Siddiq**	Signature:-
Head of Department:	**Prof. Dr. Zareen Akhter**	Signature:-

AUTHOR'S DECLARATION

I, **Ms. Hafsa Ilyas** hereby state that my Ph.D. thesis titled "**Polymer Nanocomposites reinforced with modified Graphene oxide: A Promising Material for Water Filtration**" is my own work and has not been submitted previously by me for taking any degree from this University (Quaid-i-Azam University Islamabad) or anywhere else in the country/world.

At anytime if my statement is found to be incorrect even after my Graduation the University has the right to withdraw my Ph.D. degree.

hafsa

Name of student: **Ms. Hafsa Ilyas**

PLAGIARISM UNDERTAKING

I solemnly declare that, the research work presented in the thesis titled **"Polymer Nanocomposites reinforced with modified Graphene oxide: A Promising Material for Water Filtration"** is solely my research work with no significant contribution from any other person. Small contribution/help wherever taken has been duly acknowledged and that complete thesis has been written by me.

I understand the zero tolerance policy of the HEC and **Quaid-i-Azam University Islamabad** towards plagiarism. Therefore, I as an Author of the above titled thesis declare that no portion of my thesis has been plagiarized and any material used as reference is properly referred/cited.

I undertake that if I am found guility of any formal plagiarism in the above titled thesis even after award of Ph.D. degree, the university reserves the rights to withdraw/revoke my Ph.D. degree and that HEC and the University has the right to publish my name on the HEC/University website on which names of students are placed who submitted plagiarized thesis.

Student/Author Signature: hafsa

Name: **Ms. Hafsa Ilyas**

Polymer Nanocomposites Reinforced with Modified Graphene Oxide: A Promising Material for Water Filtration

A dissertation submitted for the partial fulfillment of the degree of

Doctor of Philosophy

In

Physical Chemistry

By

Hafsa Ilyas

Supervised by

Prof. Dr. Muhammad Siddiq

Department of Chemistry

Quaid-i-Azam University

Islamabad

Pakistan

2024

ACKNOWLEDGEMENTS

My immense gratitude and credit goes towards Almighty **ALLAH (SWT)**, who created us to read and learn and ponder upon the world. As mentioned in the Quran, sura Al-Iqra "Read in the name of your Lord who created man from a clinging substance. Read, and your Lord is the most Generous-who taught by the Pen-Taught man that which he knew not." In these first few verses of Surah Al-Iqra, ALLAH instructed mankind to read and learn through the command of ALLAH. I am extremely grateful to the guidance of Holy Prophet **Muhammad (PBUH)** who taught us how to lead a life full of wisdom and gratitude by constant learning and seeking knowledge at any age of your life.

I would extend my heartfelt and deep thanks to my supervisor, **Prof. Dr. Muhammad Siddiq** Department of Chemistry, Quaid-i-Azam University, Islamabad, for his dedicated guidance and immense patience. He has been an affectionate support system for me during my Ph.D. I am also thankful to my foreign supervisor **Dr. Anjum Qureshi** (Sabanci University Istanbul, Turkey) who helped me to frame my research in a more defined manner. I am also thankful to **Tubitak Research Council Turkey** for providing me fellowship to pursue my research in **SUNUM** Sabanci University.

I appreciate Chairperson Department of Chemistry, **Prof. Dr. Zareen Akhter** and Head of Physical Section, **Prof. Dr. Hazrat Hussain**, for the accessibility of research resources and an appropriate working environment in the department to conduct research. I am indebted to all faculty members, administrative staff and laboratory technical assistants, of Quaid-i-Azam University for their assistance in accomplishing my doctorate degree.

I am highly thankful to all mentors throughout my educational carrier, faculty of **Jinnah Public School, Ali Public Academy, Hira Public Secondary School, Fatima-tuz-Zahra Degree College and University of Azad Jammu and Kashmir**. Thank you all for activating my mind, igniting the imagination and to instill a love of learning.

I would like to thank all of my lab fellows and friends specially **Sidra**, **Laraib**, **Riffat Sikandar**, **Banafshan**, **Mahwish Rabia and Esha** for being there for me during emotional breakdowns of my PhD journey.

Most importantly, I want to express my gratitude to my beloved parents, grandmother **Mrs. Ameer Nisa** and my (Late) grandfather **Mr. M. Afsar Khan** who have guided and encouraged my family to focus on higher education. I don't think I would have made it through this endeavor without my parent's prayers, financial help, moral principles, and inspiration. I am so grateful to my loving brothers **Dr. Soban Ilyas, Hafiz Roman Ilyas** and sister **Dr. Sadaf Ilyas** for all smiles, thoughts, and challenges we shared. I would like to extend thanks to my husband **Mr. Ozair Younas** for being a part of my support system in raising kids during my PhD degree. I would like to extend thanks to my mother, and my aunt **Nasadar Jan BiBi** for their unconditional love and care for my kids. I would like to appreciate my sweetest kids **Muhammad Yousaf** and **Muhammad Hashim**, their adorable giggles and cuteness keeps me happy and inspired. I am grateful to all of the wonderful people in my life who ever wish blessings and happiness for me.

Hafsa Ilyas

hafsa@chem.qau.edu.pk

ABSTRACT

Nanomaterial based polymer membranes are widely applicable for separation and purification industries. The present study is devoted to the fabrication of highly hydrophilic and antifouling polymer membranes based on graphene oxide (GO) and modified graphene oxide. Graphene oxide was prepared from graphite powder by Hummer's method. Silver functionalized GO (GO-Ag), polyethylene glycol (PEG) functionalized GO-Ag (PEG-GO-Ag), magnetic iron oxide functionalized GO (GO/Fe_3O_4) and silver functionalized magnetic graphene oxide ($Ag\text{-}GO/Fe_3O_4$) were synthesized and used to fabricate six different series of polymer membranes by using vacuum filtration assembly. Fabricated membranes include PVC/GO and PVC-GO-Ag based membranes (0, 0.25, 0.5, 1.0 wt.%), PVDF-*co*-HFP/GO-Ag, and PVDF-*co*-HFP/PEG-GO-Ag membranes, (0, 0.2, 0.6, 1.0 ,1.4 wt.%) and PVDF-*co*-HFP/GO/Fe_3O_4 and PVDF-*co*-HFP $Ag\text{-}GO/Fe_3O_4$ (1.0 wt.%) based nanocomposite membranes. Fourier transform infrared spectroscopy (FTIR), X-ray diffraction (XRD), Raman spectroscopy, scanning electron microscopy (SEM) and transmission electron microscopy (TEM) were used to explore the structural and chemical features of nanocomposites and their perspective membranes. The dead-end filtration assembly was used to investigate the membranes performance. Water flux and BSA rejection was found to increase for all the nanocomposite based membranes as compared to pure polymer membranes. Besides this, GO-Ag nanocomposite showed appreciable antibacterial properties against Escherichia coli. PEG-GO-Ag (1.0 wt.%) nanocomposite was proved to be highly effective for enhancing the hydrophilicity of PVDF-*co*-HFP membrane by lowering the water contact angle from 115°.02 to 38°.77. The water flux of PVDF-*co*-HFP/PEG-GO-Ag (1.0 wt.%) membrane increased upto 906 $Lm^{-2}h^{-1}$ as compared to pristine PVDF-*co*-HFP which showed a water flux of 216 $Lm^{-2}h^{-1}$. GO/Fe_3O_4 and $Ag\text{-}GO/Fe_3O_4$ also enhances the water flux and BSA rejection of PVDF-co-HFP membrane. Flux recovery ratio for PVC/GO-Ag (0.5 wt.%) membrane was 85% while that of PVDF-*co*-HFP/PEG-GO-Ag (1.0 wt.%) membrane was 91% and PVDF-co-HFP/$Ag\text{-}GO/Fe_3O_4$ was 92%. Furthermore, the antifouling properties and reversible fouling ratios of all the fabricated membranes increased drastically. Thermo-gravimetric analysis (TGA) of the fabricated membranes confirms their high thermal stability as well. Reusability of fabricated membranes was also explored by cyclic filtration tests. The present study is a

gateway to fabricate highly hydrophilic, antifouling and cost effective polymer membrane filters for high performance applications.

Table of Contents

List of Figures

List of Tables

List of Schemes

List of Abbreviations

BSA	Bovine serum albumin
CA	Cellulose acetate
DSC	Differential scanning calorimetry
EDX	Energy dispersive X-ray
FTIR	Fourier transform infrared spectroscopy
FRR	Flux recovery ratio
GO	Graphene oxide
Rir	Irreversible fouling
NP	Nanoparticles
PVC	Poly (vinyl chloride)
PVDF	Polyvinylidene fluoride
PEG	Polyethylene glycol
PVDF-*co*-HFP	Polyvinylidene fluoride-*co*-hexafluoro propylene
PS	Polystyrene
PA	Polyamide
PES	Polyether sulfone
Jw	Protein flux
RO	Reverse osmosis
Rr	Reversible fouling
SEM	Scanning electron microscopy
TEM	Transmission electron microscopy
TGA	Thermogravimetric analysis
Rt	Total fouling
UV	Ultraviolet
Jw	Water flux
XRD	X-ray diffraction

CHAPTER 1

INTRODUCTION

1.1 Membrane Filtration

Increased population and upswept industrialization have posed serious threats about clean water availability. World Water Council presumed that about 3.9 billion people will suffer from drinking water scarcity by 2030 [1]. Persistence of organic pollutants in water bodies is affecting the aquatic and human life. Conventional water treatment approaches like adsorption and chemical oxidation have inadequate selectivity towards many pollutants [2, 3]. Pressure driven membrane filtration has surpassed the old filtration strategies. Generally, the membrane is described as a thin layer which allows the selective transport of ions and molecules. In order to use a membrane for separation and purification purpose it must have high permeability, selectivity, mechanical durability, high thermal stability, low fabrication cost and ease of processability [4]. Membrane properties like hydrophilicity, surface charge and pore size can be tailored easily to target the specific pollutant [5].

1.2 Polymer Membranes

Polymer is a large molecule made by the repetition of small units called monomers. High thermo-mechanical stability, high chemical resistance, low cost and tunable surface properties makes polymers a suitable candidate for membrane fabrication. Polysulfone (PS) [6], Polyvinylidene fluoride (PVDF) [7], polyether sulfone (PES) [8], cellulose acetate (CA) [9], polyamide (PA) [10] and polyvinyl chloride (PVC) [11] are widely used for membranes fabrication. In order to use the polymer membranes for industrial applications, the surface properties of the polymer membranes are of fundamental importance. Membrane properties like hydro-philicity/phobicity, zeta potential, porosity and surface roughness plays a vital role in controlling the flux rate and rejection of solutes [12]. Hydrophilicity is linked with estimation of water contact angle formed between the membrane surface and sessile water droplet. Generally, the membranes are made up of

hydrophobic polymers because of their integral mechanical and thermal stability. Hydrophobic membrane surface repels the water feed away from the surface in a spontaneous manner which results in increased entropy. The foulant molecules tends to adsorb on the hydrophobic membrane surface and fouling dominates. In case of hydrophilic membranes there exists strong H-bonding interactions between membranes surface and water molecules. Hydrophilic surfaces have increased surface tension which helps in formation of strong water layer on the membrane surface. These water layers at membranes surface repel the hydrophobic pollutants and reduces the chances of their adsorption on to the membrane surface [13].

The surface charge of membranes plays an important role in controlling the rejection of solutes through the membrane. The electrostatic interactions between the foulants/solutes and the membrane surface layer are usually explored by measuring the surface zeta potential of membranes [14]. An increased negative charge on the membrane surface results in strong repulsion of salts and other negatively charged foulants. The ultrafiltration, nanofiltration and reverse osmosis membranes have negative surface charges which makes them favorable for high solutes rejections and low foulants adsorption. The negative membrane surfaces help in rejection of proteins because most of the proteins are negatively charged under neutral conditions [15]. Membranes surface charge can be tuned by increasing the pH of feed solution which results in dissociation of carboxylic and sulfonic groups. Apart from the surface charge, membranes surface roughness/smoothness influences the transport properties as well. A rougher surface layer provides more sites for adhesion of colloids and microorganisms which results in clogging of porous surface and reduced permeate flux. Besides the physicochemical texture of membranes surface, presence of active antifouling agents and biocides on the top layer of membrane can control the fouling in an efficient manner. Formation of hydrophilic polymer sites on the surface of membrane material minimize the attachment of foulants by steric repulsion mechanism [16]. Depending upon the size of pores different types of filtration membranes are being used which include microfiltration, nano-filtration and reverse osmosis membranes as shown in **Figure 1.1**.

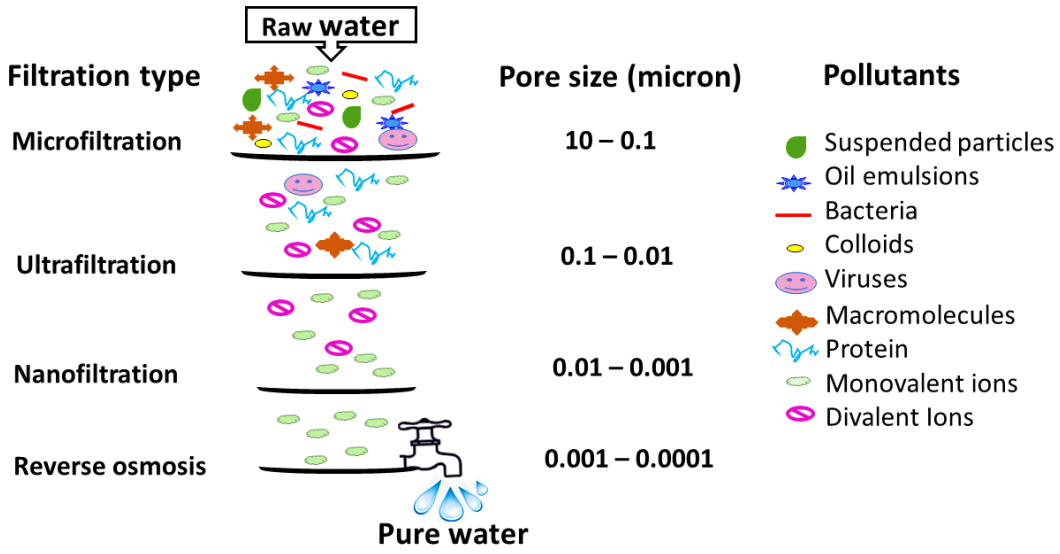

Figure 1.1. Different types of filtration membranes

1.3 Membrane Fouling

Since the emergence of membrane separation techniques during 1960, s the membrane fouling is a subject of high concern. Fouling of polymer membranes is a multidimensional phenomenon which occurs because of deposition of colloids, micro-organisms, salts and macromolecules either on the membrane surface or within the porous structures [17]. Depending upon the nature of foulants the membrane fouling can be categorized as organic fouling, inorganic fouling, biofouling and colloidal fouling. Organic fouling occurs due to the accumulation of proteins, polysaccharides and natural organic matter (NOM) from the feed water. Inorganic fouling is related to super saturation and precipitation of inorganic salts on the membrane surface. Colloidal fouling occurs due to the presence of undispersed particles and colloids (size) which includes oxides and hydroxides of heavy metals [18]. Biofouling involves the biological pollutants and microorganisms like bacteria, viruses, fungi and biopolymers. Biofouling is the most complicated type of fouling because of rapid growth and multiplication of adhered sessile cells by consuming the feed water nutrients. Bacteria once adhered to the membrane surface will continue to grow and spread in the form of biofilms on the membranes surface. Fouling instigated flux decline, reduced separation efficiency, low solute rejection and biodegradation of membrane. High

operating pressure needed to compensate the biofilm resistance as well as frequent cleaning of membrane surface increases the cost of separation process. Biofouling reduces the membranes life span and deteriorates the water quality [19]. Currently many strategies are being developed to treat the membrane fouling which include the surface modification of polymer membranes by direct printing, template synthesis, incorporation of hydrophilic nano additives etc. Membrane fouling can be reversible or irreversible based on the type of physical and chemical interactions between the foulants and the membrane surface. Foulants can interact with polymer membrane surface by hydrophobic interactions, electrostatic interactions, hydrogen bonding and van der Walls attractions. Therefore, by tuning the membranes surface charges and increasing the hydrophilicity of membranes surface one can minimize the undesirable interactions between polymer membrane and foulants. This can be accomplished by the incorporation of hydrophilic nano additives either within the polymer matrix or on the membrane surface [12, 13]. Surface modification of Polymer membranes can be done by interfacial polymerization [20, 21] irradiation of high energy particles [22] plasma treatment [23] and coating/incorporation of nanoparticles [24].

1.4 Nano-materials

Nanomaterials are materials with 1 to 100nm dimensions of a single unit structure. Nanomaterials are proved to have outstanding performance in dealing with polluted water. Their exceptional features like high surface area, eco-friendliness, high selectivity, reusability and extent of adsorption elucidate their competence in water treatment. Nanomaterials can deal with several pollutants including biological/microbial contaminants, heavy metal ions like Hg and Pb, natural organic matter and industrial wastes. Nanomaterials can tackle the pollutants by undergoing various processes like adsorption, absorption, oxidation, repulsion and filtration as well [25, 26]. Nanomaterials can be classified into four major categories depending on their source of origin *i.e.* organic-nanoparticles, inorganic-nanoparticles, carbonaceous-nanoparticles and composite-nanoparticles

1.5 Metal based Nano-materials

The high hydrophilicity of metal nanoparticles (Ag, Au, Pt etc.) along with their antimicrobial nature significantly improves the properties of polymer nanocomposites [27]. Subair et al. [28] fabricated a dopamine modified poly (ethylene imine) (PEI) membrane with in situ synthesized gold nanoparticles. These AuNPs decorated membranes were applicable for degradation of methylene blue, Congo red and reduction of p-nitro phenol. Liu et al. [29] used PtNPs/ bacterial cellulose and CNTs to synthesize the conductive hydrogels where the PtNPs increases the electrocatalytic activity of bacterial cellulose. Due to their low toxicity and cost effectiveness AgNPs are broadly used in membrane processes. Ag-GO functionalized poly (lactide-co-glycolide)-chitosan polymeric mat has been reported to be effective in inactivating gram negative (Escherichia coli) and gram positive bacteria (Staphylococcus aureus) [30]. Mahmoudi et al. [31] reported the synthesis of highly hydrophilic and antibacterial polysulfone membranes embedded with GO-Ag. Improved fouling resistance was attributed to the uniform dispersion of AgNPs in polysulfone membrane by combining the AgNPs with GO nanoplatelets. Besides these bare metal nanoparticles many metal oxide particles of nano-size are being used for nanocomposite fabrication. Among these metal oxide-based nanoparticles most widely used nanomaterials are iron oxide nanoparticles [32], manganese dioxide nanoparticles (MnO_2) [33], alumina nanoparticles [34], titanium dioxide nanoparticles [35]. Park Jung et al. [36] used chitosan coated Fe3O4 nanoparticles to fabricate highly hydrophilic PVDF membranes and used them for removal of a toxic heavy metal chromium. Jahankhan et al. [37] prepared an adsorptive membrane by coating a tea filter bag with PVC blends and Fe_3O_4/polydopamine/Ag nanocomposite. The synthetic membrane exhibits elevated water flux and high adsorption of Rhodoamine B and Auramine O. Naseem et al. [38] developed a novel janus membrane by using solar active nanocomposite RbxWO3@ Fe_3O_4/ and PET substrate. This membrane was aimed to purify waste water by the simultaneous evaporation and photocatalytic transfiguration of pollutants. Among these metal and metal oxide nanostructures silver nanoparticles and magnetic iron oxide nanoparticles are employed in our present study to get antibacterial and antifouling filtration membranes.

1.5.1 Synthesis of Metal Nanomaterials

Metal nanoparticles are generally fabricated by physical methods, chemical methods or biological methods as listed in **Figure 1.2**.

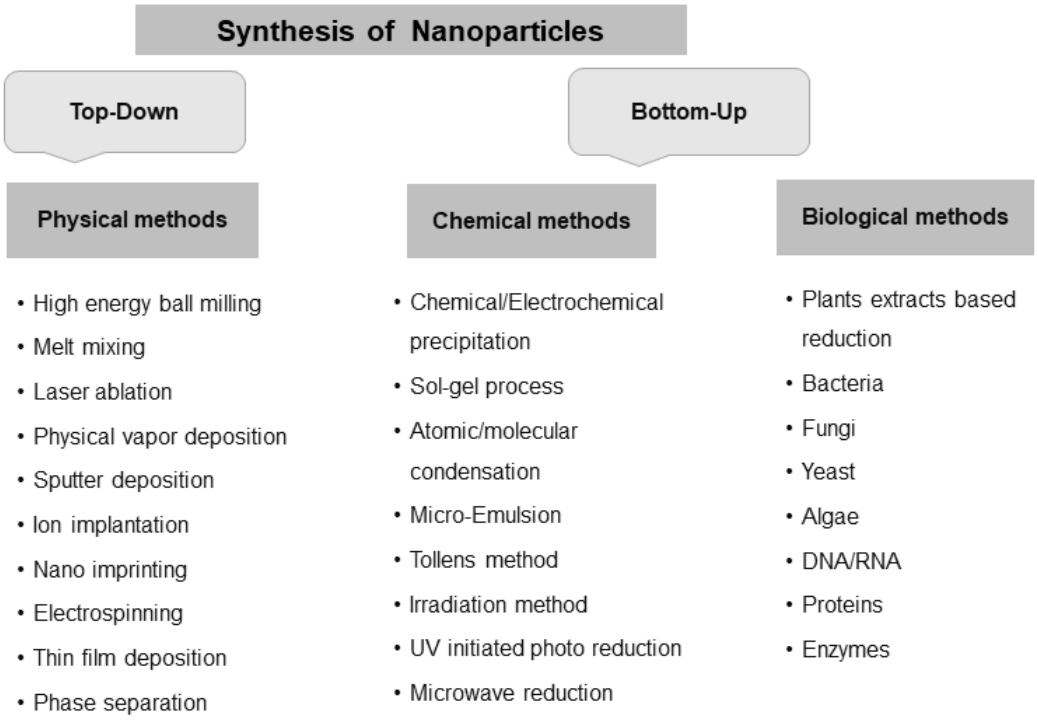

Figure 1.2. Different methods used for synthesis of nanoparticles [39].

Physical methods involve a variety of fabrication techniques which include laser ablation, laser Pyrolysis, ball milling, evaporation and electrospinning etc. Chemical methods used for fabrication of metal nanoparticles usually require hazardous chemicals for reduction of metal ions. Hydrazine and sodium borohydride are the widely used reducing agents [39]. Silver and gold metal nanoparticles are usually synthesized by chemical reduction method in which the metal precursor solution is treated with a reducing agent like sodium borohydride to reduce the metal ions. Magnetic iron oxide nanoparticles are obtained by a fast and facile co-precipitation method. Biological or green methods involves the use of microbes/plant extracts as reducing agent. Biological methods are environmental friendly methods because these methods don't involve the toxic chemicals and byproducts as in case of chemical methods [40].

1.6 Carbon Nano-materials

By the advent of graphene in 2004, carbon nanofillers have gained enormous interest in scientific research. The family of carbon nanofillers include graphite, graphene oxide and graphene, nano diamonds, fullerene, and cylindrical carbon nanotubes [41]. **Figure 1.3** represents the overview of carbon nanofillers.

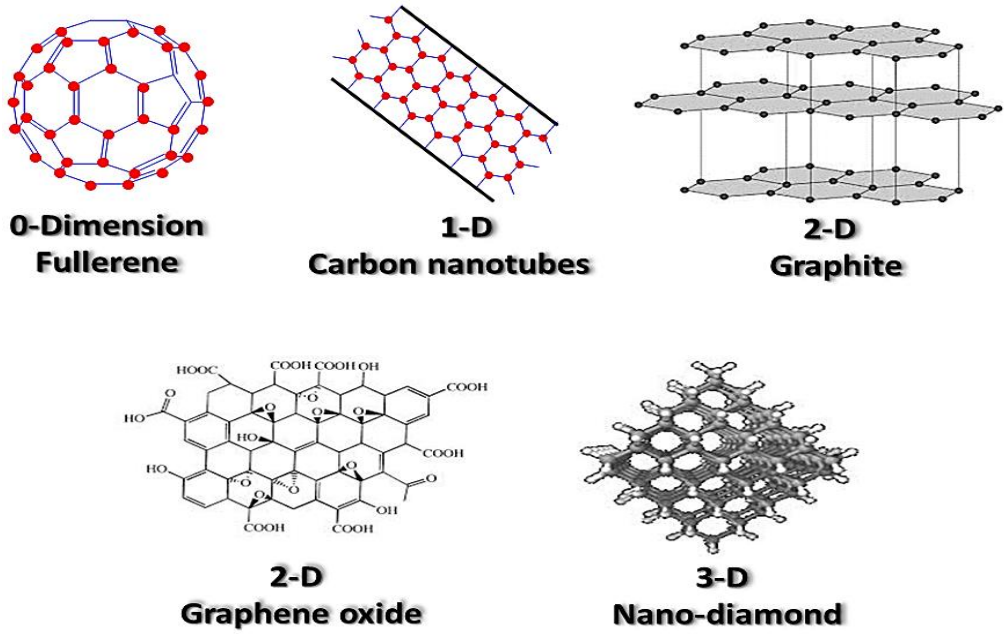

Figure 1.3. The overview of carbon nanofillers [41].

Carbon nanofillers specially graphene, graphene oxide and CNTs have excellent adsorption capacity and widely used for fabrication of aerogel and hydrogels [42]. Bhakta et al. [43] explored that maghemite/multi walled carbon nanotubes (MWCNTS) can remove methylene blue dye from aqueous media. Zheng et al. [44] synthesized a TPG-ZnO nanocomposite by using tea polyphenols, reduced graphene oxide (rGO) and zinc oxide. The synthesized TPG-ZnO nano-adsorbent showed the remarkable adsorption efficiency of Pb^{+2} (98.9%). Along with high adsorption power carbonaceous nanocomposites have great antibacterial features against both gram negative and gram positive strains. Fengjuan et al. [45] fabricated a GO/copper based antibacterial coating for titanium sheets. Hamed et al. [46] reported that GO/ZnO nanocomposite showed excellent antibacterial activities

against various bacterial strains and used this material for antimicrobial/anticancer weapon. based. The inhomogeneous dispersion of carbon nanofillers like GO and CNTs causes aggregation effect at high filler content. Therefore, many different modification strategies are being researched to get the desired results. Hussain et al. [47] reported that the carbon nano-adsorbents have excellent removal efficiency for most of the persistent organic pollutants. The mechanisms presumed for adsorption of pollutants by nanomaterials involve electrostatic interactions, hydrogen bonding, van der Waals forces, pi-pi interactions and hydrophobic interactions as well.

1.6.1 Graphene Oxide

Graphene oxide is a single atomic layered structure made by oxidation of graphite flakes. Certain features of GO like high surface area, chemical/mechanical stability, high young's modulus/tensile strength and hydrophilicity gains the interest of researchers from past two decades. Graphene oxide consists of hexagonal carbonated rings in a honey comb like pattern decorated with oxygenated moieties. In graphene oxide structure definite amount of hydroxyl and epoxide groups are present on the layers while carbonyl and carboxyl groups are located on the edges. These functionalities escalate the applicability of GO by launching different tailoring sites on the surface of graphene oxide. Graphene oxide can be functionalized very easily to achieve the desired features. Because of inadequate analytical techniques the accurate number of oxygenated functional groups on the structure of GO is still a matter of concern [48]. The functional groups on the GO layers knock out the bonding electrons and facilitates its surface modification as well as better dispersion in water. Besides water the GO can be dispersed in organic solvents like THF and DMF easily to assemble homogeneous GO layer within the nanocomposite membranes. Because of high hydrophilicity and small particle size, it is difficult to recycle GO nanofiller by simple centrifugation method. Therefore, many modifications like magnetic functionalization of GO nanofillers are being done to promote the reusability of GO by using an external magnetic field to recollect the processed nanofillers [49]. Zhong at al. [50] fabricated a highly stabilized magnetite-graphene oxide based antimicrobial membrane for water treatment. The magnetite nanoparticles reduce the swelling prospects of GO sheets and the synthesized membrane retains its permeability and rejection performance even at high

ultrasonic destabilization. Rastgar et al. [51] synthesized thin film nanocomposite membrane based on magnetic graphene oxide GO/Fe_3O_4. This membrane was used for forward osmosis with an improvement of water flux and total fouling as compared to pristine membrane.

1.6.2 Structure of Graphene Oxide

Graphene oxide is a non-stoichiometric compound possessing variety of compositions depending on particular synthesis route. Because of its extraordinary physical, thermal, mechanical and optical properties graphene oxide have become the point of interest for scientists. Inspite of its demanding nature, precise structure of GO is still a matter of concern. However different structural models have been presented to understand the structural framework of GO [52]. According to Lerf et al. [53] GO consists of an aliphatic as well as aromatic part (unoxidized benzene rings) and size of these two parts vary with extent of oxidation. Presence of alternating single and double bonds in GO was confirmed by Kudin et al. [54] and Ammar et al. [55]. Hofmann and Holst proposed the sp^2 hybridized model of GO in which epoxy groups are spreaded along the basal planes of graphite sheets [56]. Ruess modify the Hofman model by assuming that the hydroxyl groups are present along the sp^3 hybridized basal plane. According to Ruess model in the lattice structure of GO 1,3 position of cyclohexane contain epoxides and 4th position is occupied by hydroxyl moiety [57]. However, substitution of quinoidal species in puckered backbone and complete removal of epoxides and ether groups was suggested in Scholz and Boehm model [58]. Besides this Nakijima and Matsuo [59] models are based on the lattice framework of GO. But recently lattice based models are invalidated, focusing on the nonstiochiometric and amorphous nature of GO. Different models about structure of GO are shown in **Figure 1.4**. At present the most widely accepted structural model of GO is proposed by Lerf and klinowski [60] they used solid state nuclear magnetic resonance (NMR) spectroscopy to analyze the material and this model is based on materials reactivity. In 13C NMR spectrum of GO three resonance peaks were noted by cross polarization/magic angle spinning experiments. Hypothesizing that all carbon atom in GO are quaternary (Mermoux model) the peak at 130 ppm was assigned to mixture of alkenes, the peak at 70 ppm was assigned to epoxy (1,2 ether-groups) while the peak at 60 ppm was attributed to tertiary alcohols. 3

Significant inter- platelet hydrogen bonding between alcohols and epoxides was noted which contribute to the stacked structure of graphene oxide. In order to judge the distribution of alkenes (isolated or clustered in aromatic rings) Lerf and co-workers performed number of experiments in which GO is treated with maleic anhydride and D2O.

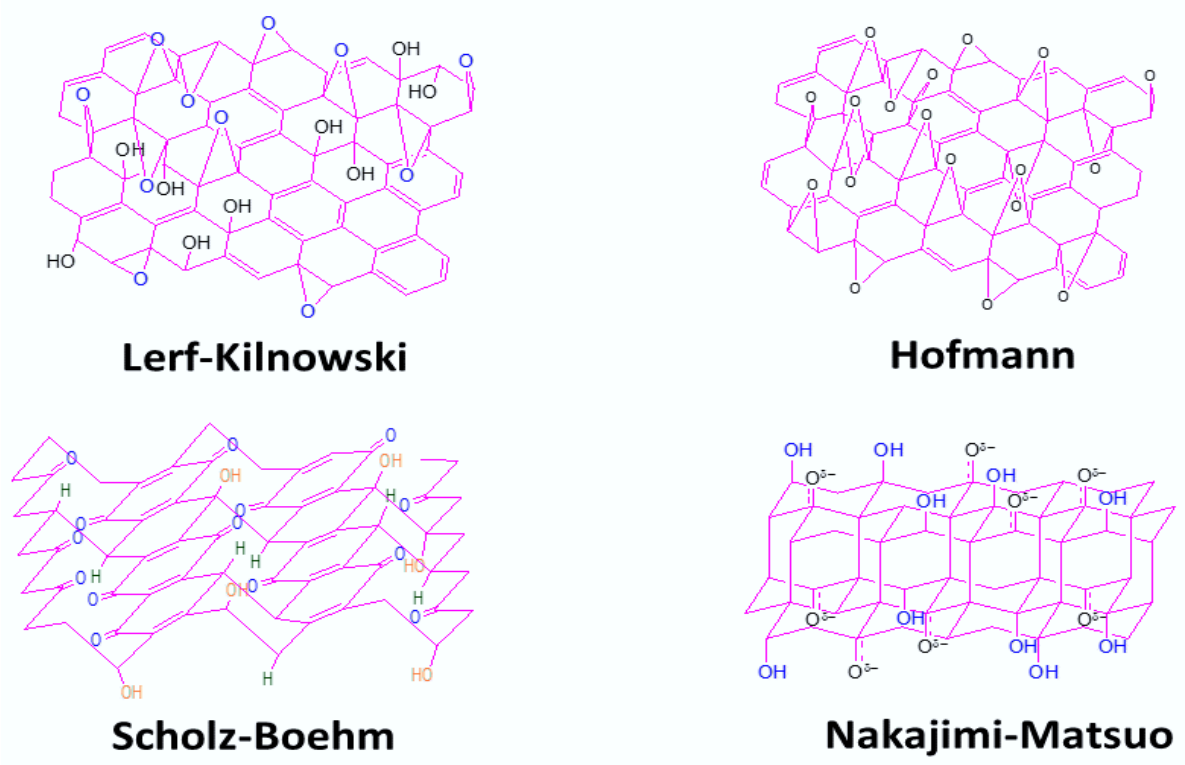

Figure 1.4. Structural models of graphene oxide

In the reaction of GO and maleic anhydride (conjugated) non aromatic alkenes must react but the results of 1H and 13C NMR spectra was observed to be similar to that of starting material which suggest that no reaction has occurred. However, disappearance of water peak in 1H NMR spectra, while treating the GO with D2O was helpful in studying the resolution of proton signals which were badly suppressed by the strong resolution of water molecules associated with surface of GO. For tertiary alcohols the signals δ = 1.3 ppm remains unchanged, which depicts that exchange is slow as compared to water molecules. Presence of two magnetically inequivalent alcohol species was confirmed by the appearance of a peak at δ=1.0ppm. Based on these experimental observations, tertiary alcohols and ethers (1,2 ethers *i.e.* epoxides) were considered as most dominating functionalities in structure of graphene oxide. Hydrogen bonding between water and

epoxides (oxygen moiety) of GO is strongly responsible for the stacked behavior of GO. Updating the earlier models of Ruess and Scholz-Boehm in Dekany model it was suggested that GO has quinoidal structure having trans-linked cyclohexyl system functionalized with 1,3 ethers and tertiary alcohols. Dekny model proposed that the 1713 cm^{-1} peak in IR spectrum of GO indicate the presence of ketones/quinones instead of carboxylic acids [61].

1.6.3 Synthesis background of GO

Graphene oxide was first prepared by an Oxford chemist Benjamin C. Brodie in 1859 while the term graphite was introduced by a scientist A.G. Werner in 1789. He used potassium chlorate ($KClO_3$) and fuming nitric acid (HNO_3) as an oxidant in addition to graphite to synthesize graphene oxide [62]. This method has many drawbacks as it was a time taking process which continuous four days at least. At least four cycles of oxidation were required. Besides this the nitric acid and chlorate result in the production of acid fog, N_2O and ClO_2 which are very harmful. In 1898 Staudenmaier introduced the use of a blend of two thirds of sulphuric acid and one third of nitric acid in addition to $KClO_3$. In contrast to Brodie's method, complete oxidation of graphite to graphene oxide takes place just in one step. But this method is also very time consuming and produce ClO_2 gas. In fact, a risk of explosion is always there while performing Brodie's and Staudenmaier experiments. In 1958 a new method is proposed for large scale production of graphene oxide by Hummer [63]. Hummer synthesized GO by using Sodium nitrate ($NaNO_3$), Potassium permanganate ($KMnO_4$), sulfuric acid (H_2SO_4), hydrogen peroxide (H_2O_2), and graphite powder. In this method first of all graphite flakes, $NaNO_3$ and H_2SO_4 are mixed and stirred to form homogeneous solution. Then by placing the solution in ice bath for 2h $KMnO_4$ (6g) was added slowly into it. Solution will become dark green. Again stirred the solution for 30 min at 35°C and added distilled water. Now the flask was placed in a 90°C water bath, for 15 min and again distilled water is added to the solution. The color of the solution turned dark yellow. Then hydrogen peroxide was added under continuous stirring for another two hours. The solution was filtered and subjected to washing with one molar hydrogen chloride solution and repeated washing with distilled water. Centrifugation can be done in order to remove impurities. Then the obtained graphene oxide is dried at 60°C and finally grinded to get fine powder of graphene oxide. Hummer, s method can be modified in

variety of ways. In modified hummers method one can use excess of sulphuric acid (90 mL and potassium permanganate (12g) for better oxidation of graphite powder [64]. **Table 1.1** summarizes the oxidizing agents used for synthesis of GO by different scientists. Hummer's method is a fast method because of strong oxidant $KMnO_4$ which reduces the oxidation time of graphite flakes. Besides this, no explosive ClO_2 or acid fog is observed during the reaction. Although it has some drawbacks like formation of NO_2/N_2O_4 due to the use of $NaNO_3$ and presence of Na^+ and NO_3^- in waste water formed during this process. Incomplete oxidation is also a big problem and affects the yield of the product. Repeated centrifugation to completely remove the residuals is time and energy consuming. **Figure 1.5** shows the scheme for hummer's method [65].

Table 1.1. Synthesis of GO by using different oxidizing agents [62-64].

Year	Scientist	Oxidizing agents for GO synthesis
1859	Brodie	$KClO_3$ and HNO_3
1898	Staudenmaier	HNO_3 and H_2SO_4
1858	Hummer	$KMnO_4$, H_2O_2, $NaNO_3$ and H_2SO_4

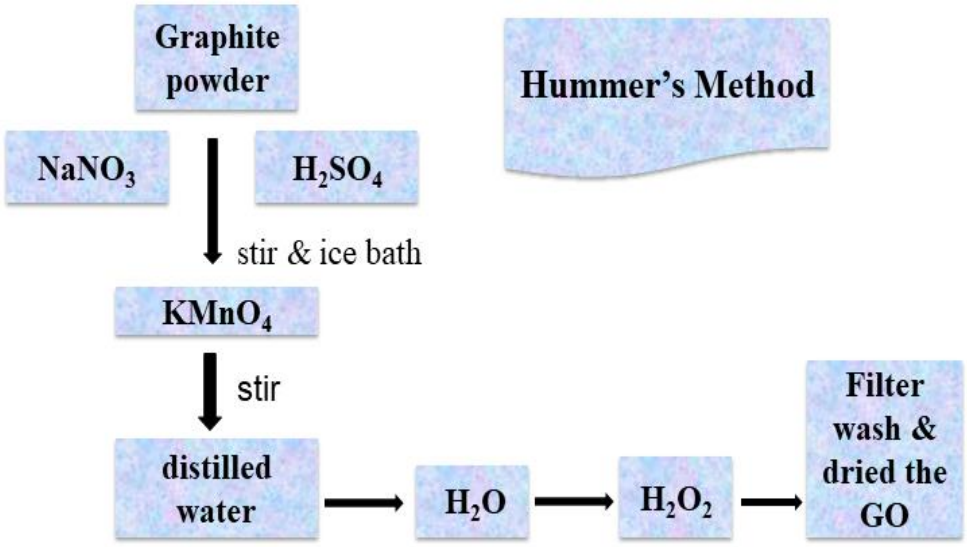

Figure 1.5. Hummer's method for synthesis of GO [64].

Tour's method is one of the adaptations of Hummer's method. In contrast to Hummer's method $NaNO_3$ is not used here. In this method graphite powder and potassium permanganate (1:6 by weight) are mixed together. By stirring the graphite and permanganate mixture with one hand, mixture of sulphuric acid and phosphoric acid will be added to it and stirred. Then placed it on heating stirrer while stirring at 50°C for 12 hours. Then the reaction flask was allowed to cool at room temperature. Added the ice made form de-ionized water to a large glass container. Poured the graphite acid mixture over the ice. Then hydrogen peroxide will be added to the mixture and stirred. Now the product formed is graphene oxide. The GO could be synthesized by the Tang - Lau method also known as "bottom-up" synthesis. In this method graphene oxide is synthesized from glucose. This method is simple and safe as compare to other methods (top-down) in which strong oxidizing agents are used. Thickness of the GO layers can also be controlled very easily by this method [66].

1.7 Potential of GO in Water Treatment

1.7.1 Removal of Heavy Metals

Among various pollutants found in water, heavy metals need special attention as they are toxic even in minute quantity and can be fatal for living organisms. Sreeprasad et. al. [67]

reported the use of GO and RGO-metal/metal oxide composites for removal of mercury from polluted water. In case of these composites the values of distribution co-efficient (Kd values) are found to be an order of magnitude higher than that of pristine GO and RGO. For RGO and composites distribution coefficient was found to be higher than 10 Lg^{-1} for Hg (II). Time dependent removal of mercury was studied by using GO, RGO, RGO-MnO_2, RGO-Ag and Ch-RGO-Ag as shown in **Figure 1.6**. Due to the presence of large functionalities on GO, one would expect greater uptake in case of GO. But mercury uptake by GO and RGO was similar which depicts that the carboxylic functional group of GO and RGO *i.e.* COO- would be responsible for uptake of mercury as this functional group is common in GO and RGO. TEM and EDAX supports that MnO_2 and Ag were significantly helpful in adsorption of mercury.

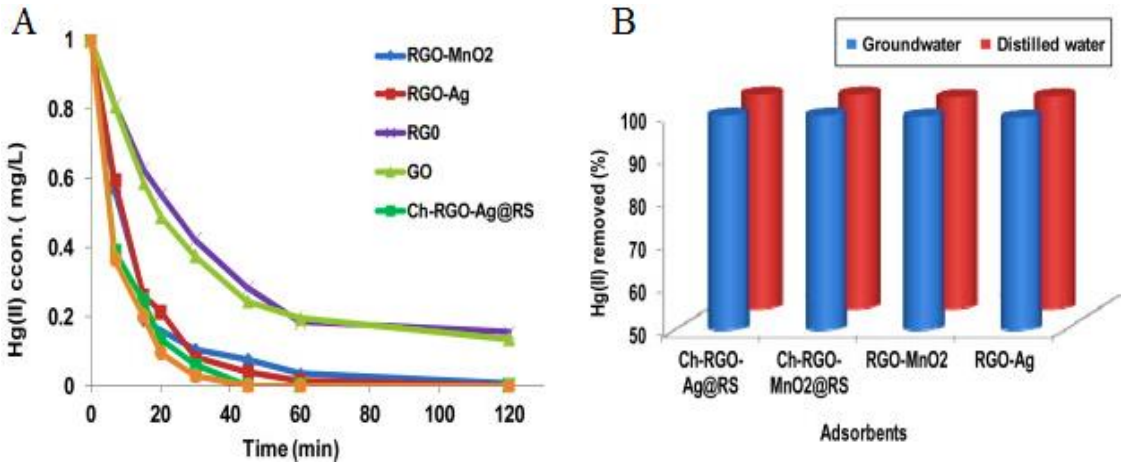

Figure 1.6. (A) kinetics of Hg (II) adsorption by different adsorbents, (B) comparison of different composites for removing mercury Hg (II) from water samples [67].

One of the most carcinogenic and toxic chemical when consumed >10 ppb is arsenic. According to an estimation about 60 million people are drinking arsenic containing water (>10 ppb) and it leads to skin cancer in Wisconsin even at <10 ppb concentration [68]. Zhang et al. [69] studied the removal of arsenate from drinking water by using GO-ferric hydroxide composite. GO was first treated with ferrous sulphate and then oxidized with hydrogen peroxide and ammonium hydroxide. Successful impregnation of ferric hydroxide was confirmed by using XRD, SEM and TEM. **Figure 1.7** represent the SEM micrographs of GO and GO–Fe-5, and energy dispersive X-ray spectroscopy (EDS) of GO–Fe-5.

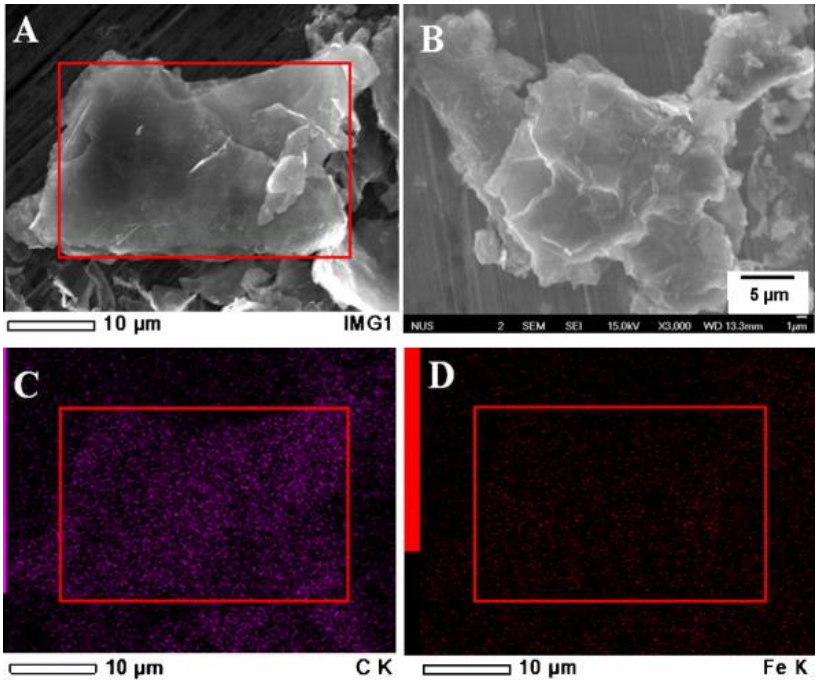

Figure 1.7. SEM micrographs of GO and GO–Fe-5, and EDS (energy dispersive X-ray spectroscopy) of GO–Fe-5. (A) SEM of GO–Fe-5, (B) SEM of GO, (C) carbon mapping of GO–Fe-5, and (D) iron mapping of GO–Fe-5 [69]

Five composites of GO-ferric hydroxide were prepared by varying ratio of GO/$FeSO_4 \cdot 7H_2O$ *i.e.* GO/Fe-1 (345mg GO/100mg $FeSO_4 \cdot 7H_2O$), GO/Fe-2 (345 mg/300 mg), GO/Fe-3 (345 mg/500 mg), GO/Fe-4 (345 mg/750 mg) and GO/Fe-5 (345 mg/1000 mg). The composite GO/Fe-5 was able to absorb 95% of arsenate from the contaminated water containing 51.14 ppm arsenate concentration. Absorption capacity of GO/Fe-5 composite was found to be 23.78 mg arsenate/g of composite. Arsenate was effectively removed in a wide range of pH (from 4 to 9) but at higher pH *i.e.* greater than 8 the efficiency of arsenate removal was found to decrease. **Table 1.2** shows the effects of iron on arsenic removal. Chandra et al. [70] synthesized water dispersible magnetite-reduced graphene oxide composites for removal of arsenic from water. Composites were fabricated by a chemical reaction between graphene oxide and magnetite particles (~10 nm). External magnetic field was used to separate the superparamagnetic composites.

Table 1.2. The effect of loaded iron on removal of arsenate ([a]-calculated from TGA tested in air, [b]-percentage of arsenate removed, [c]-arsenate absorbed by absorbents [d]-Iron conc. of the filtrate) [69].

	$Fe(OH)_3$ content (%)[a]	R_{AS} (%)[b]	q_{AS} (mg/g)[c]	L_{Fe} (ppm)[d]
GO-Fe-1	8.17	80.4	4.91	2.97
GO-Fe-2	19.62	98.1	5.98	7.74
GO-Fe-3	28.22	99.2	6.04	3.22
GO-Fe-4	42.26	100	6.10	0.64
GO-Fe-5	54.12	100	6.10	0.25
GO-Fe-5	54.12	95.7	18.55	15.82
GO-Fe-5	54.12	95.3	23.78	14.93

Magnetite-RGO composites have high affinity for adsorption of As (III) and As (V) as compared to bare magnetite particles. The reason for this high affinity is the increased adsorption sites in magnetite-RGO as a result of reduction of bare magnetite aggregates. These composites have great advantage in practical applications for removal of arsenic from drinking water because magnetite-RGO composites were able to effectively remove 99.9 % arsenic within 1ppb. Yang et al. [71] reported the application of graphene oxide in removal of Cu^{2+} from water. Graphene oxide has excellent capacity to absorb Cu^{2+} ions and by this absorption GO sheets tends to aggregate. Atomic force microscopy and confocal microscopy confirms the folding of GO sheets and hence aggregation in aqueous solutions of Cu^{2+}. As compared to bare active carbon the absorption capacity of GO for Cu^{2+} was about 10 times greater. The interaction between oxygen of GO sheet and Cu^{2+} ions render GO an effective absorbent for removal of cupper ions.

1.7.2 Disinfection and Antifouling Properties

One of the biggest challenges in waste water treatment is to control membrane fouling which shortens the life span of membrane filters by disturbing pore size and flux rate. Nanotechnology have introduced some antibacterial agents including Ag, Cu, ZnO, and TiO_2. Among these Ag nanoparticles have low cytotoxicity towards human beings. However, uniform dispersion of nanoparticles in aqueous media is a critical issue for

industrial applications. To avoid aggregation and achieve homogeneous dispersion one can use macroscopic support for loading nanoparticles. Graphene oxide provides and effective support for nanomaterial loading due to its low cost, hydrophilicity, ease of processing and functionalization [72, 73]. Bao et al. [74] synthesized the silver-graphene oxide nanocomposite as an antibacterial agent for water disinfection. GO-Ag composites were fabricated by *in situ* reduction of adsorbed Ag ions by hydroquinone and characterized by UV-visible, TEM, FTIR etc. Antibacterial properties were tested for both gram negative and gram positive strains of bacteria *i.e. Escherichia coli* and *Staphylococcus aureus*. **Figure 1.8** shows the antibacterial strength of GO and GO-Ag composites by paper disc method.

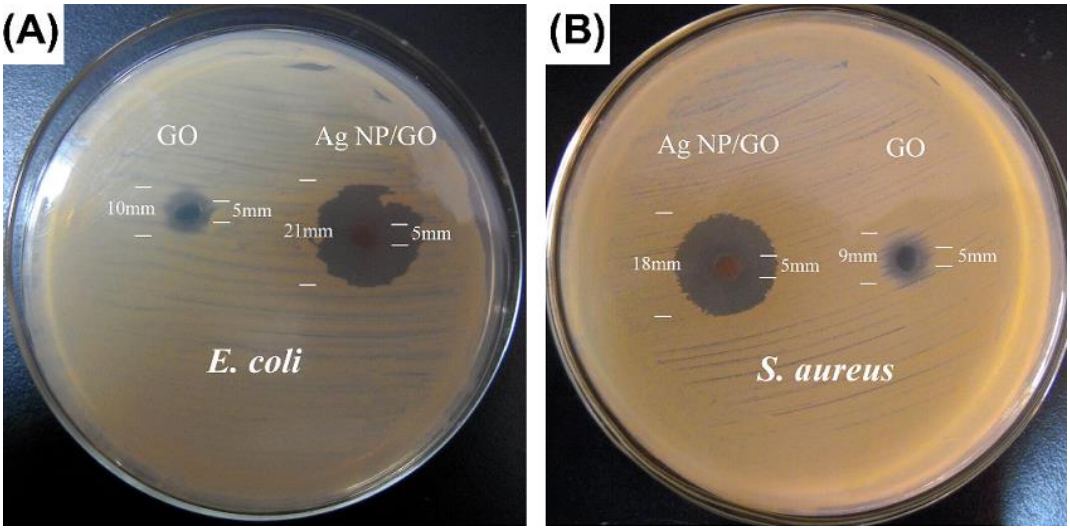

Figure.1.8. Kirby–Bauer antibiotic activity test for the GO paper disk and the Ag NP/GO paper disk against (A) *E. coli* and (B) *S. aureus* [74].

After 48h incubation a small inhibition zone was seen around GO which depicts the low toxicity of GO. However, a significantly larger and clear inhibition zone appears in case of GOAg composite. Diameter of inhibition zone for GO-Ag composite was almost a hundred times larger than that of bare GO. Ag ions or silver nanoparticles would be released to the surrounding media which either kill bacteria by disrupting cell membranes, or damaging protein to minimize the chances of microbial growth. To check the effectiveness of

prepared antibacterial composites in aqueous media, GO and GO-Ag were immersed in water infected by bacteria. After proper incubation plate counting method was used to check the level of disinfection. **Table 1.3** enlists the number of bacterial cells surviving in the presence of GO and GO-Ag composites.

Table 1.3. Number of bacterial cells surviving after contact with GO and Ag-GO composite [74].

Bacteria	Sample (cfu/mL)	Survival (cfu/mL)	Reduction (%)
E. coli	Blank	$1.33*10^6$	_
	GO	$6.40*10^5$	51.9
	Ag-GO	0	100
S. aureus	Blank	$6.67*10^5$	_
	GO	$2.52*10^5$	61.3
	Ag-GO	$8.27*10^4$	87.6

E. coli cells in contact with GO and GO-Ag composites were reduced to 51.9 % and 100 % respectively. While *S. aureus* was reduced by 61.3% and 87.6% respectively in the incubated GO and GO-Ag. Difference in membrane structure of both bacterial strains (thickness and integrity) was the main factor for lower efficacy of GO and composites towards S. aureus. Chung et al. [75] used ZnO-GO composite to improve the antifouling properties of polysulfone nanohybrid membranes. ZnO and ZnO-GO nanoparticles were synthesized by employing sol-gel method while the nanohybrid membranes of polysulfone impregnated with ZnO (1, 2, 3 wt.%) and ZnO-GO (0.1, 0.3, 0.6 wt. %) were fabricated by wet phase inversion technique. Although all membranes exhibited better properties but the best performance was noted in case of 2 wt.% ZnO and 0.6 wt.% Zn-GO. All the membrane properties like porosity, high hydrophilicity and high permeability contribute to overcome

the biofouling of polysulfone membranes. Liang et al. [76] used graphene oxide modified by hyper branched polyethylenimine (HPEI) to synthesize antibacterial polyethersulfone ultrafiltration membranes. For pure PES membrane the protein adsorption amount was noted to be 65.11 μg/cm^{-2} which was decreased to 25.89 μg/cm^2 for hybrid membranes containing 5 wt. % HPEI-GO. As adsorption of protein on membrane surface results in fouling, hybrid membranes containing HPEI-GO displayed excellent antifouling properties as compared to pure membranes. Besides improved antibacterial properties, these hybrid membranes have high tensile strength and high Young's modulus. Lei et al. [77] synthesized the high performance TiO_2-GO-Ag composites for water decontamination and disinfection under solar irradiation. As compared to GO and TiO_2 the composites show remarkable photocatalytic degradation of phenol and acid orange under solar irradiation. Due to the presence of silver nanoparticles, composites bear excellent antibacterial activities towards *E. coli*. The advanced photocatalytic activities make such composites highly useful for water purification.

1.7.3 Desalination

Desalination is one of the most powerful technique to secure the availability of neat water. Mostafa et al. [78] studied the applications of nano porous graphene oxide membrane for water desalination. Molecular dynamics proved that the nano porous membranes having pore size in the range of 0.29 to 0.45Å showed > 89% salt rejection at pressure less than 50 MPa. Water flux was also noted to be high (2-5 orders of magnitude) as compared to other reverse osmosis membranes. As compared to graphene membranes graphene oxide based membranes possess ~77% better water permeability due to the presence of large number of functional groups and such water desalination plants are cost effective. Keng et al. [79] reported the successful synthesis of wood-GO composite for solar steam generation. For desalination and water purification processes solar steam generation is highly efficient technology. Deposition of GO layer on wood (microporous) results in increased optical absorption and great photo thermal conversion which rapidly increases the temperature at the surface of liquid. Wood act as insulator to prevent the heat loss by confining it to the evaporative surface and helps in water transport from bulk to the surface. At a power density of 12 KW/m^2 the solar thermal efficiency of wood-GO composite was

noted to be ~83%. Euntae Yang et al. [80] introduced the forward osmosis membrane for desalination based on reduced graphene oxide and polydopamine. Due to the facile fabrication, controllable pore size and ultra-thin thickness GO based membranes can be used as an alternative to polymeric membranes. Hydrophilic polydopamine layer was coated on reduced graphene oxide laminates which increases the chances of water absorption. As a result, the reduced graphene oxide-polydopamine membranes shows water flux of 36.6 L/m^2h, with a reverse solute flux of 0.042 mol/m^2h and a high salt rejection rate of 92.0% in FO. Finnerty et al. [81] synthesized a novel graphene oxide leaf for solar desalination with zero liquid discharge. GO leaf displayed a broadband absorption and high stability in saline medium. When GO leaf was lifted in a tree like structure above the water, steam was generated at the rate of 2.0 LMH (Liter m^2 per hour) with an energy conversion efficiency of 78% under 0.82 solar flux. While the GO leaf floating on the surface of water generated steam at 1.1 LMH with energy efficiency of 54%. The rate of evaporation was directly related to the light intensity and inversely to the salinity. Despite of severe accumulation of salt on the leaf surface GO leaf maintain stability in a 15 wt.% NaCl solution. However, restoration of GO leaf just need scraping of deposited salt and rinsing the leaf with water. Due to ease of processing and low cost GO-leaf opened up new ways to desalination technology. Hegab et al. [82] reported that GO can be used in different ways for desalination purpose including GO membrane, GO surface modified membrane and GO incorporated in polymeric membranes. By the incorporation of GO mechanical strength, selectivity, water flux, antifouling properties of membranes increases significantly. Bin et al. [83] studied the use of GO/polyacrylonitrile membrane for water desalination. Vacuum filtration assembly was used to fabricate the thin film of GO on polyacrylonitrile membrane. At 90˚C the GO/PAN membrane possess a high water flux (65.1 Lm^{-2} h^{-1}) with high rejection (99.8%) by pervaporation for desalination. Such membranes exhibit high performance for desalination even in high salinity *i.e.* salt concentration upto 100,000 ppm. So GO-assisted membranes can be used for brackish and sea water desalination and reverse osmosis treatment as well. Abraham Jijo et al. [84] reported the tunable sieving of ions using graphene oxide membrane. According to Jijo GO based membranes exhibit 97% rejection for NaCl. Zahirifar Jafar et al. [85] synthesized a noval dual layer desalination membrane by incorporating GO-ODA (octadecylamine) in

PVDF (polyvinylidene fluoride) matrix. Different techniques (XRD, TGA, FE-SEM) were used for characterization and investigation of properties of GO-ODA and their membranes. PVDF membranes containing GO-ODA possess superior properties in terms of increased hydrophobicity, surface roughness, water flux and salt rejection as well. Betterment of membrane properties was attributed to the formation of high surface area nano-channels by GO-ODA which results in high salt (NaCl) rejection and increased water flow.

1.8 Stability Concerns of Graphene Oxide and Metal Nanoparticles

One of the main challenges of GO to form nanocomposite membranes is swelling of GO sheets in aqueous media which results in leaching of GO nanofiller. These swelling effects limits the long term usability of GO. Another challenge to hinder the applicability of GO is associated with its π-π stacking. The π-π stacking of GO sheets results in its agglomeration within polymer matrix and affects its applications. One of the quick method to overcome agglomeration is functionalization of GO with different metal and metal oxide nanoparticles [50, 86]. GO-Ag [87], GO-ZnO [88], GO-TiO_2 [89], and GO-nanodiamond are widely studied to improve the stability of polymer membranes in water treatment [90].

The antimicrobial property of AgNPs is directly linked with their size and shape. Low colloidal stability of AgNPs results in their aggregation which decreases their surface area and antimicrobial activity. So the main problem associated with the use of graphene oxide and silver nanoparticles is their agglomeration property. Functionalization of GO with AgNPs results in high exfoliation of GO nano-sheets, by increasing the interlayer distance of GO nanolayers. On the other hand, using highly oxygenated substrate like GO provides high binding sites for nucleation and growth of AgNPs [91]. So functionalization of GO with AgNPs helps in uniform dispersion of AgNPs and exfoliation of GO nanosheets as well. Cobos et al. [92] reported the use of PVA/GO-Ag nanocomposite against two pathogenic bacteria Staphylococcus aureus and Escherichia coli.

1.9 Polymer Nanocomposite Membranes

In contrast to the classical polymer membranes, nano filler based membranes are springing up for separation and purification. Nanotechnology plays a remarkable role in controlling

water pollution. The two dimensional nanomaterials have integral atomic thickness properties which controls the membranes transport resistance. Besides this the adjustable pore size and selectivity to certain particular pollutants makes nanomaterials a wonder in the field of separation and purification industry. Polymer nanocomposites can be fabricated by using highly antifouling nano fillers by using melt intercalation, exfoliation/adsorption and in situ polymerization. Carbon nanofillers are one of the most fascinating material used for fabrication of nanocomposite membranes [93]. **Figure 1.9** enlists some common applications of polymer nanocomposites. Physical and chemical stability of nanocomposite membranes is still a matter of concern. According to a study proposed by Zodrow at al. [94] (Ag^{+}) silver ions leach from the silver impregnated polysulfone membrane surface resulting in water flux decline and reduced antimicrobial activities. CNTs are proved to have better stability than metal nanoparticles. MWCNT are proved to increase the stability of polyamide membranes [95]. In order to maintain the high performance and reusability of membranes, different strategies are being used for immobilization of nano fillers on polymer surface. Xin Li et al. [96] studied that pluronic F127 restrict the leaching of TiO_2 from a polyether sulfone mixed matrix membrane. The synthesized membrane shows highly antifouling effects for BSA and humic acid foulants.

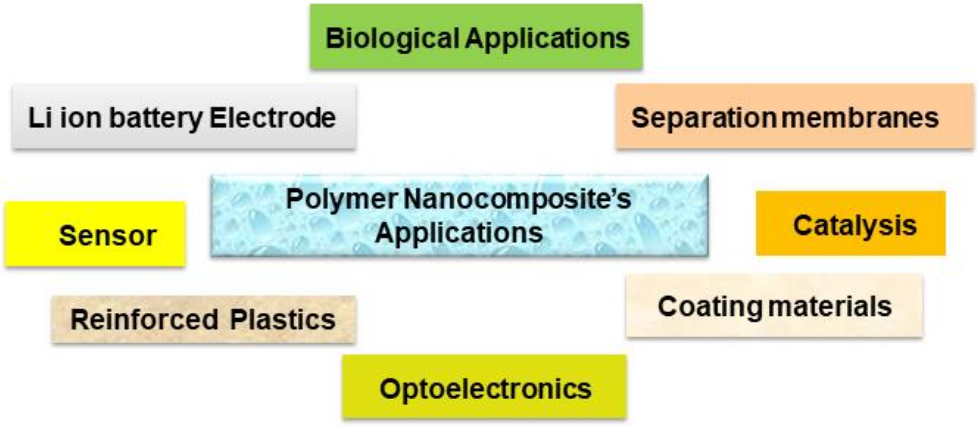

Figure 1.9. Applications of polymer nanocomposites

1.10 Methods for Fabrication of Polymer/Nanocomposite Membranes

The most prevalent techniques used for manufacturing nano porous membranes are phase inversion, electrospinning, solution casting, interfacial polymerization, track in polymer membranes. Solution casting involves the mixing of nanocomposites and polymer beads/powder into a solvent under continuous stirring to form a homogeneous solution. This homogeneous solution was than casted on the glass plates or a supporting substrate and allowed to dry. While the phase inversion process involves the change of homogeneous liquid phase to solid state. During phase inversion the homogeneous polymer or polymer/nanocomposite solution was casted by using a casting blade (to control the thickness of membranes) onto the glass substrate. Than the substrate was immersed in a non-solvent, usually water to allow the inversion of phase which leads to thin film formation [97]. To obtain the desired properties of polymer membranes different approaches are being used which include, thermally induced phase inversion, immersion precipitation and vapour/evaporation induced phase inversion. [98, 99]. Nanofibrous membranes are usually synthesized by electrospinning method. Viscosity of the casting solution and electric potential controls the porosity and pore size distribution of membranes generated by electrospinning [100]. Interfacial polymerization involves a poly condensation reaction between polyamines and polyacyl chlorides monomers (dissolved in immiscible solvents). A thin film (10nm to several m thick) generate at the polymer substrate interface and attached to the substrate. The reverse osmosis and nanofiltration membranes were generally synthesized by interfacial polymerization [101]. The structure and morphology of the as-synthesized membranes depends on the solvent type, monomer concentration and reaction speed. Polymer membranes fabricated by phase inversion or solution casting methods involves mixing of nanofillers within the polymer matrix and membrane surface remain deficient of hydrophilic moieties. Resin infiltration technique can help in surface availability of nanocomposites to tackle the hydrophobic and fouling concerns of polymers. Resin infiltration assembly is reciprocal to layer by layer assembly in which the layered components interact with each other by electrostatic attraction or H-bonding [102-104]. **Figure 1.10** represents the fabrication methods of polymer/nanocomposite membranes.

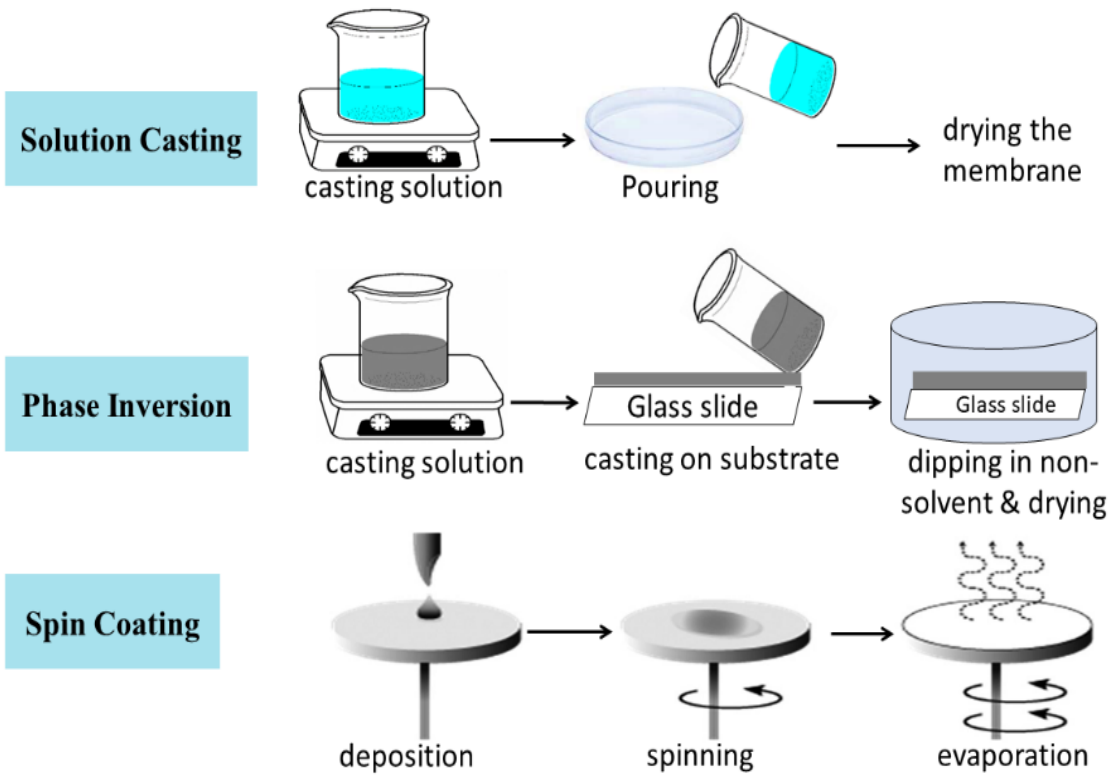

Figure 1.10. Fabrication methods of polymer/nanocomposite membranes

1.11 Literature Review

1.11.1 Graphene Oxide/ Silver Nanoparticles Composites

Silver nanoparticles acts as a natural defense system against various microorganisms. Nano silver when come in contact with bacterial cell wall. They rupture the cell structure and penetrate into the cell interior where they generate free radicals causing bacterial cells death. Antibacterial features of silver nanoparticles are well explored in the field of medicine as well [105]. Suhalim et al. [106] analyze the silver/GO additive to increase the water flux and rejection properties of PSF membrane. The PSF membranes with 0.5 wt.% GO-Ag loading exhibit the highest ionic rejection and lowest water contact angle. Faria et al. [107] synthesized forward osmosis membranes functionalized with graphene oxide silver. GO-silver and thin film composite membrane were covalently cross linked by their carboxyl groups. The GO-silver based composite membrane exhibits 80% inactivation of

Pseudomonas aeruginosa. These membranes exhibit high anti biofouling property during cross flow filtration tests. Soroush at al. [108] also used GO-silver for surface functionalization of forward osmosis membrane. The GO/Ag nanocomposite was covalently bonded to the thin film composite membrane through amide forming condensation reaction by using ceastamine. These membranes showed excellent hydrophilic properties with water contact angle below 25º. Besides this the fabricated membranes showed 95% inactivation of *Escherichia coli* without compromising the membrane transport properties. Another study done by Vatanpour et al. [109] showed that boron nitrite-GO/Ag nanocomposite improves the water permeability, antifouling, antibacterial and high rejection properties of PES membranes. Furthermore, the boron nitrite-GO/Ag nanocomposite increases the negative surface charge of PES membrane which exhibited 88.9% rejection of reactive black 5 and 77.7 % rejection of reactive red 120. Kwanyong et al. [110] used Ag-GO nanocomposite as an antifouling and antibacterial coating on PVDF membranes by a facile pressurized filtration method. Water flux performance of the coated membrane increased 50% as compared to the pristine PVDF membrane. The modified membranes maintained high flux recovery and antibacterial features after membrane back wash. Jose et al. [111] fabricated a Ag-GO coated nylon membrane for water purification by vacuum filtration technique. The designed membrane exhibited 46.7 $Lm^{-2}h^{-1}$ water flux and appreciable rejection of Congo red (95%), Rhodamine B (88%) and Methylene blue (85%). Antibacterial performance test showed that the Ag-GO nanocomposite inhibits the bacterial growth of *Staphylococcus aureus and Escherichia coli*. Another study done by Heba Isawi [112] showed that Ag-GO nanocomposite enhances the desalination performance of polyamide thin film composite membrane. The water flux performance increases from 27 to 43.4 $Lm^{-2}h^{-1}$ while the salt retention increases from 93% to 99%. Antibacterial properties were also tested by using Escherichia coli. X.F Sun et al. [113] used Ag-GO composite for modification of cellulose acetate membrane. SEM analysis showed that the silver nanoparticles preserve their nanostructure properties on the modified membrane surface which results in inactivation of 86% of Escherichia coli. The Ag-GO modified membrane showed significant low flux drop as compared to unmodified membrane and membranes based on bare GO and Ag nanoparticles. Mahmoudi et al. [114] reviewed the multifunctional applications of silver

doped graphene oxide composites. He concluded that aggregation effect of the plasmonic silver nanoparticles can be diminished by grafting the AgNPs on GO sheets, which results in extraordinary antibacterial results. GO-Ag nanocomposites have extraordinary environmental and biomedical applications as well as high optical sensitivity to detect heavy metals. Alkhouzaam et al. [115] presented an overview of GO based membranes regarding the water treatment and desalination approaches. This overview showed that both the pristine GO and functionalized GO nanofiller based membranes increases the hydrophilicity, antifouling, antibacterial and rejection properties of reverse osmosis membranes. Zhou et al. [116] fabricated the highly antibacterial thin film composite reverse osmosis membranes based on GO quantum dot-mediated AgNPs. GOQD-AgNPs was incorporated into PA thin films by employing interfacial polymerization. The obtained TFN membrane exhibits 98.9% rejection of NaCl salt and a water flux of 39.1 $Lm^{-2}h^{-1}$. GOQD-AgNPs based membrane possessed remarkable antibacterial features against *Staphylococcus aureus* (96.5%) *and Escherichia coli* (98.6%).

1.11.2 Graphene oxide/Polyethylene glycol Composites

Polyethylene glycol (PEG) is an important thermoplastic polymer which possess extraordinary properties like high hydrophilicity, crystallinity and solubility in organic solvents. Recently PEG has been used as an additive and surface modifier to improve water permeability and antifouling properties of polymer membranes. Hydrophilicity of GO can be improved by surface functionalization of GO sheets with PEG [117]. Strong hydrogen bonding between GO and PEG is proved to be very successful in fabrication of organic-inorganic hybrids to achieve high performance membranes. Mansourpanah et al. [118] reported that incorporation of PEG/GO nanosheets increases the hydrophilicity, salt rejection and antifouling properties of polyamide thin film composites. Li-guang and coworkers [119] reported the in-situ polymerization of polyimide/PEG-GO hybrid membranes. PEG grafting results in formation of defective structures on GO surface which enhances the gas separation property of membranes. Chen et al. [120] synthesized the PVDF/PEG-graphene composite by employing solution blending method in which PEG-graphene was obtained by amidation reaction between GO and methoxy polyethylene glycol followed by reduction using sodium borohydride. The water flux and selectivity

performances of GO functionalized membrane primarily determined by its functionalized active layer as well as its concentration and aggregation of GO sheets, which obstruct the effective driving force for water flux due to slow diffusion of solute on the functionalized active layer of porous surface of membrane. Therefore, in order to fabricate GO membranes with high selectivity and water flux properties, it is extremely critical to structurally engineer the functionalized GO membrane layer so that it rejects or minimize unwanted solute transport. Jatoi at al. [121] fabricated PEGylated GO based lamellar nanofiltration membrane for separation of rhodamine B, evans blue and methylene blue. PEGylated GO based membrane showed ~ 155 ± 10 $Lm^{-2}h^{-1}$ methol permeability. PEGylation enhanced the interlayer spacing of GO sheets upto 1.12nm and additionally increases the stability of GO membranes in organic solvent. M.A. jihad et al. [122] synthesized the PEG functionalized GO nanoparticles incorporated with *Nigella sativa* extracts and used them for drug delivery system. The synthesized nanocomposite was observed to inactivate the *Staphylococcus aureus and Escherichia coli* bacteria by interacting the the bacterial cell structure and destroying the nucleic acid. Yuan Peng et al. [123] Graphene functionalization was found to decrease the thermal resistance at PEG-graphene interface and uplift the heat capacity and phase change temperature as well. M.veerapandian [124] used GO functionalized with Ag@silica-PEG nanohybrid for electrochemical detection of quercetin. A. kumar et al. [125] used PEG and GO functionalized cotton to fabricate the thermos-regulating textile fabric material. The and highly efficient UV rays' protection. GO/PEG-CuS nanocomposite are applicable for cervical cancer treatment [126]. The anticancer drug doxorubicin was effectively loaded on the GO/PEG-CuS nanocomposite and used to decrement the tumor by combining the photothermal and chemothermal therapies. DR Rout et al. [127] synthesized PEG functionalized reduced GO/ZnO composite for removal of phenolic pollutants from waste water. The analysis showed that the synthesized PEG-GO/ZnO nanocomposite remove 86.54% of industrial effluents in 45 min. P.A jeshvaghani et al. [128] reported a novel green nanoemulsification method to obtain a GO/PEG-fibroin protein based nanocarrier for cancer treatment. Mohammadi and Babaei [129] proposed a novel nanocomposite based on PVA/chitosin/PEG-GO for biomedical use and food packaging industry. Their study revealed that the surface fuctionalization of GO with PEG reduces the toxicity of GO at high loading.

PVA/chitosin/PEG-GO sample showed the highest mechanical strength, low biodegrability and better antibacterial properties against *S. aureus and E. coli.*

1.11.3 Graphene oxide/Magnetic Fe_3O_4 Composites

The presence of hydrophilic groups like carboxyl and hydroxyl groups on GO sheets makes the GO adsorbent highly dispersible in aqueous media. The conventional centrifugation or filtration techniques are not useful in successful retrieval of GO from the sample. On the other hand, magnetic nanoparticles are very easy to separate from the reaction mixtures. So the fabrication of magnetic graphene oxide is widely explored for the simple and fast recovery of graphene oxide just by applying an external magnetic field [130]. Wang et al. [131] used a magnetic β-cyclodextrin graphene oxide nanocomposite for the removal of malachite green from aqueous solution. The maximum adsorption capacity of the magnetic nanocomposites was 990.10mg/g and these nanocomposites were used for 5 cycles with 80% recovery ratio. Hossienzadeh et al. [132] synthesized high performance ultrafiltration membranes by using the functionalized magnetic graphene oxide. The magnetic nanofiller was proved to enhance the permeability and water flux of polysulfone membranes along with high antimicrobial/antifouling properties. Abdi et al. [133] studied that the hydrophilicity and antifouling property of PES membranes drastically increased by incorporation of magnetic GO/metformin hybrids. These modified membranes were used for removal of heavy metal ions (cupper ions) and direct red/16 dye. Xu et al. [134] fabricated the Fe_3O_4/GO based PVDF membranes by using magnetic field induced casting and phase inversion process. A magnetic field of 0.1- 0.2T was used to induce the migration of magnetic GO to the membranes top surface. This migration behavior raises the hydrophilic character of PVDF membranes. Hydrophilicity of PVDF membranes significantly increases with a water flux of 595.39 $Lm^{-2}h^{-1}$. BSA rejection and flux recovery ratio was also appreciable. Another study proposed by Mirzaei et al. [135] uses GO/ Fe_3O_4 for fabrication of PES mixed matrix ultrafiltration membranes. A magnetic field of 0.1T was used during casting process to obtain the magnetic properties in PES-GO/ Fe_3O_4 membrane. Comparing the membranes fabricated with and without magnetic field induction, it was concluded that in the case of magnetic field induced membrane the water contact angle reduces by 35 % which increases the pure water flux upto 76.2 %.

Furthermore, the BSA rejection was 92 % while the flux recovery ratio (FRR) was 87.9 %. P.V. Chai et al. [136] synthesized the highly antifouling PSf membranes by incorporating the GO/ Fe_3O_4. Co-precipitation method was used to obtain the magnetic GO and phase inversion technique was used for membrane fabrication. The 0.6 wt.% GO/ Fe_3O_4 membrane exhibits the 87.01 $Lm^{-2}h^{-1}$ water flux and 98 % rejection of congo red with a FRR of 95%. Zhang et al. [137] used magnetic graphene oxide to fabricate immobilized metal affinity adsorbant for selective enrichment of cytokinins in plants. Rastgar et al. [51] [fabricate GO/Fe_3O_4 nanohybrid based forward osmosis membrane by in-situ interfacial polymerization of polyamide monomer solution. Thin film composite membranes synthesized both in the presence of magnetic field and in the absence of magnetic field were tested to compare their water permeability, salt rejection and antifouling properties. Magnetic field assisted membrane depicts 117.4% and 63.2% enhancements of water flux as compared to pristine TFC membrane and non-magnetic GO/Fe_3O_4 based TFC membrane. Nusrat Tara et al. [138] synthesized magnetic *Nigella sativa* –GO based composite for highly active antibacterial water treatment tests. Magnetic iron oxide nanoparticles were incorporated in cellulosic black cumin seed powder functionalized with GO. The synthesized BC-GO@ Fe_3O_4 composite was characterized and used against Gram-positive and Gram-negative bacterial strains. Besides this, the BC-GO@ Fe_3O_4 composite showed excellent adsorption of methylene blue and arsenic from water.

1.12 Plan of Work

To the best of our knowledge, PVC membranes were mostly fabricated by phase inversion or solution casting methods. These methods involve mixing of nanofiller within polymer matrix and membrane surface remain deficient of hydrophilic moieties. Resin infiltration technique can help in surface availability of nanocomposites to compensate the hydrophobic issues of polymers. In the present strategy the GO was synthesized and modified with silver nanoparticles (AgNPs), poly ethylene glycol (PEG), magnetic iron oxide (Fe_3O_4) and silver functionalized magnetic GO (Ag-GO/Fe_3O_4). These nanocomposites (GO-Ag, PEG/GO-Ag, GO/Fe_3O_4 and Ag-GO/Fe_3O_4) were incorporated into the PVC and PVDF-*co*-HFP polymer resins by using a vacuum filtration assembly to fabricate surface active `hydrophilic polymer membranes. The synthesized nanocomposites and their membranes were characterized by XRD, FTIR, Raman, UV, SEM TEM, and water contact angle measurements. Magnetic membranes were mostly fabricated by using an external magnetic field to move the magnetic nanoparticles to the top of the membrane surface. Herein, we used resin infiltration method to fabricate magnetically active membranes without using any external magnetic field. The fabricated membranes were tested in terms of water and BSA filtration, antifouling ratios, cyclic filtration tests, flux recovery ratios, and thermal stability as well.

1.13 Aims and Objectives of Present Study

The aim of the present study was to fabricate a highly hydrophilic, fouling resistant and thermally stable PVC and PVDF-*co*-HFP membranes. This aim was achieved by working on following objectives.

- To synthesize the graphene oxide (GO) and modified GO (GO-Ag, PEG/GO-Ag, GO-Fe_3O_4 and Ag/GO-Fe_3O_4) nano-fillers
- To use the synthesized nano-fillers for fabrication of hydrophilic and antifouling polymer membranes.
- To use the resin infiltration fabrication technique for the surface availability of nanofillers.

- To explore the effect of GO, GO-Ag, PEG/GO-Ag, GO-Fe_3O_4 and Ag/GO-Fe_3O_4 nano fillers incorporation on water contact angle of membranes.
- To investigate the pure water flux and BSA protein flux of fabricated nanocomposite membranes.
- To evaluate the effect of nano fillers addition on BSA rejection of nanocomposite membranes.
- To inspect the total fouling ratio, irreversible fouling ratio and reversible fouling ratio of fabricated membranes
- To examine the antibacterial features of GO and GO-Ag nanofillers
- To analyze the cross-sectional morphology and thermal stability of synthesized membranes.
- To evaluate the durability and reusability of membranes.

CHAPTER 2

EXPERIMENTAL WORK

2.1 Materials and Methods

All the chemicals were of analytical grade and used without further purification. Graphite powder, silver nitrate ($AgNO_3$), sodium nitrate ($NaNO_3$), potassium permanganate ($KMnO_4$) and sulfuric acid (H_2SO_4) were purchased from Sigma Aldrich. Tetra hydro furan (THF), sodium borohydride ($NaBH_4$), poly vinyl chloride (PVC), dimethyl acetamide (DMAc), sodium borohydride ($NaBH_4$) and sodium citrate ($Na_3C_6H_5O_7$) were supplied by Daejung China. Polyethylene glycol (PEG) (Mw=1500 g), ferric chloride ($FeCl_3.{}_6H_2O$), ferrous chloride ($FeCl_2.{}_4H_2O$), hydrogen peroxide (H_2O_2), ammonium hydroxide (NH_4OH) and poly (vinyledene fluoride-co-hexaflouropropylene) (PVDF-*co*-HFP) were obtained from Merck.

2.2 Synthesis of Nanocomposites

2.2.1. Synthesis of GO and GO-Ag

Graphene oxide was synthesized by using modified Hummer's method as shown in **Figure 2.1**. [139] [140]. Sulfuric acid and $KMnO_4$ were used to oxidize the graphite flakes. Briefly, sulfuric acid (25 mL) was slowly added in to the mixture of graphite flakes (1 g) and sodium nitrate (1 g) under vigorous stirring. Subsequently, $KMnO_4$ (3 g) was added and mixed homogenously on the ice bath. Then, 50 mL water was added in a drop wise manner (to avoid explosion because of highly exothermic reaction). The solution was refluxed at 100 $^{\circ}C$ for 15 min and then 100 mL distilled water was added followed by the addition of 30% H_2O_2 solution. The resulting final product was centrifuged and washed with excess amount of water and dried overnight at 50 °C in vacuum oven.

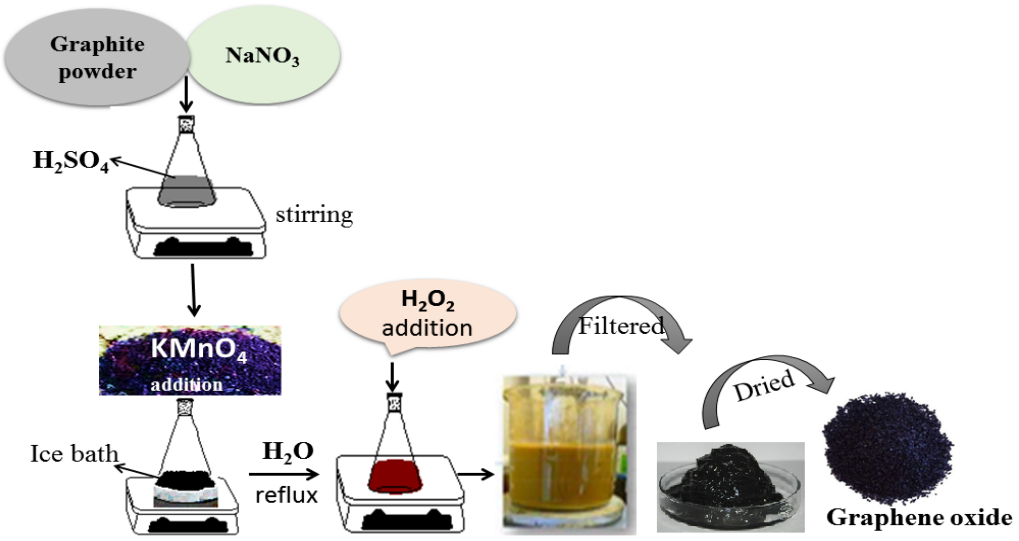

Figure 2.1. Synthesis of graphene oxide

Synthesized GO was then functionalized with AgNPs by following chemical reduction method shown in **Figure 2.2**. GO (0.5g) was dispersed in 0.01M $AgNO_3$ solution by ultrasonication. Than freshly prepared $NaBH_4$ solution was added drop wise to the above suspension of GO under continuous stirring. $NaBH_4$ reduces the Ag ions decorated on the surface of GO functionalized sheets. Silver functionalized GO nanosheets were than washed with deionized water and dried in vacuum oven at 50°C [141].

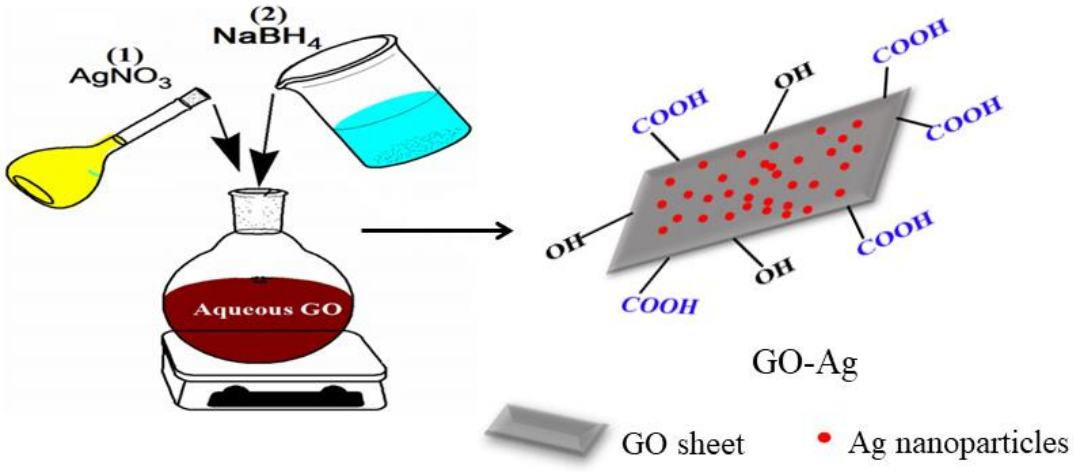

Figure 2.2. Silver functionalization of GO by chemical reduction method

2.2.2 Synthesis of PEG-GO-Ag

PEG modified GO-Ag nanofiller was synthesized by following method. GO-Ag (0.05 g) was dispersed in 30 mL deionized water by sonication. After uniform mixing of solution, 0.5 g PEG was added and again sonicated for 1 h. The above mixture was stirred for 2 h at room temperature and finally centrifuged and washed with excess amount of water to remove unreacted PEG [142].

2.2.3 Synthesis of Magnetic GO (GO/Fe_3O_4)

Magnetic graphene oxide was synthesized by following chemical co-precipitation route as shown in **Figure 2.3** [143]. The powdered GO (0.5 g) was dispersed in (100 mL) distilled water by bath sonication. Than the freshly prepared salt solution (1.2 g $FeCl_3.6H_2O$ and 0.6 g $FeCl_2.4H_2O$) was added dropwise to the GO solution under continuous stirring and heated up to 90°C for 30min. Afterwards, the ammonium hydroxide (30 mL) solution was added at once to the above mixture. By the addition of ammonium hydroxide blackish precipitates of magnetic GO (GO/Fe_3O_4) were noticed. The obtained GO/Fe_3O_4 nanoparticles were separated with the help of a magnet and washed with plenty of deionized water to neutralize the pH. Then the GO/Fe_3O_4 nanocomposite was dried at 50°C. For comparison, bare Fe_3O_4 nanoparticles were also synthesized following the same co-precipitation method.

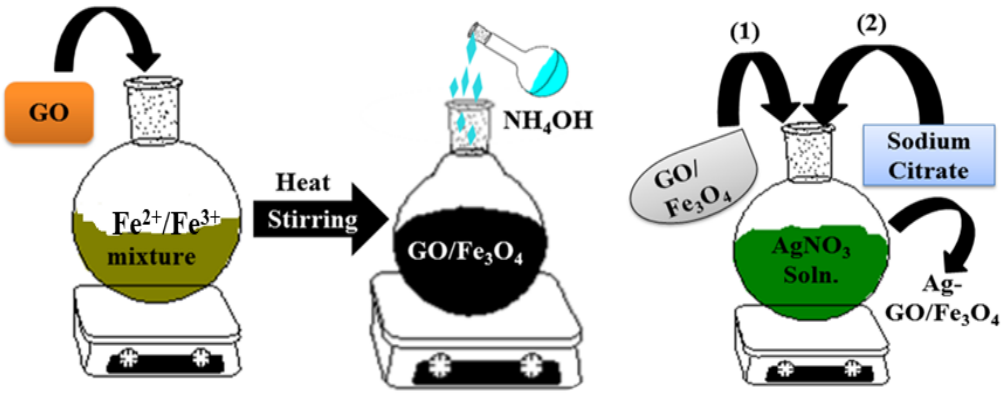

Figure 2.3. Synthesis of GO/Fe_3O_4 and Ag-GO/Fe_3O_4 [143].

2.2.4 Silver functionalization of Magnetic GO

Finely grinded magnetic graphene oxide (0.05g) was added to the silver nitrate (0.01M) solution and undergo sonication to ensure uniform nucleation of nanoparticles. Than the sodium citrate solution (0.01M) was added dropwise to the above suspension and let the solution to be sonicated for 1h. Silver functionalized GO/Fe_3O_4 nanoparticles were than washed many times by magnetic decantation and dried at 50°C in vacuum oven [144]. **Figure 2.3**. shows the method for silver functionalization of GO/Fe_3O_4.

2.3 Fabrication of Polymer/Nanocomposite Membranes

2.3.1 Fabrication of PVC/GO and PVC/GO-Ag Membranes

PVC/GO-Ag nanocomposite membranes were fabricated by employing resin infiltration technique as shown in **Figure 2.4**. GO-Ag (0.25, 0.5 and 1 wt. %) nano additives were dispersed in THF (10ml) by ultrasonication. Well dispersed GO-Ag suspensions were filtered through a 0.2 µm PES filter paper fitted in a vacuum filtration assembly. After partial drying of GO-Ag layer, PVC resin (10g in 80 mLTHF) was dropped on to this GO-Ag layer and allowed to filter through the nano additive layer. Resin infiltration of PVC through GO-Ag nano channels helps in gripping of GO-Ag particles resulting in increased stability of PVC/GO-Ag membrane. The obtained membrane was peeled off from the surface of filter paper and dried at room temperature. PVC-GO membranes were synthesized following the same above mentioned method. The pristine PVC membrane was fabricated by using solution casting method. **Table 2.1** explicate the compositions and assigned codes of fabricated membranes.

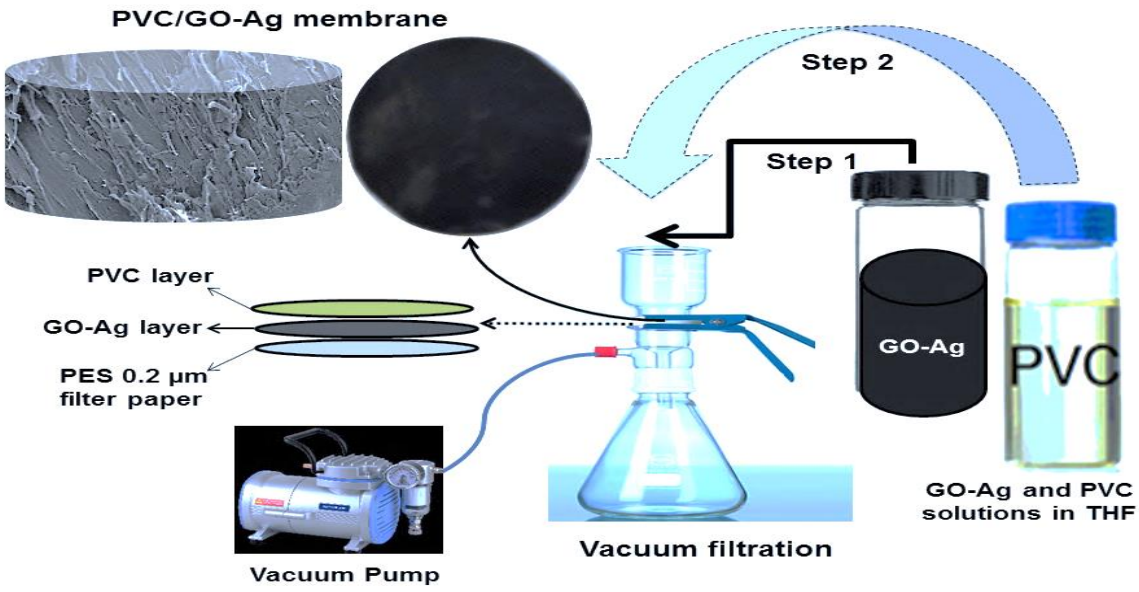

Figure 2.4. Fabrication of GO-Ag based PVC membranes by resin infiltration

Table 2.1. Composition and sample codes of PVC/nanocomposite membranes

Material	PVC wt.%	Nanofiller wt.%	Membrane code
PVC	10	0	PVC
GO	10	0.5 GO	P/GO 0.5 wt.%
GO-Ag	10	0.25 GO-Ag	P/GO-Ag 0.25 wt.%
GO-Ag	10	0.5 GO-Ag	P/GO-Ag 0.5 wt.%
GO-Ag	10	1 GO-Ag	P/GO-Ag 1 wt.%

2.3.2 Preparation of GOAg/PVDF-*co*-HFP and PEG-GO-Ag/ PVDF-*co*-HFP Membranes

All the membranes were fabricated by resin infiltration method using PEG-GO-Ag nanofiller as active layer on PVDF-*co*-HFP support membranes. Different concentrations of PEG-GO-Ag (0.2, 0.6, 1 and 1.4 wt.%) nanofiller were dispersed in THF (10 g) and sonicated for 1 h. In the first step, PEG-GO-Ag (0.2, 0.6, 1 and 1.4 wt.%) as active layer

was deposited on Whatman filter paper (0.45 µm) using vacuum filtration assembly at room temperature (25 °C) and under low vacuum condition. A homogenous solution of PVDF-*co*-HFP (10 g) was prepared by dissolving in DMAc (80 g) in parallel. When the PEG-GO-Ag layer is about to dry completely, the PVDF-*co*-HFP solution was poured onto this layer to undergo vacuum filtration which results in PVDF-*co*-HFP resin intercalation into the PEG-GO-Ag layer. PEG/GO-Ag active layer based PVDF-*co*-HFP membrane was then peeled of and dried in an oven at 80 ºC to remove residual solvent. For comparison, control membranes of pristine (PVDF-*co*-HFP) and PVDF-*co*-HFP membrane containing 1wt.% GO-Ag were also prepared using the same procedure (1 GOAg-P). The fabricated nanohybrid membranes with PEG-GO-Ag additive with 0, 0.2, 0.6, 1 and 1.4 wt. % were designated as Pristine-P, 0.2 PEG-GOAg-P, 0.6 PEG-GOAg-P, 1 PEG-GOAg-P and 1.4 PEG-GOAg-P, respectively. **Scheme 2.2** represents the scheme for fabrication of PEG-GOAg-P membranes.

Table 2.2. Composition and sample codes of PVDF-*co*-HFP/nanocomposite membranes

Material	PVDF-*co*-HFP wt.%	Nanofiller wt.%	Membrane code
PVDF-*co*-HFP	10	0	Pristine-P
GOAg	10	1 GO-Ag	1 GOAg-P
PEG-GO-Ag	10	0.2 PEG-GO-Ag	0.2 PEG-GOAg-P
PEG-GO-Ag	10	0.6 PEG-GO-Ag	0.6 PEG-GOAg-P
PEG-GO-Ag	10	1 PEG-GO-Ag	1 PEG-GOAg-P
PEG-GO-Ag	10	1.4 PEG-GO-Ag	1.4 PEG-GOAg-P

2.3.3 Fabrication of GO/Fe_3O_4 and Ag-GO/Fe_3O_4 based Membranes

In order to synthesize the magnetic membranes, resin infiltration approach was used. Magnetic graphene oxide (GO/Fe_3O_4 1.0 wt.%) was dispersed in THF and sonicated properly to obtain a consistent distribution of GO/Fe_3O_4. Separately, PVDF-*co*-HFP resin was synthesized by dissolving PVDF-*co*-HFP beads in DMAc under continuous stirring at 70°C. Than the homogeneous solution of GO/Fe_3O_4 was filtered slowly through a 0.2 µm

polyether sulfone (PES) filter paper fitted in vacuum filtration assembly and dried at room temperature until a smooth layer of magnetic graphene oxide was formed. After this, we poured the PVDF-*co*-HFP resin gently on the GO/Fe_3O_4 layer and undergo resin infiltration under low vacuum. The infiltration of PVDF-*co*-HFP resin through the stacked GO/Fe_3O_4 layer successively griped the magnetic graphene oxide resulting in a stable membrane pattern. The fabricated membrane was peeled off carefully from the surface of filter paper and dried at 70°C. **Table 2.3** shows the composition and sample codes of PVDF-*co*-HFP/magnetic nanocomposite membranes Ag-GO/Fe_3O_4 (1.0 wt.%) membrane was fabricated following the same above mentioned method. The pure PVDF-*co*-HFP membrane was obtained by using solution casting method.

Table 2.3. Composition and sample codes of PVDF-*co*-HFP/magnetic membranes

Material	PVDF-*co*-HFP wt.%	Nanofiller wt.%	Membrane code
PVDF-*co*-HFP	10	0	Pristine-P
GO/Fe_3O_4	10	1.0	GO/Fe_3O_4-P
Ag-GO/Fe_3O_4	10	1.0	Ag-GO/Fe_3O_4-P

2.4 Characterization of Nanocomposites

Purity and crystallinity of GO and GO-Ag, PEG-GO-Ag, GO/Fe_3O_4 and Ag-GO/Fe_3O_4 nanocomposites were studied XRD (Bruker D2 phaser XE-T edition) technique. The structural functionalities of the synthesized nanofillers were characterized by FTIR (Nicolet iS10 FTIR spectrometer, 600-4000 cm^{-1} with 4 cm^{-1} resolution). The UV-visible spectroscopy (NanoDrop 2000 UV-Vis spectrophotometer) was used to investigate the silver functionalization of GO, and GO/Fe_3O_4. Raman spectra of samples were recorded using Renishaw in Via Reflex spectrometer (laser wavelength 532 nm with 5 cm^{-1} spectral resolution). To record Raman spectra of synthesized samples, 10 µL of nanofiller suspension in water (1 mg/mL) was drop casted on a clean silicon substrate and dried at room temperature. Thermal stability of the nanofiller samples were analyzed by TGA analyzer (NETZSCH STA 449 C thermo-microbalance with TG resolution of 1 µg) at a heating rate of 10 ºC/min in air (flow rate 30 mL/min) from 25 ºC to 550 ºC. The surface morphology of the samples was studied by SEM and TEM (scanning electron microscopy,

Leo Supra 35VP) analysis. The samples were pre-coated with gold at a 0.04 volt/ohm using Cressington sputter coater (108/SE) before taking SEM images.

2.5 Characterization of Membranes

Surface morphology of pristine PVC, PVDF-*co*-HFP membranes and the nanocomposites based membranes i.e. PVC/GO, PVC/GO-Ag, GO-Ag/PVDF-*co*-HFP, PEG-GO-Ag/PVDF-*co*-HFP, GO/Fe_3O_4/PVDF-*co*-HFP and Ag-GO/Fe_3O_4/PVDF-*co*-HFP was studied by SEM and TEM. Cross-sectional morphology was also viewed by SEM analysis. Chemical nature and functionalities of all the membranes were explored by FTIR spectra over a range of 500 to 4000cm^{-1}. XRD patterns of all the synthesized membranes were also explored to check the crystalline or amorphous nature of membranes. TGA was used to study the thermal stability of all the nanocomposite membranes. Membrane coupons were heated from 25 to 700°C and weight loss of each sample was noted accordingly. DSC study was done to check the glass transition temperature and melting temperature of the prepared membranes.

2.6 Membrane Performance Study

All the fabricated membranes were tested in terms of permeability, hydrophilicity and rejection by using different equations as discussed below.

2.6.1 Porosity and Water Contact Angle

Porosity (ε) of all the nanocomposite membranes was explored by using gravimetric analysis. Following equation was used to evaluate the porosity of membranes [145].

$$\varepsilon = \frac{w1 - w2}{A \times l \times \rho\text{-}w} \times 100 \ \ldots\ldots\ldots\ldots (1)$$

where, w2 and w1 are the weight of dry and wet membrane, l is the membrane thickness (m), A is active area of membrane (m^2) and $\rho w$is the density of water (0.998g/cm^3). Water contact angle is directly linked with hydrophobic or hydrophilic nature of composites. High contact angle refers to more hydrophobic character and less permeability of water. Water

contact angle of all the membranes was measured by using tensiometer KSV apparatus to check the effect of GO, GO-Ag, PEG-GO-Ag, GO/Fe_3O_4 and Ag-GO/Fe_3O_4 nanocomposites on hydrophilicity of polymer membranes.

2.6.2 Water Flux and BSA Rejection

Water permeability of all the unmodified and nanocomposite modified membranes was checked by undergoing water flux (Jw) measurement. Initially the membranes were compressed for 0.5h by applying 0.1MPa nitrogen gas pressure. Than the water flux (Jw1) was calculated by using following equation [146];

$$Jw1 = \frac{V}{A \times \Delta T} \times 100 \quad \ldots\ldots\ldots\ldots (2)$$

Where V is the permeated volume (L) of liquid, A is total area of membrane in m^2, and ΔT is time required for permeation. After 30min the feed was replaced by 0.5g/L BSA solution and BSA flux was noted using the above mentioned equation. BSA rejection was measured by employing UV spectroscopy to check the concentration of feed and permeate solution. Following formula was applied to calculate of BSA rejection [146].

$$\text{Rej} = 1 - \frac{Cp}{Cf} \times 100 \quad \ldots\ldots\ldots\ldots (3)$$

C_p and C_f are the concentrations of permeate and feed solution in mole/dm^{-3}.

2.6.3 Antifouling Ratio and Flux Recovery

Fouling resistance of all the fabricated membranes was explored by measuring the water flux and BSA flux of all the membranes. After measuring the BSA flux, the membranes were washed with distilled water for 0.5h to remove the adsorbed foulants and then water flux was noted again for another 0.5h to measure the flux recovery ratio. Total fouling ratio (Rt), reversible fouling ratio (Rir), irreversible fouling ratio (Rir) and flux recovery ratio (FRR) were calculated using following equations [147];

$$\text{Rt} = \frac{1 - Jp}{Jw1} \times 100\% \quad \ldots\ldots\ldots\ldots (4)$$

$$\text{Rr} = \frac{Jw2 - Jp}{Jw1} \times 100\% \quad \ldots\ldots\ldots\ldots (5)$$

$$\text{Rir} = \frac{Jw1 - Jw2}{Jw1} \times 100\% \quad \ldots\ldots\ldots\ldots (6)$$

$$\text{FRR} = \frac{Jw2}{Jw1} \times 100\% \quad \ldots\ldots\ldots\ldots (7)$$

Where J_{w1} is pure water flux, Jp is BSA protein flux and J_{w2} is water flux after washing the membrane.

2.6.4 Antibacterial Performance

Microbial resistance of GO and GO-Ag nanocomposites was studied against *Escherichia coli* (10^5cfu) strain. 1mg/ml of GO and GO-Ag nanocomposite solution was incubated with *E. coli* and SEM images were taken at different incubation times to compare the bactericidal properties of GO and GO-Ag.

2.6.5 Leaching Effect of GO and GO-Ag

The leaching effect of fabricated nanofillers from membranes was studied by using UV-visible spectroscopy. The fabricated PVC/GO 0.5 wt.% and PVC/GO-Ag 0.5 wt.% membranes were dipped in water and sonicated to check the stability of nanofillers. Membrane samples remain dipped for one week and UV spectra were recorded to study the leaching of nanofillers.

CHAPTER 3

RESULTS AND DISCUSSION

3.1. Influence of GO-Ag Nano-filler on the Antibacterial, Antifouling and Hydrophilic Characteristics of Polyvinyl Chloride Membrane

3.1.1. Characterization of GO and GO-Ag

3.1.1.1.XRD of GO and GO-Ag

Purity and crystallinity of GO and GO-Ag nanosheets was studied by XRD spectroscopy. XRD pattern of GO (**Figure 3.1 (a)**) shows a clear peak at 11.59 θ° while that of graphite at 26 θ° (**Figure 3.1 (b)**). XRD peak of GO in GO-Ag nanocomposite slightly shifts towards lower theta i.e. 10.39 θ° which suggested the strong intercalation of AgNPs between GO sheets [72]. This intercalation of AgNPs between stacked GO layers results in increased d-spacing of GO nanosheets. Increased d-spacing in GO-Ag nanosheets (8.5Å) as compared to GO nanosheets (7.6Å) depicts the excellent features of GO-Ag in terms of stability and dispersion. Besides this, the appearance of AgNPs peaks at 38.12 θ°, 64.40 θ° and 77.40 θ° confirms the successful functionalization of GO nanosheets.

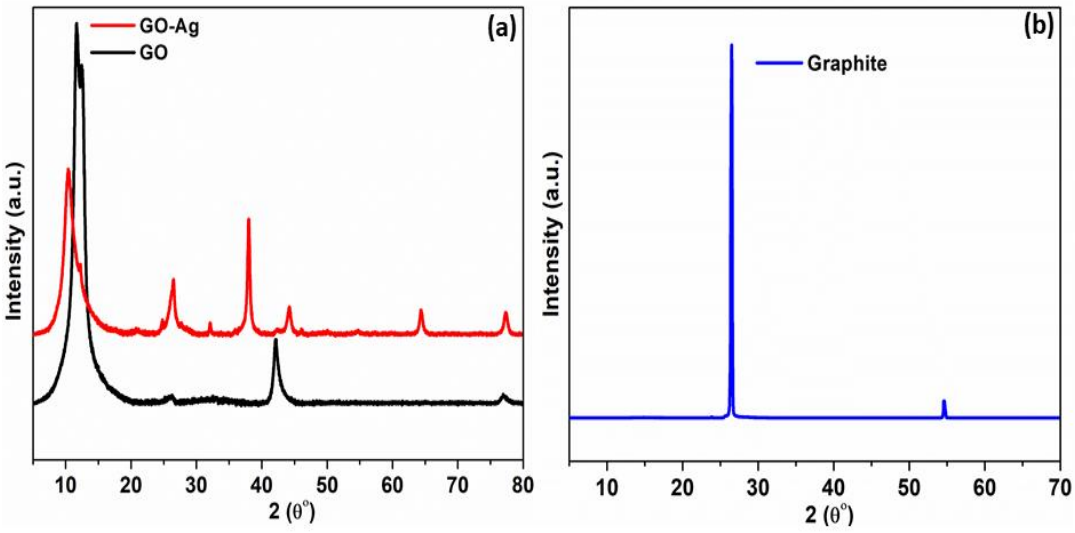

Figure 3.1. The XRD spectra of GO and GO-Ag (a), XRD of graphite (b)

3.1.1.2. SEM and TEM Analysis of GO and GO-Ag

In order to explore the morphological features of GO and GO-Ag nanocomposites, SEM and TEM analysis were performed. SEM and TEM images of GO (a,b) and GO-Ag (c,d) are represented in **Figure 3.2**. SEM micrograph of GO shows multilayer patterns of GO stacked upon each other. On the other hand, GO-Ag microstructure reveals unfolded sheets of GO. TEM images further clarify the uniform dispersion of GO-Ag nanosheets. TEM micrographs of GO-Ag manifest crumpled nanosheets of GO decorated with uniformly distributed AgNPs. SEM and TEM images proves that silver functionalization helps in better dispersion of GO nanosheets which results in increased d-spacing of GO patterns and unfurling of stacked GO sheets. Uniform distribution of AgNPs results in increase in specific surface area of AgNPs and hence increases their availability.

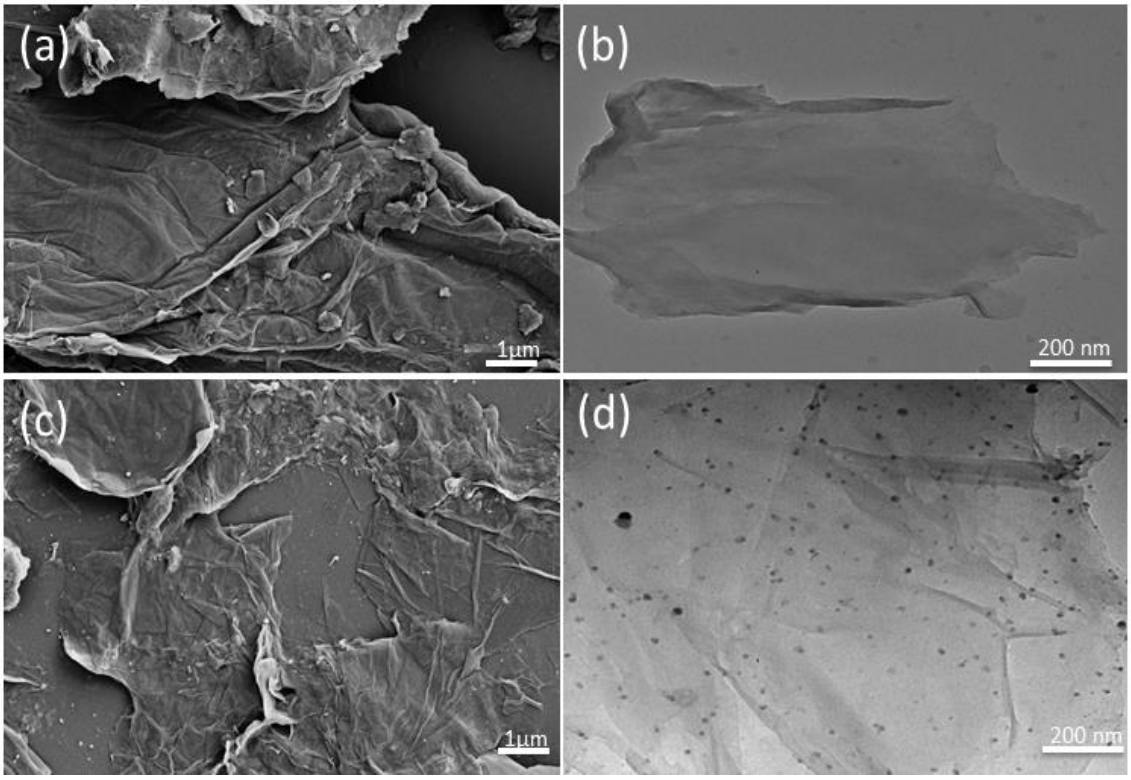

Figure 3.2. SEM and TEM images of (a & b) GO and (c & d) GO-Ag

3.1.1.3. FTIR Analysis of GO and GO-Ag

To investigate the functionalities of GO and GO-Ag nanocomposite FTIR spectra were recorded in the range of 4000 to 400 cm^{-1} as shown in **Figure 3.3**. Appearance of a clear hump at 3124 and 3147 cm^{-1} represents the presence of OH functional group in GO and GO-Ag. The peak at 1710 cm^{-1} and 1613 cm^{-1} in GO nanocomposite confirms the stretching vibration of C=O and C=C respectively. The peak at 1026 cm^{-1} deals with the epoxy stretching vibration of C-O. In case of GO-Ag nanocomposite a small shift in stretching vibrations of C=O and C=C was observed. This shift in peaks from 1710 to 1719 cm^{-1} and 1613 to 1570 cm^{-1} indicates the interaction of AgNPs with carbonyl and carboxyl moieties of GO nanosheets [148].

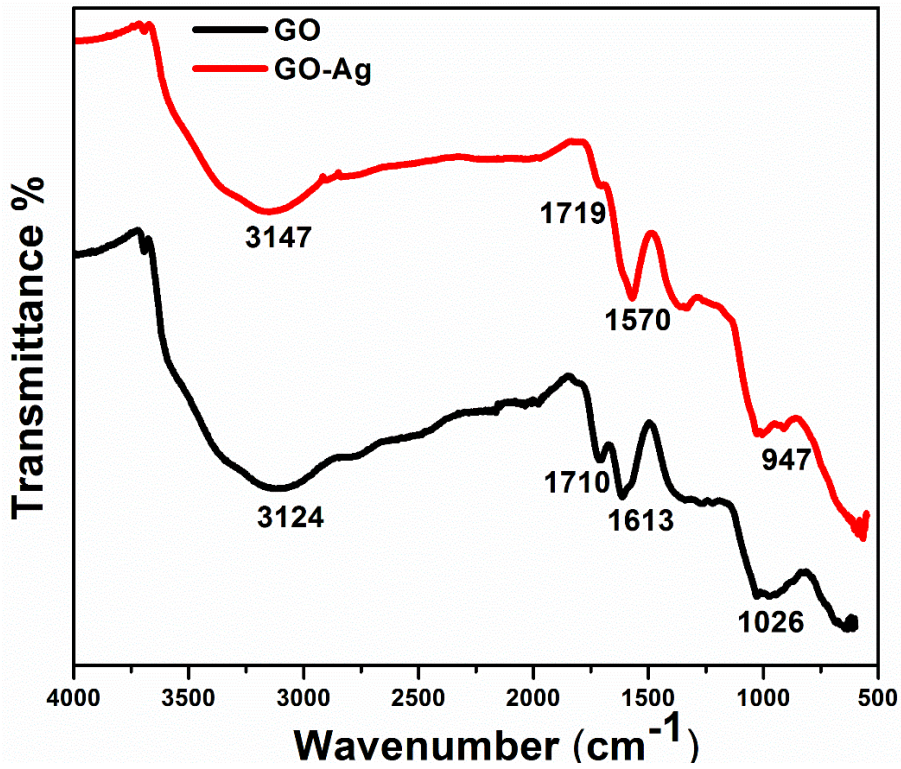

Figure 3.3. FTIR spectra of GO and GO-Ag

3.1.1.4. UV and Raman Analysis of GO and GO-Ag

Successful functionalization of GO by AgNPs was further explored by UV spectra. **Figure 3.4. A (a)** shows the UV spectra of GO and GO-Ag. In the UV spectra of GO two clear absorption peaks were observed due to n-pi and pi-pi transitions. In UV spectra of GO the absorption peaks at 214 nm and 236 nm represents the pi-pi and n-pi transitions of C=C and C=O functional groups. In GO-Ag nanocomposite the absorption peak at 390 nm indicates strong resonance of AgNPs. Furthermore, the Raman spectra of GO and GO-Ag **(Figure 3.4. A (b))** clarify the presence of sp^2 and sp^3 hybridized carbon atoms. The appearance of D and G bands in Raman spectral analysis of GO was due to the vibrations of $sp^3$and sp^2 carbon atoms. The drastic increase in intensities of D (1360 cm^{-1}) and G (1598 cm^{-1}) bands of GO in GO-Ag was attributed to the fast charge transfer mechanism due to silver functionalization of GO nanosheets [149, 150].

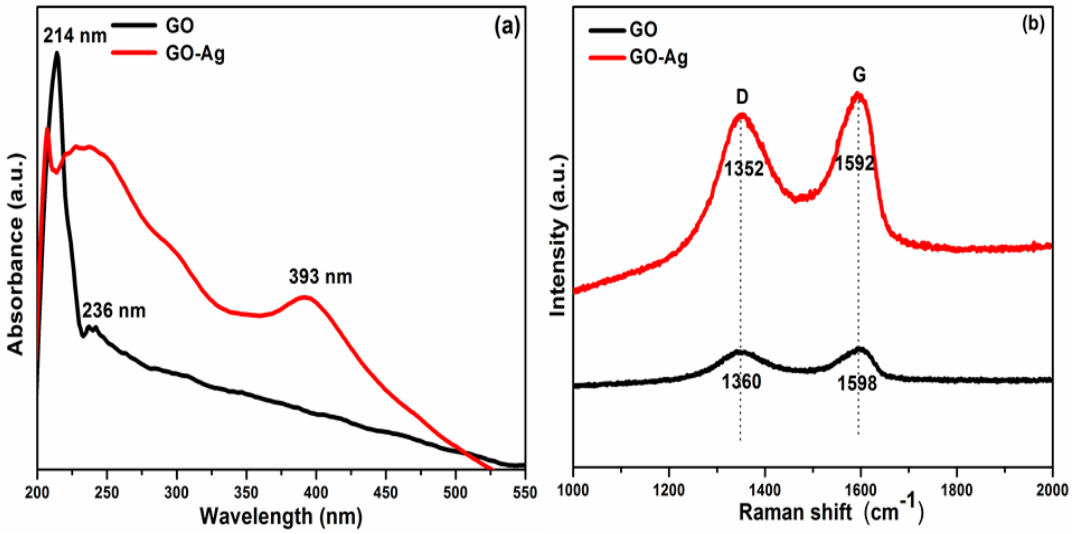

Figure 3.4. (A) UV spectra (a) and Raman spectra (b) of GO and GO-Ag

Surface charges of nanofillers play a crucial role in controlling the permeability and rejection of different molecules. Zeta potential gives a better estimation of surface charges of nanofillers. Zeta potential of freshly prepared GO and GO-Ag solutions (1 mg/mL) was measured three times for each sample (Figure 3.4. (B)). Increased surface charge of GO-Ag nanocomposite will result in increased hydrophilicity and high electro-static repulsion of BSA foulant.

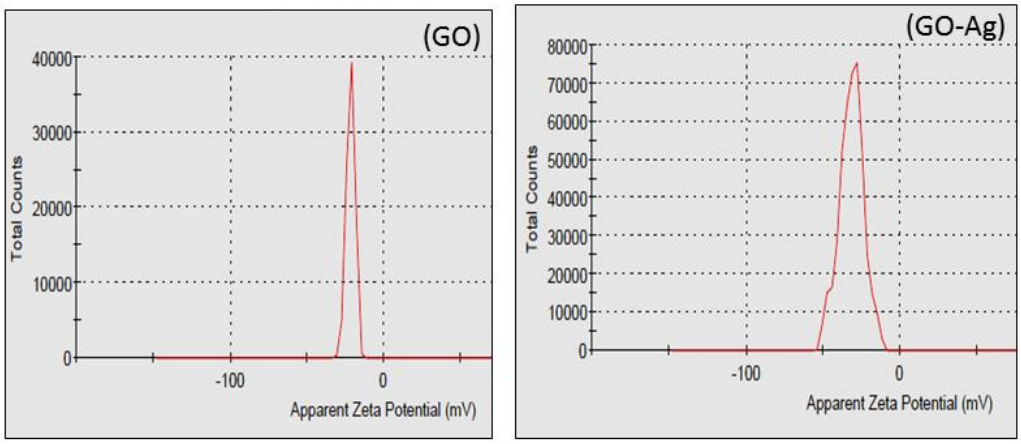

Figure 3.4. (B). Zeta potential of GO and GO-Ag nanoparticles

3.1.2. Characterization of Membranes

3.1.2.1. XRD of Membranes

XRD patterns of all the PVC membranes with and without addition of GO and GO-Ag are represented in **Figure 3.5**. XRD spectra of pure PVC membrane consist of a minute hump at 23.2 θ° which suggests the amorphous nature of PVC. The amorphous nature of pure PVC was supported by literature (Abdelghany, 2019) [151]. In GO and GO-Ag loaded membranes the characteristic peaks of GO and AgNPs merged together within the polymer matrix. XRD patterns of P/GO and P/GO-Ag membranes consist of a clear hump in the range 36 to 40 θ° as compared to PVC membrane. By increasing the GO-Ag content from 0.25 to 1 wt.% a small shift in position of hump towards higher theta value was observed. At a very high filler content i.e P/GO-Ag 1 wt%, the appearance of minute peaks at 12.8 θ° and 38.4 θ° was noticed, which can be attributed to the characteristic XRD peaks of GO and AgNPs.

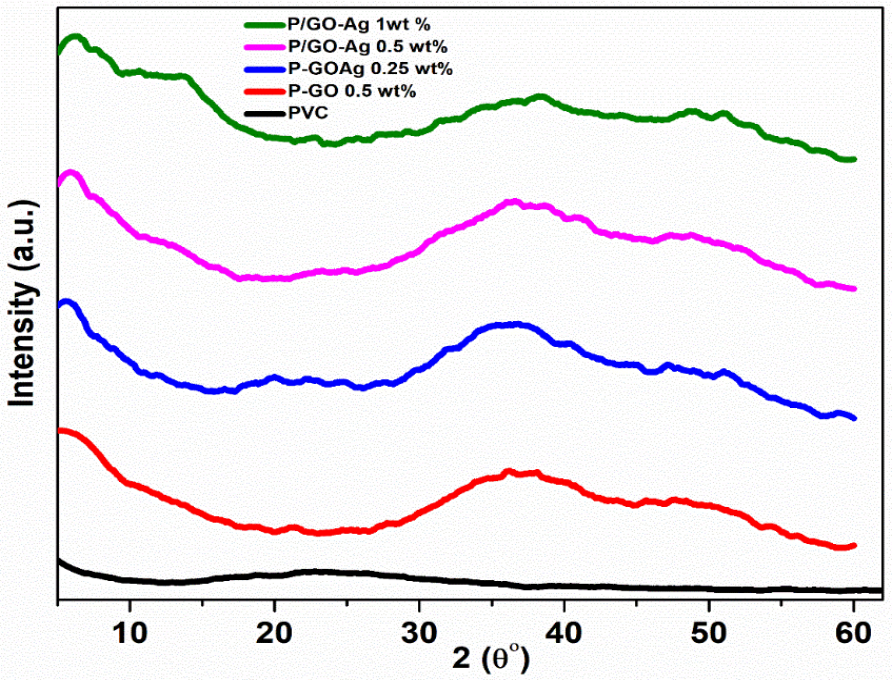

Figure 3.5. XRD patterns of the GO and GOAg based membranes

3.1.2.2. SEM Analysis of Membranes

Surface morphology of all the PVC membranes incorporated with GO and GO-Ag nanofiller was explored by SEM analysis. **Figure 3.6** Shows the SEM images of PVC, P/GO (0.5 wt.%) and P/GO-Ag (0.25, 0.5, 1 wt.%). The SEM image of pure PVC shows a very dense membrane surface. SEM micrographs of GO based PVC membrane shows the clusters of undispersed GO sheets. While GO-Ag based membranes depicts regular patterns of GO sheets dispersed throughout the PVC matrix. FESEM images of P/GO-Ag membranes prove that AgNPs helps in better dispersion of GO which results in well exfoliation of GO. However, at a very higher filler content (1 wt.%) the GO-Ag nanoparticles tends to agglomerate but this aggregation was much less as compared to un-functionalized GO. The particle size of agglomerated GO sheets clearly reduced in P/GO-Ag membranes which manifest strong intercalation of silver nanoparticles between GO sheets, resulting in increased interlayer spacing and better dispersion. Thickness of the fabricated membranes lies between 100 µm to 190 µm respectively. Thickness of pure PVC was 100 µm while that of P/GO-Ag (0.5 wt.%) membrane was 160 µm and P/GO-Ag (1 wt.%) membrane was 190 µm respectively.

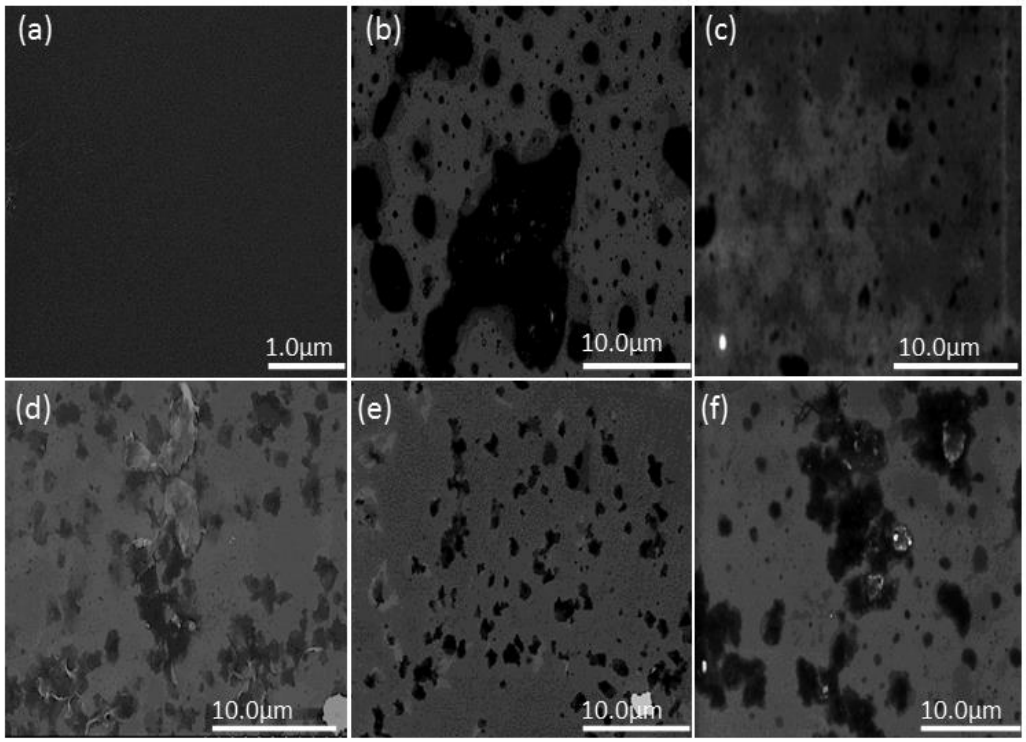

Figure 3.6. SEM images of (a) PVC and (b) P/GO 0.5 wt.%, (c) P/GO-Ag 0.25 wt.%, (d, e) P/GO-Ag 0.5 wt.% and (f) P/GO-Ag 1wt.%

Cross-sectional SEM images of PVC membrane with and without GO-Ag nanoadditive are represented in **Figure 3.7**. Cross-sectional SEM images of pure PVC membrane comprises of a dense skin layer while that of P/GO-Ag 0.5 wt.% membrane shows some finger like projections and micro voids throughout the membrane cross-section. Presence of a porous sub layer in addition to the surface skin layer in case of P/GO-Ag 0.5 wt.% membrane can be attributed to the interactions of GO-Ag nanosheets with PVC chains by covalent bonding, along with displacement of Cl atoms from PVC backbone, resulting in disordering the PVC chains and increasing the porous structures.

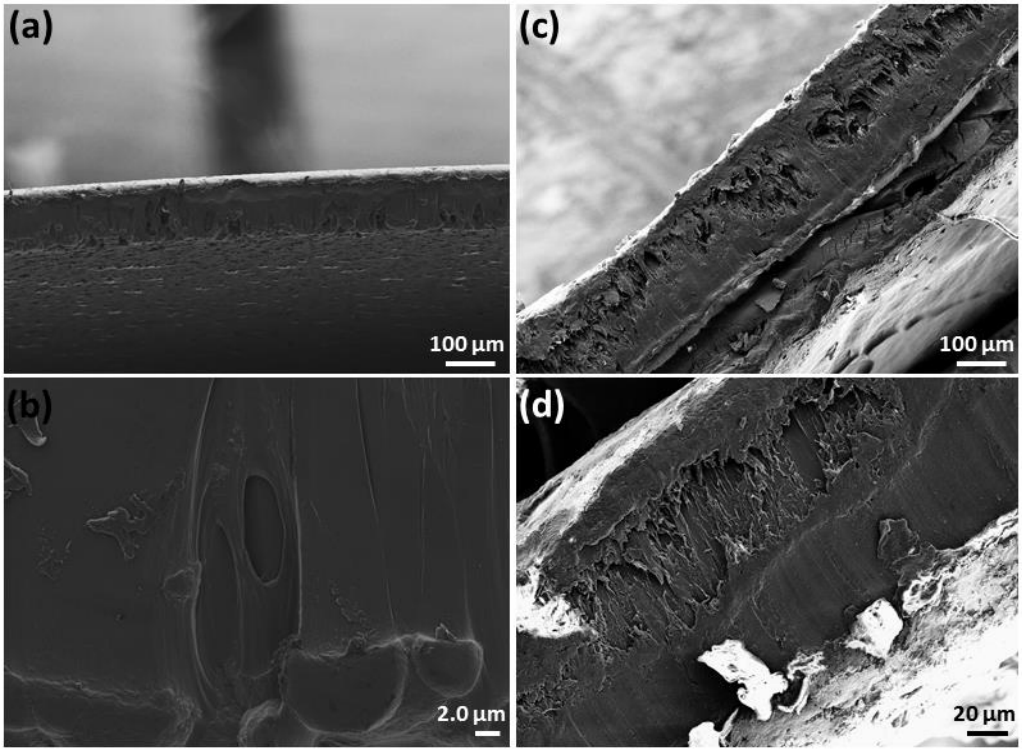

Figure 3.7. SEM images of (a,b) PVC and (c.d) P/GO-Ag 0.5 wt.% membrane

3.1.2.3. TEM Analysis of Membranes

Surface features of P/GO 0.5 wt.% and P/GO-Ag 0.5 wt.% were further investigated by TEM analysis as shown in **Figure 3.8**. TEM image of P/GO membrane was comprised of stacked GO sheets while that of P/GO-Ag TEM displays crumpled silk like patterns of unfolded GO-Ag sheets. **Figure 3.8** portrayed the uniformly decorated GO-Ag nanolayers throughout the polymer matrix resulting in increased surface roughness and hydrophilicity of P/GO-Ag membranes. The TEM images of P/GO-Ag at 200 nm resemble the TEM micrographs of pure GO-Ag nanoadditive which ensures the availability of GO-Ag nanofiller on the top of the membrane surface. The TEM micrographs of P/GO-Ag indicate that silver functionalization helps in preventing the stacking of GO sheets which results in decreased agglomeration of nanoadditives within the polymer matrix. These results suggest that P-GO-Ag nanocomposite comprises excellent features as compared to pristine PVC and P/GO membrane. SEM and TEM analysis validate that the surface properties of the PVC membranes are robustly influenced by incorporation of GO and GO-Ag nanocomposites. According to Hosseini et al, [152] the BET (Brunauer-Emmett-Teller)

surface area of PVC membrane was about 14.61 m^2/g. Another study of Zaheen Ullah et al. [153] reported that the BET surface area of PVC/GO membrane was 474.03 m^2/g. These studies illustrate that GO plays and important role in increasing the specific surface area of PVC membranes.

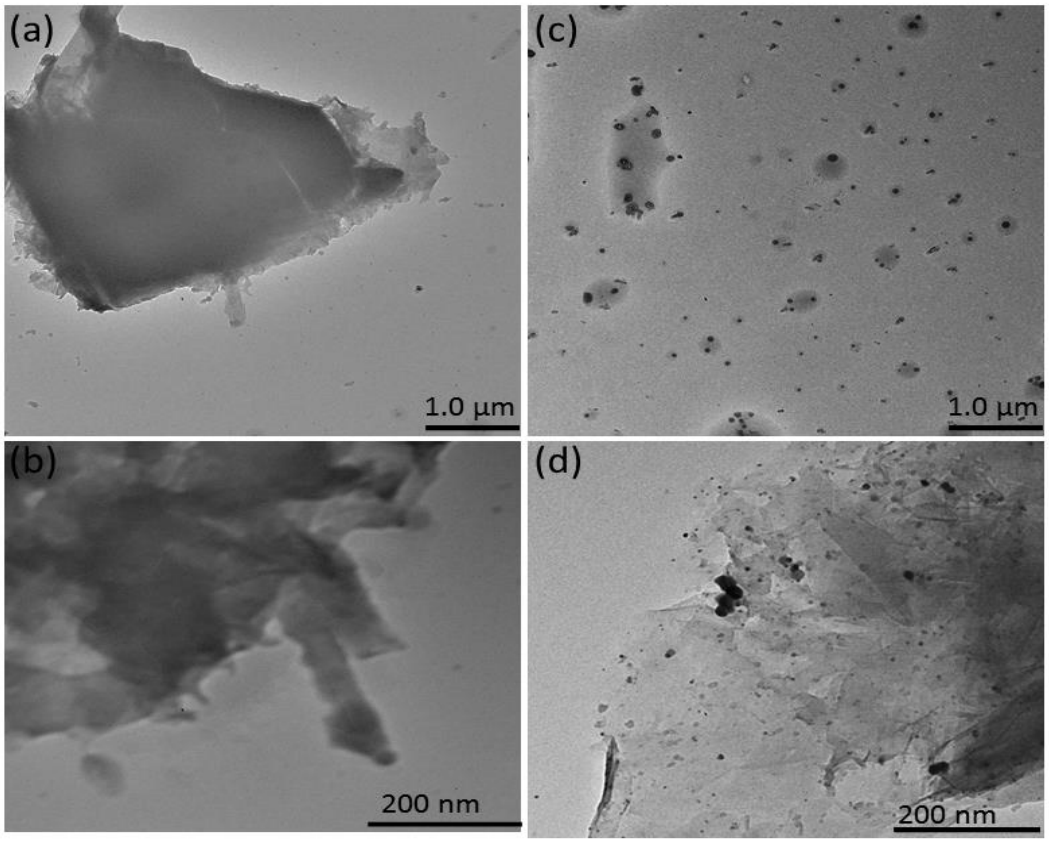

Figure 3.8. TEM images of (a,b) P/GO 0.5 wt.% and (c,d) P/GO-Ag 0.5 wt.%

3.1.2.4. FTIR Analysis of Membranes

Surface functionalities of the P/GO and P/GO-Ag membranes were explored through FTIR spectra as shown in **Figure 3.9**. A clear shift in peak from 1642 to 1715 cm^{-1} was observed in GO-Ag containing membranes which clarify the interaction of C=O moieties of GO with PVC resin. A slight shift in peak positions of C=O, C-O and C=C was observed in P/GO-Ag spectra as compare pure FTIR peaks of GO-Ag (**Figure 3.9**) which suggests the favourable interaction of PVC resin filtered through GO-Ag nanolayers.

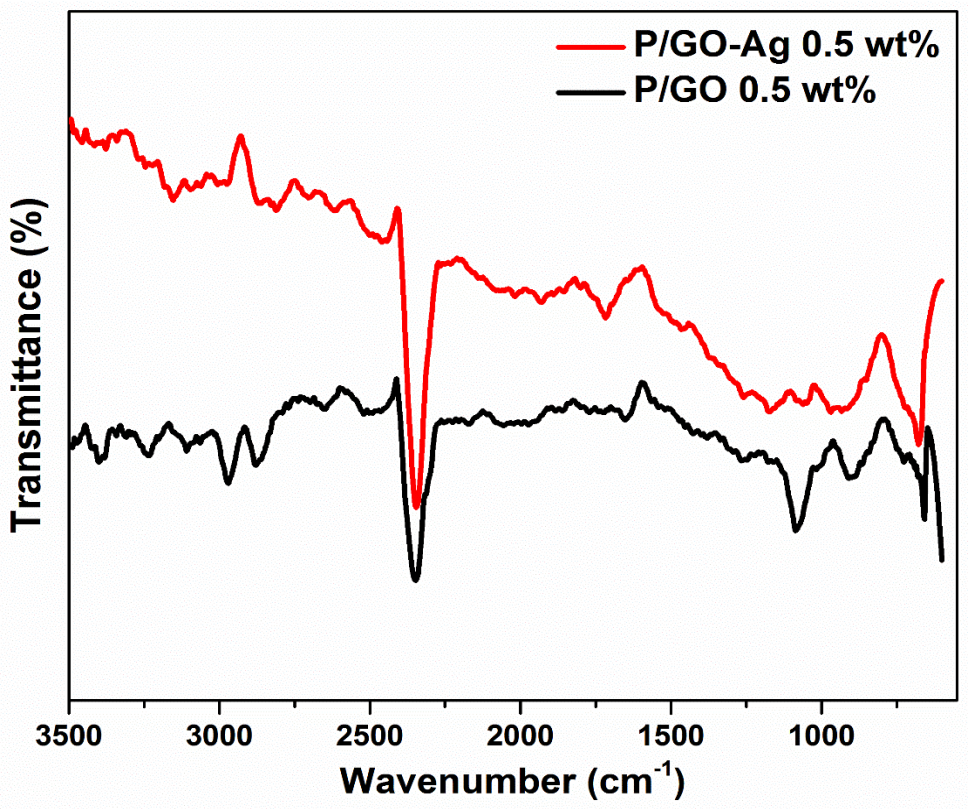

Figure 3.9. FTIR spectra of P/GO 0.5 wt.% and P/GO-Ag 0.5 wt.% membranes

3.1.2.5. Thermal and Mechanical Stability of Membranes

To investigate the thermal stability of fabricated membranes, all the membrane samples were heated from 25 °C to 700 °C in an inert atmosphere. A two-step degradation behavior was observed in TGA curves of all the membranes (**Figure 3.10 (a)).** TGA curve of pure PVC membrane shows first degradation step at 209 °C and degradation continuous up to 370 °C. This degradation mainly corresponds to the elimination of small molecules like HCl. At this stage the Cl-radical formed from cleavage of C-Cl bond withdraws H^+ from the nearby C-H bond and results in HCl evolution. A major weight loss of the PVC membrane occurs involving dislocation of all the Cl atoms and leaving behind polyene backbone [154]. No weight loss was observed from 370 °C to 446 °C, which suggests the stability of polymer backbone in this region. Another minor weight loss was noted in the temp range of 446 °C to 508 °C. In case of P/GO 0.5 wt.% membrane the first degradation

temperature increases up to 249 °C while for P-GOAg 0.5 wt.% membrane initial degradation starts at 263 °C. This increase in degradation temperature corresponds to the strong interaction of GO-Ag nanosheets with C-Cl bonds of PVC matrix. A total weight loss of 98 % was obtained for pure PVC membrane and for P/GO and P/GO-Ag 0.5 wt.% membrane the weight loss decreases to 86.72 % and 45.62 % respectively. TGA curves of P/GO-Ag 1 wt.% membrane shows a weight loss of 80.02 % which indicates the aggregation of nanofiller at high filler content. Such aggregations weaken the polymer-GO interaction and results in poor stability of membranes. So the thermal stability of all the modified membranes increases appreciably up to 0.5 wt.% filler content and decreases again on further increase in filler content.

Thermal stability of PVC and P/GO and P/GO-Ag based membranes was further explored by DSC analysis (**Figure 3.10 b**). Membrane coupons were heating from 25 to 300 °C at the rate of 10° per minute and then cooled back to room temperature. Glass transition temperature (Tg) of all the modified PVC membranes was found to be increased as compare to pure PVC. Tg of the pure membrane was 55.27 °C and increased to 64.5 °C by the addition of 1 wt.% GO-Ag nanocomposite.

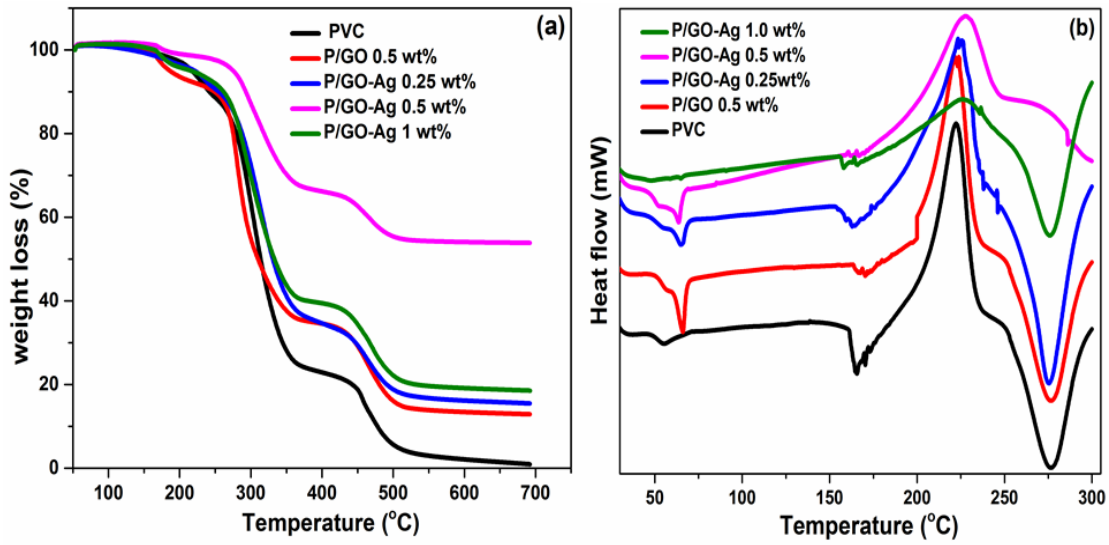

Figure 3.10. TGA (a) and DSC (b) curves of all membranes

As the glass transition temperature depends on the mobility of polymer molecules, addition of nanofillers like GO and GO-Ag increases the compactness of polymer chains and Tg shifts to the higher temperature. Moreover, the crystallization temperature (Tcrys) and melting temperature of the GO-Ag modified PVC membranes also increases. Tcrys of pure PVC was noted by an exothermic curve at 222 °C while that of P/GO-Ag 0.5 wt.% was at 228 °C. Unmodified PVC membrane shows an endothermic melting curve at 276 °C while P/GO-Ag 0.5 wt.% membrane undergoes melting at 286 °C. So the increase in Tg, Tcrys and Tm represents the strong intercalation of GO and GO-Ag nanosheets within the polymer chains resulting in increased thermal stability. As reported in literature [155, 156], introduction of highly functional nanosheets in polymer resin limits the chain mobility of host polymer and hence changes the Tg, Tcrys and Tm subsequently.

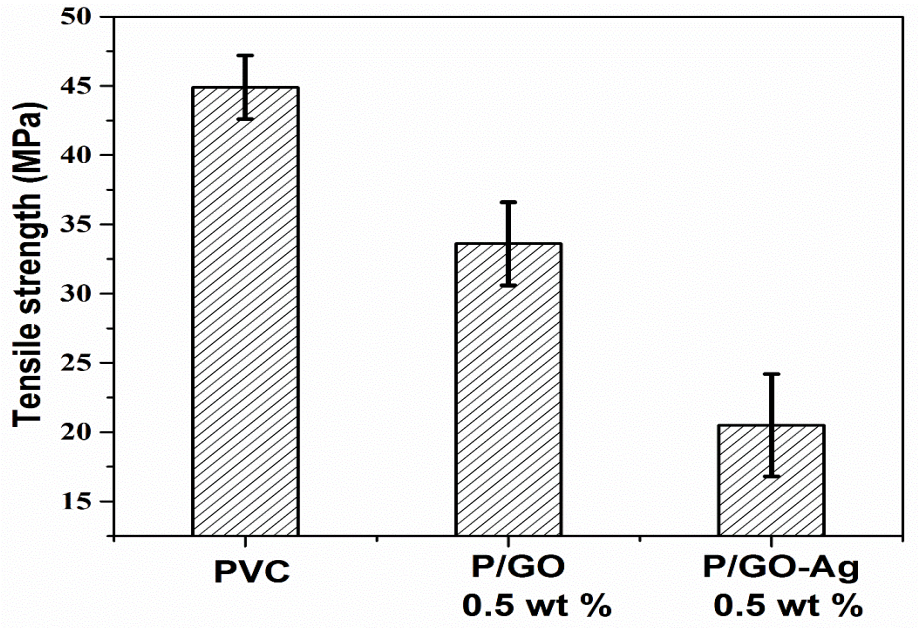

Figure 3.11. Tensile strength of fabricated membranes

Mechanical stability of pristine PVC, P/GO 0.5 wt.% and P/GO-Ag 0.5 wt.% membranes was monitored by tensile testing and reported in **Figure 3.11**. Tensile strength of PVC membrane was noted as 44.9 MPa while that of P/GO 0.5 wt% and P/GO-Ag 0.5 wt% membrane was 33.6 MPa and 20.5 MPa respectively. This decrease in tensile strength insinuate the increased porosity of GO and GOAg based membranes. The presence of large number of microporous cavities and high porosity as observed in **Figure 3.7 (c,d)** are the main reasons behind decreased tensile strength of GO-Ag based membranes [145].

3.1.2.6. Water Contact Angle and Porosity of Membranes

Porosity and water contact angle are the two main features in controlling the membrane performance. Although in general, a highly porous membrane corresponds to excellent water permeation but in many cases all the pores are not equally available for reaction. Aggregation of nanocomposites may result in pore blocking and hence decreases their availability. Porosity of all the GO-Ag based membranes (**Figure 3.12 (a)**) was found to be increased as compared to pure PVC and GO based PVC membrane. Porosity of PVC membrane was 62.6 % while that of 0.5 wt.% P/GO-Ag was 82 % respectively. Further increase in filler content decreases the membrane porosity. These results are in good

agreement with SEM micrographs of membranes and shows that P/GO-Ag 0.5 wt.% membrane was best in terms of increased porosity and excellent dispersion of nanofiller. In case of 1 wt.% P/GO-Ag membrane, the GO sheets tends to agglomerate which results in congestion of water channels and pore blockage.

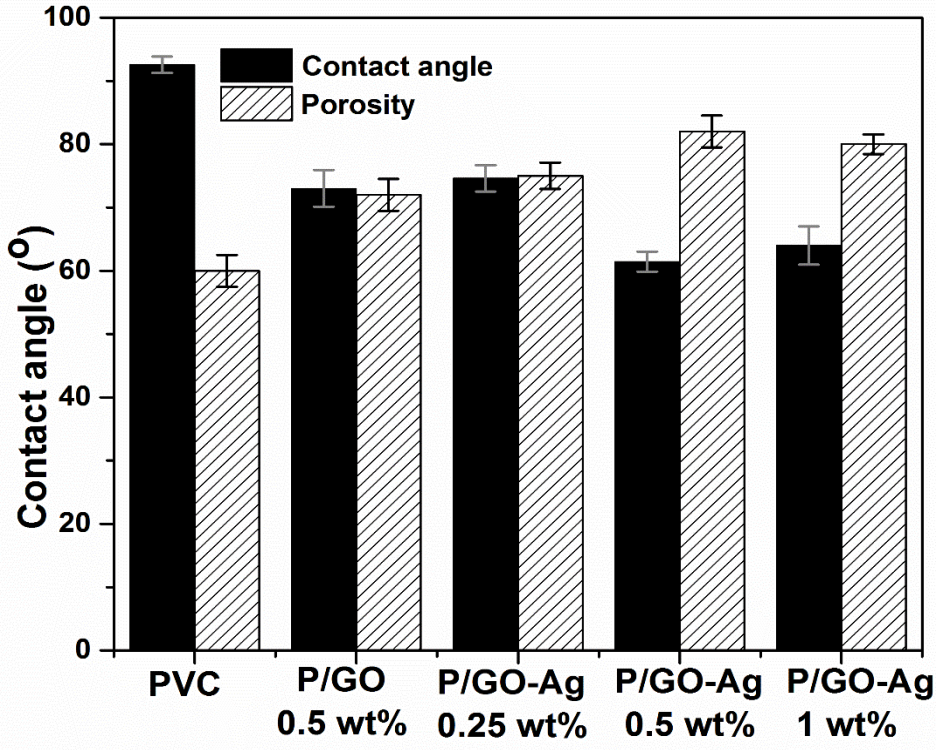

Figure 3.12. (a). Porosity and Contact angle of all fabricated membranes

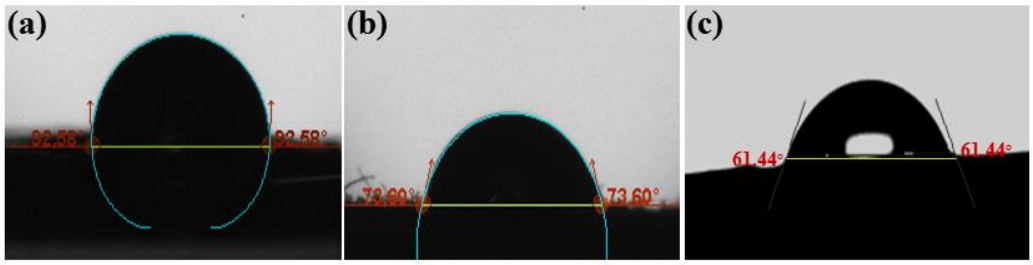

Figure 3.12 (b). Contact angle images of (a) PVC and (b) P/GO 0.5 wt.%, (c) P/GO-Ag 0.5 wt.%

Hydrophilicity test of PVC membranes was carried out by measuring the static water contact angle on all the membrane surfaces. Contact angle is a surface property and linked primarily with the quantity and quality of nanoadditives dispersed in polymer matrix as well as with surface roughness of membrane. Addition of hydrophilic nanocomposites results in increased hydrophilic character of PVC membranes [157, 158]. Water contact angle of pristine PVC and all the modified membranes are listed in Figure 3.12. (a), while **Figure 3.12 (b)**. represents the water contact angle images of PVC, P/GO 0.5 wt.% and P/GO-Ag 0.5 wt.% membrane respectively. The unique infiltration approach of PVC resin through the GO and GO-Ag nanosheets results in availability of GO nanosheets on the membrane surface (as confirmed from TEM images of membrane **Figure 3.8**) and decreases the water contact angle of P/GO-Ag based membranes by increasing the surface roughness of membranes. Water contact angle of pristine PVC decreases from 92° to 73° for P/GO 0.5 wt.% and 61° for P/GO-Ag 0.5 wt.% membrane. However, in case of P/GO-Ag 1 wt.% nanocomposite the water contact angle was found to increase up to 64° which corresponds to the aggregation of GO-Ag nanolayers at high filler content, resulting in poor hydrophilicity. These results of decreased contact angle of P/GO-Ag based membranes indicating an increased surface roughness of membrane are consistent with the literature [159]. Ahmed Sari et al. [160] reported a consistent decrease in water contact angle with increased surface roughness, entailing an increased hydrophilic character to the membrane surface.

3.1.3. Membrane Performance

3.1.3.1. Water flux and BSA Rejection of Membranes

Pure water flux (Jw) and BSA flux (Jp) of all the membranes was evaluated and shown in **Figure 3.13 (a)**. Addition of water friendly nanocomposites to the PVC matrix leads to the successful tuning of membranes properties. Water flux of all the modified membranes was found to be increased as compare to pure PVC membrane. Water flux for PVC membrane was 192 $Lm^{-2}h^{-1}$ while that of P/GOAg 0.5 wt.% was 613 $Lm^{-2}h^{-1}$, which gives an increase of 219 %. Water flux was found to increase linearly with the increase of GO-Ag content

up to 0.5 wt.% but a further increase in GO-Ag wt.% leads to the reduction of water transport through the P/GO-Ag channels. At a very high filler content i.e. 1 wt.% P/GO-Ag, the aggregation increases, resulting in pores clogging and decreasing the water permeation. In P/GO 0.5 wt.% and P/GO-Ag 0.5 wt.% membrane water flux increases by 1.9 folds and 3.2 folds in comparison with pure PVC membrane. The P/GO-Ag 0.5 wt.% was noticed to be the best membrane in terms of higher water flux and increased hydrophilicity. These results support the earlier results of SEM, porosity and contact angle as all these analysis depicts that for 1 wt.% membrane aggregation effect surmounts and results in malfunctioning of membrane.

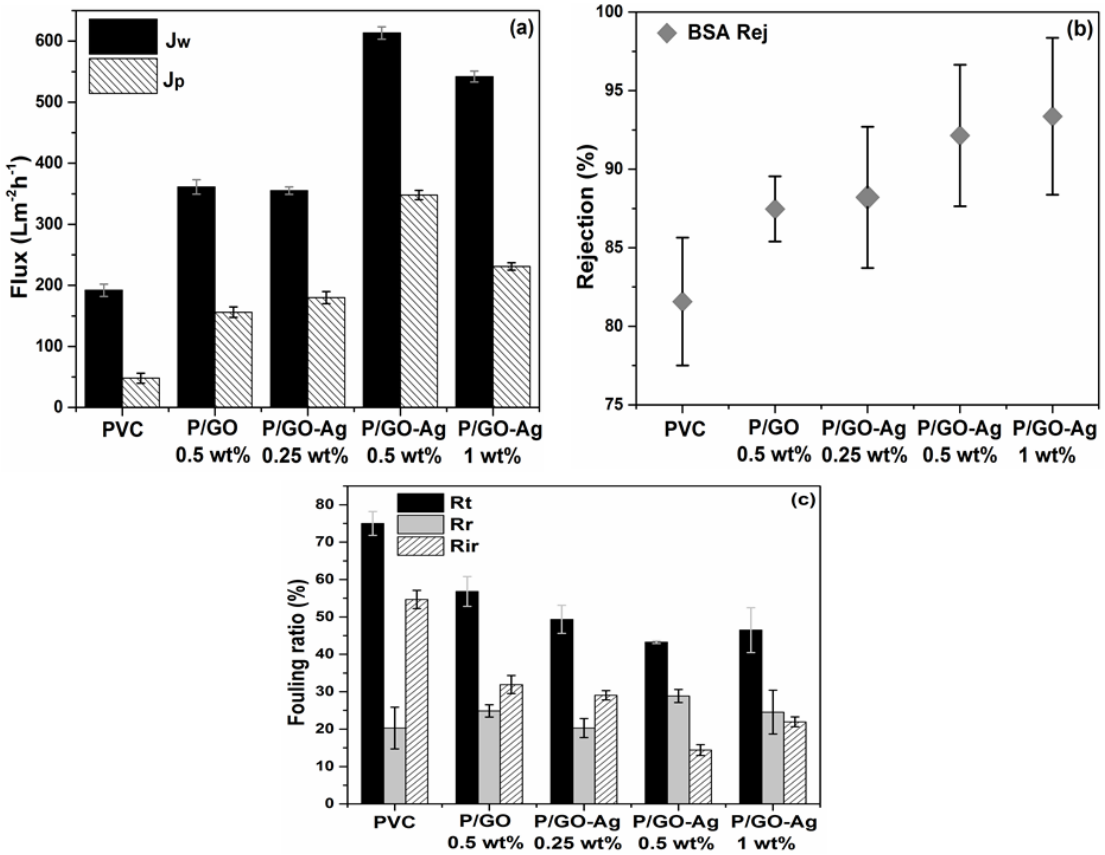

Figure 3.13. (a) Water flux (Jw), BSA protein flux (Jp), (b) BSA rejection and (c) total fouling (Rt), reversible fouling (Rr) and irreversible fouling (Rir) ratio of membranes

In order to assess the BSA rejection of PVC membranes the pure water was replaced with BSA feed solution. By changing the feed water with BSA protein solution, the flux of P/GO-Ag 0.5 wt.% membrane decreases to 348 $Lm^{-2}h^{-1}$. Decline in BSA flux was attributed to the surface adsorption of BSA foulants, resulting in blocking of water channels and hence lowering the permeability. The BSA flux decreases drastically for pure PVC membrane, which corresponds to the highly hydrophobic nature of PVC resulting in adsorption of BSA molecules on the membrane surface as shown **Figure 3.13**. Increased water permeation as well as high BSA rejection can be attributed to the combined effect of H-bonding as well as electrostatic forces on the membrane surface and interface. In case of P/GO-Ag based membrane, formation of a dense water layer on the membrane surface, repels the hydrophobic BSA molecules and increases their rejection.

Although the BSA flux of all the membranes decreases with time but this decrease was slightly low in case of P/GO-Ag based membranes. BSA molecules are negatively charged at pH 7, an increase in membrane surface charge increases the electrostatic repulsion between BSA and membrane surface resulting in decreased BSA adsorption [161]. BSA rejection for PVC membrane was 81.5 % while that of P/GO 0.5 wt.% and P/GO-Ag 0.5 wt.% was 87% and 92.1% as shown in **Figure 3.13 (b)**. In contradiction with water flux the BSA rejection of 1 wt.% P/GO-Ag membrane increases significantly (93.3%). This increase in BSA rejection was supported from literature. High filler content may induce pore blocking and decreases the permeability but it provides increased active surface for adsorption of BSA molecules within the stacked layers of GO [161].

3.1.3.2. Antifouling Efficiency of Membranes

Antifouling efficiency of a filtration membrane is closely associated with its hydrophobic or hydrophilic property. Microorganisms and Proteins (BSA) are considered as main pollutants causing membrane fouling. These pollutants badly affect the membrane performance by setting down on the surface of membranes or inside the pores. However, availability of hydrophilic surfaces on the top layer of membrane could hinder the protein adsorption by forming a water layer on the membrane surface (**Scheme 3.1**) [162].

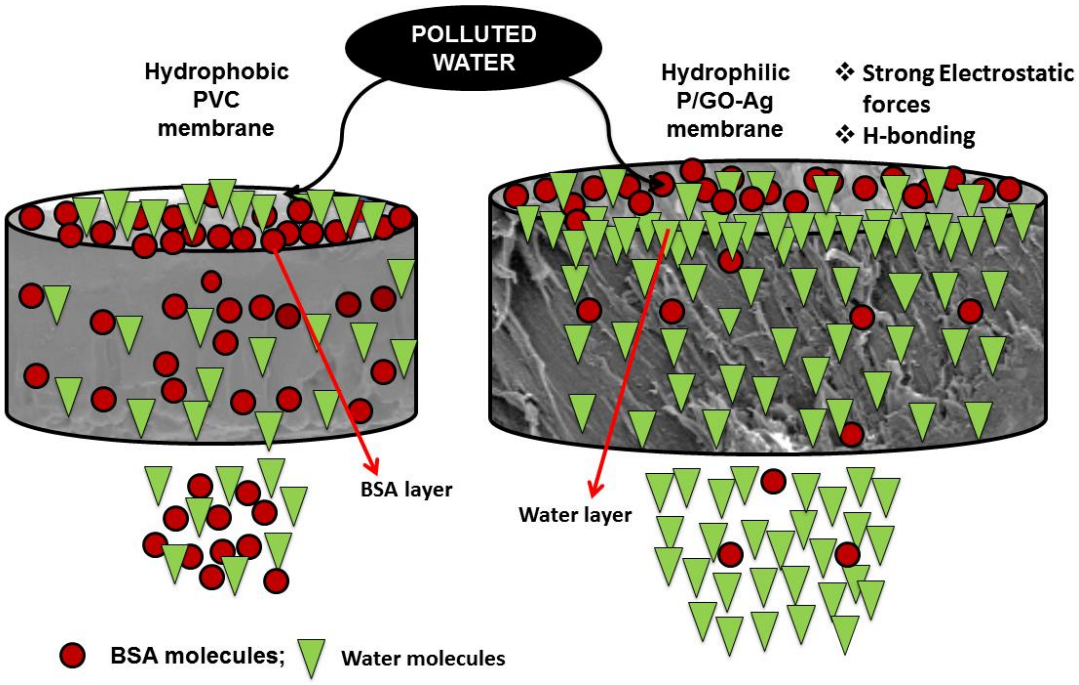

Scheme 3.1. Schematic representation of water and BSA filtration from PVC membrane and P/GO-Ag 0.5 wt% membrane

Synergistic effects of GO and AgNPs excels the hydrophilicity of P/GO-Ag membrane. Fouling ratios of all the fabricated membranes are shown in **Figure 3.13 (c)**. Among all the fabricated membranes, highest total fouling ratio and highest irreversible fouling ratio was noticed in case of PVC membrane i.e. 74.9 % and 54.6 %. Fouling ratio decreases to 56 % by the addition of 0.5 wt.% P/GO, and decreases to lowest value of 43.23 % for P/GO-Ag 0.5 wt.% membrane. Temporary fouling can be reversed by back flushing or washing the membrane with distilled water. Permanent blocking of pores by adhesion of membrane foulants results in irreversible membrane fouling and decreases the efficiency and life spain of membrane filters. These results indicate that GO-Ag nanofiller plays an essential role in decreasing the membrane fouling and hence increases the water transport through the modified membranes.

3.1.3.3. Flux Recovery Ratio of Membranes

After sequential filtration of water and BSA solutions through the membranes, all the membranes were washed with water for 30 min and water flux was measured again to estimate the flux recovery ratio of membranes. FRR of all the fabricated membranes are shown in **Figure 3.14 (a)**. Irreversible fouling of membranes either by adsorption of BSA on the surface or by pore blocking results in poor flux recovery. FRR was highest for P/GO-Ag 0.5 wt.% membrane (85.6 %) and lowest for PVC membrane (45.3 %). P/GO 0.5 wt.% membrane exhibit 68.1 % FRR while that of P/GO-Ag 0.25 wt.% shows FRR of 70.9 %. These results revealed the appreciable hydrophilic features of GO-Ag in tailoring the surface properties of PVC membranes. BSA molecules are hydrophobic in nature and availability of highly hydrophilic GO-Ag nanosheets on the membrane surface helps in controlling the BSA adsorption on membranes.

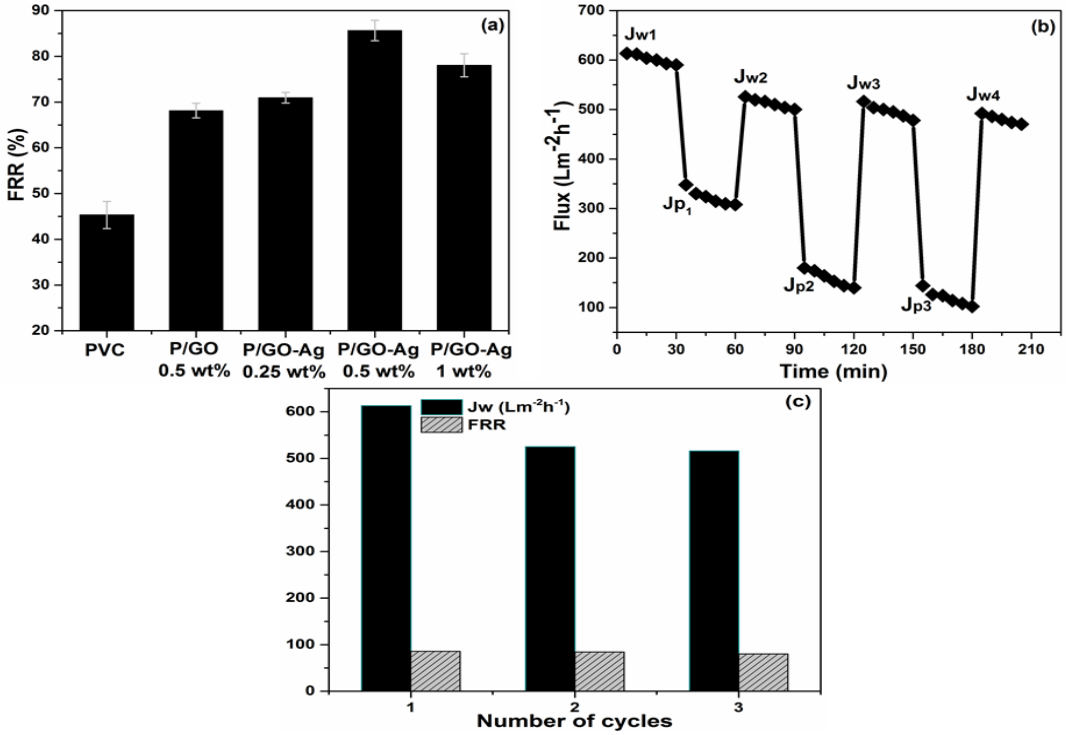

Figure 3.14. (a) FRR of all fabricated membranes, (b) cyclic filtration of P/GO-Ag 0.5 wt.% membrane and (c) Jw and FRR of P/GO-Ag 0.5 wt.% membrane

3.1.3.4. Cyclic Filtration

Due to high risks of polymer membrane foiling, the re-usability of polymer membranes is quite challenging. Among all the PVC/GO-Ag based membranes, P/GO-Ag 0.5 wt% showed the best performance in terms of permeability and rejection. In order to check the reusability of P/GO-Ag 0.5 wt.% membrane four successive cycles of water permeation were designed. Cyclic flux and FRR of P/GO-Ag 0.5 wt.% membrane was shown in **Figure 3.14 (b,c)**. Water and BSA permeation was noted over a period of 3.5 h. After initial compaction of membrane, Jw1 was noted every 5 min up to 0.5 h, after that BSA permeation flux (Jp) was noted in the same way for next 0.5 h. BSA flux was found to decrease appreciably, suggesting the adsorption of BSA molecules within the nanochannels of GO. The fouled membrane was washed with distilled water for another 0.5 h and then Jw2 was measured to figure out the flux recovery ratio. The same sequence of water and BSA filtration followed by membrane washing was repeated for 3.5 h. Jw1, Jw2, Jw3 and FRR for cyclic flux were calculated by using the equation (1) and (7) (as explained in section 2.1.6.1 and 2.1.7.2) respectively. Water flux of P/GO-Ag 0.5 wt.% membrane for three filtration cycles was 613 $Lm^{-2}h^{-1}$, 525 $Lm^{-2}h^{-1}$ and 517 $Lm^{-2}h^{-1}$. Flux recovery ratio of P/GO-Ag 0.5 wt.% membrane was 85.64 %, 84.17 % and 80.26 %, which reveals high stability and reusability of P/GO-Ag 0.5 wt.% membrane.

3.1.3.5. Leaching Effect of GO and GO-Ag

Rapid release of nanoparticles from the membrane matrix can affect the durability and performance of a membrane filter. Leaching of GO and AgNPs from the fabricated PVC membranes was monitored by UV-spectroscopy (**Figure 3.15**). The fabricated P/GO 0.5 wt.% and P/GO-Ag 0.5 wt.% membranes were dipped in 50 ml distilled water and sonicated by bath sonication for 1h. The UV-spectra reveals the stability of both GO and AgNPs as no any peak was observed in the range of 200 to 450 nm after 1h sonication.

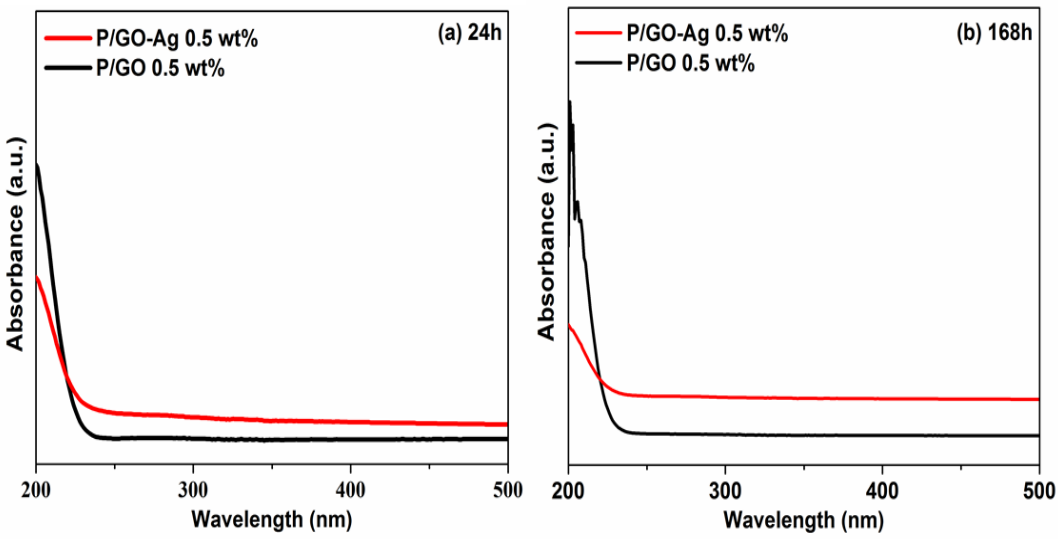

Figure 3.15. UV spectra of silver nanoparticles leaching (a) after 24h (b) 168h

The membranes were remain dipped in water and UV spectra was noted again after 24h (1day) and 168h (1week). The UV spectra of both samples after 24h justify the stability of GO-Ag. However, a long term interaction with water results in negligible leaching of GO from P/GO 0.5 wt.%, but the P/GO-Ag 0.5 wt.% membrane still persists its stability (**Figure 3.15**). The infiltration of PVC resin through the GO-Ag nanolayers results in immobilization of silver nanoparticles on GO surfaces which hinders the leaching of silver nanoparticles and increases the stability of P/GO-Ag membranes. Li Jingchun et al. [163] studied that GO helps in controlling the release of AgNPs from polymer membranes by providing large number of anchoring sites in terms of functional groups. Saranya et al. [164] also supports the negligible leaching of GO-Ag nanofiller and confirms the stability of GO-Ag. Besides this, cyclic filtration of water and BSA solutions also depicts the stability of GO-Ag based membranes.

3.1.3.6. Antibacterial Features

Another big issue associated with membrane filtration is formation of biofilm or cake layer on polymer membrane due to accumulation of microorganisms on the membrane surface. Using antibacterial nanoparticles to reduce the chances of biofilm formation is an effective strategy to enhance membrane performance [165]. In order to assess the antibacterial properties of synthesized GO and GO-Ag nanocomposites, a gram negative bacteria

Escherichia Coli was chosen as biofoulant. Usually gram negative bacteria are considered to be more resistant to antibiotics due to their compact cell wall as compared to gram positive bacteria. So if a substance is resistant to gram negative bacteria it would also be effective to gram positive bacteria [31].

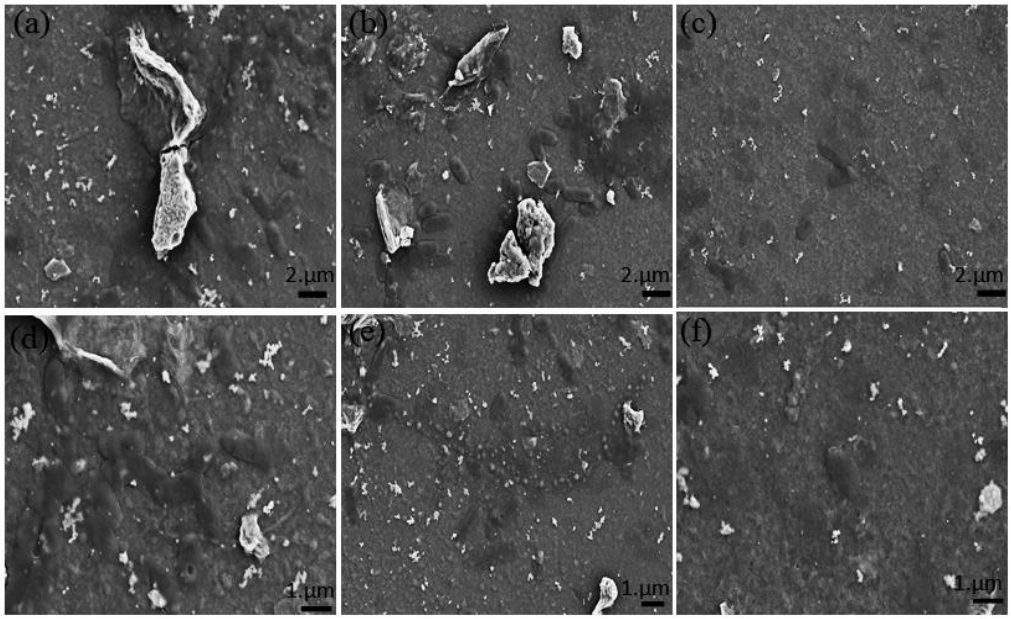

Figure 3.16. SEM images of antibacterial tests of GO (a,b,c) and GO-Ag (d,e,f) nanocomposites at 0.5h (a,d), 3h (b,e) and 6h (c,f) incubation

In order to explore the antibacterial features of GO and GO-Ag nano-composites *E. coli* culture (10^5cfu) was incubated with freshly prepared 1 mg/mL GO and GO-Ag nanocomposite. SEM micrographs of both samples were recorded after 0.5 h, 3 h and 6 h incubation. **Figure 3.16** represents the SEM micrographs of GO and GO-Ag nanocomposites incubated with *E. coli* culture at different incubation time. SEM images of GO and GO-Ag nanocomposite manifest the minimal adhesion of *E. coli* on the surface of GO nanosheets. SEM micrographs of GO nanocomposite at 3 h incubation comprises a large number of E. coli cells, while in case of GO-Ag nanocomposite the number of E. coli cells decreases appreciably. This decrease in *E. coli* cells suggest the interaction of Ag nanoparticles with the *E. coli* cell wall resulting in rupturing of cell wall and killing of *E. coli* cells. After 6 h incubation only two *E. coli* cells diffused in GO-Ag nanocomposite were viewed through SEM as shown in **Figure 3.16 (f)**. These results manifest the

effectiveness of GO-Ag nanocomposite in controlling bacterial growth. So the intercalation of GO-Ag nanocomposite in PVC membranes can successfully assist in minimizing microbial fouling of membranes.

3.1.4. Proposed Interactions Between PVC/GO-Ag and H_2O Molecules

In the PVC/GO-Ag membranes polar groups of graphene oxide may interact with Cl groups of PVC resulting in disordered PVC chains. These interactions result in increased roughness and porosity of membranes. On the other hand, polar groups of GO interact with external water molecules resulting in H-bonding. In P-GOAg membranes a covalent bond exists between C-C atoms of PVC and GO. **Scheme 3.2** represent the possible interaction between PVC and GO-Ag sheets as well as with water molecules. Presence of strong H-bonding and high polarity increases the hydrophilicity and permeability of P/GO-Ag membranes.

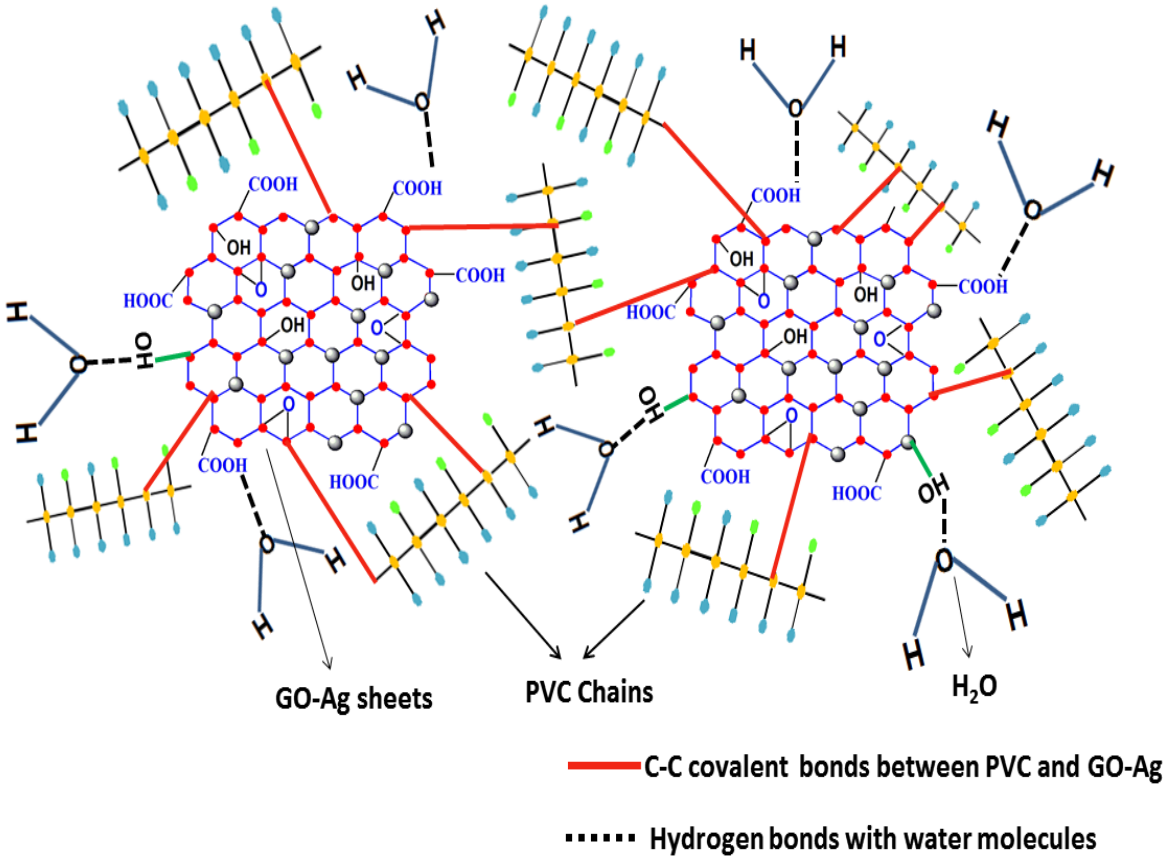

Scheme 3.2. Proposed mechanism of interaction between PVC chains, GO-Ag nanosheets and water molecules

3.2. PEG Functionalized Graphene Oxide-silver Nano-additive for Enhanced Hydrophilicity, Permeability and Fouling Resistance Properties of PVDF-*co*-HFP Membranes

3.2.1. Characterization of PEG-GO-Ag Nano-additive

3.2.1.1. SEM and EDX Analysis of PEG-GO-Ag Nano-additive

Surface morphology of PEG functionalized and non-functionalized GO-Ag nano-additive was observed by SEM imaging (**Figure 3.17 (a-d**)). SEM images of non-functionalized GO shows AgNPs decorated uneven distribution of large GO flakes. Functionalization of GO-Ag with PEG resulted in highly exfoliated and transparent sheets of GO as seen in SEM images. Further, crumpled silk like patterns of PEGylated GO layers were also observed in PEG-GO-Ag nano-additive images, which render the homogeneity and smoothening effect of PEG chains (**Figure 3.17 (c-d)**).

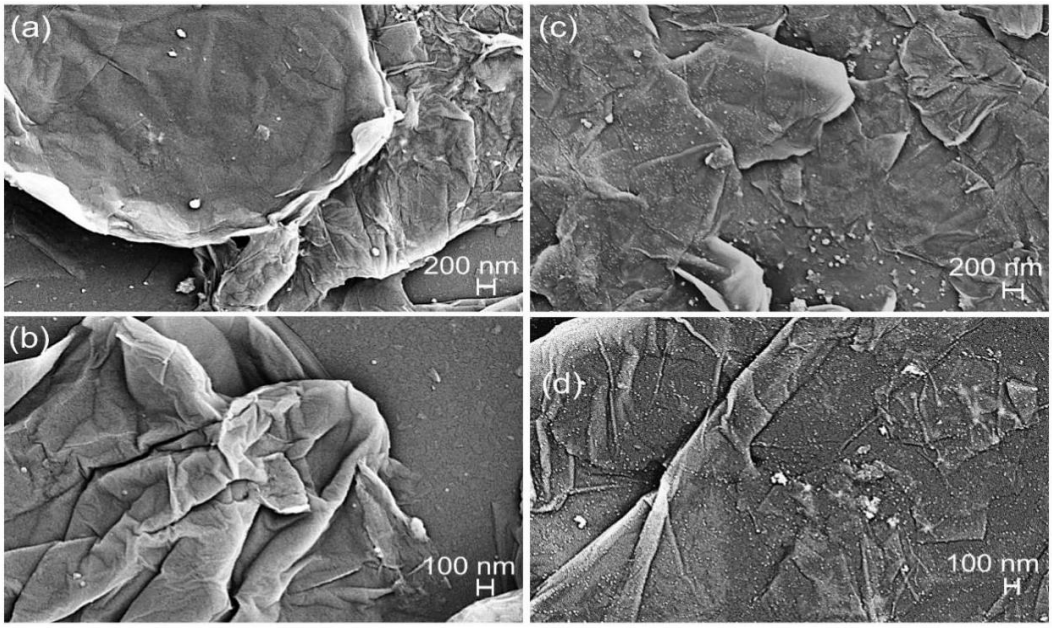

Figure 3.17. SEM images of (a-b) GO-Ag, and (c-d) PEG functionalized GO-Ag

Further, the elemental composition of Ag in PEG-GO-Ag as examined by the EDX mapping confirmed the presence of Ag NPs in PEG-GO-Ag with characteristic X-ray peaks at 3 keV as shown in **Figure 3.18 (a-d)**. The EDX plot also revealed the presence of Na and Si that originated from the glass substrate background. EDX elemental analysis showed that weight % of carbon (C), oxygen (O) and silver (Ag) was 19 %, 80.8 % and 0.10 %. It is evident from the EDX analysis that the Ag NPs content in PEG-GO-Ag was less than 1%. Moreover, as-synthesized membranes were stable in water upto 8 weeks and that the negative/toxic effects of Ag ion release into the operational environment could be minimum or undetectable, especially considering the small percentage of Ag NPs in PEG-GO-Ag membrane.

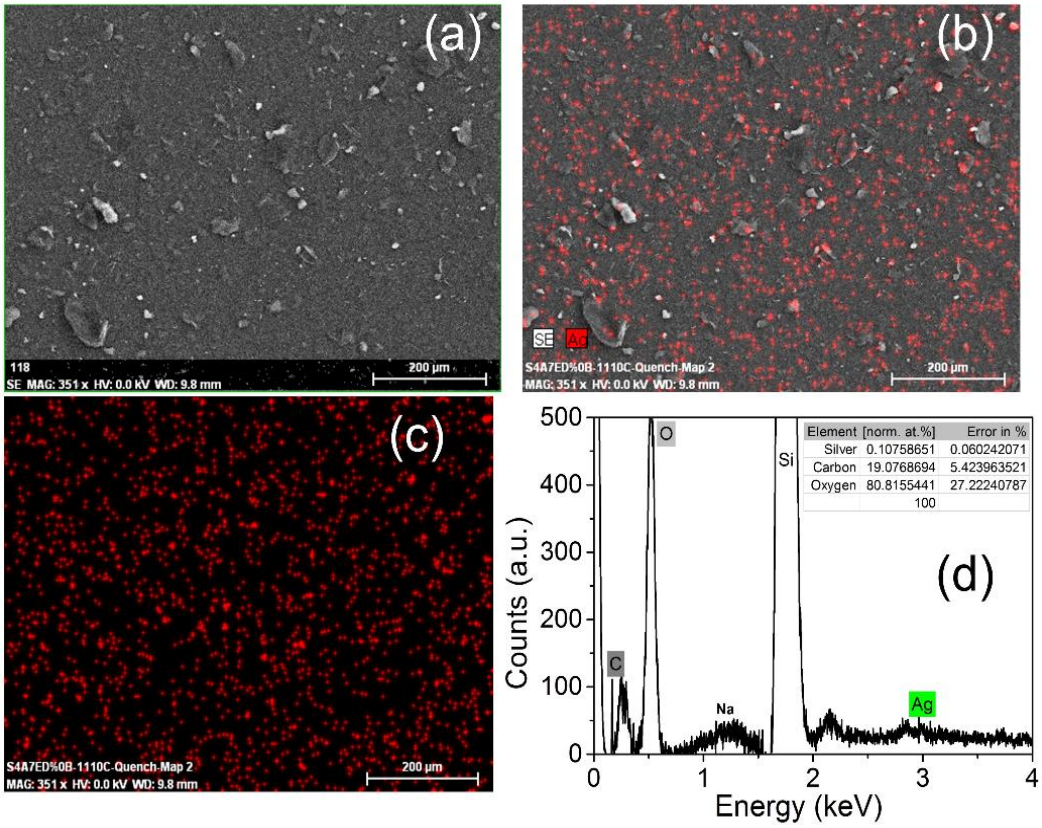

Figure 3.18. EDX mapping of PEG-GO-Ag (a-d). (a) SEM image of PEG-GO-Ag, (b) distribution of Ag NPs, (c) the overlay of the SEM image and (d) The EDX spectrum of the PEG-GO-Ag indicated the presence of Ag NPs

3.2.1.2. FTIR Analysis of PEG-GO-Ag Nano-additive

The chemical composition of PEG functionalized GO-Ag surface was analyzed by FTIR spectroscopy. FTIR spectrum of GO showed the stretching vibrations of C=O from carbonyl or carboxyl groups at 1711 cm^{-1} and epoxy stretching vibration of C-O at 1040 cm^{-1}, which indicates presence of oxygenated functional groups on GO surface (**Figure 3.19 (a)**) [166]. FTIR plot of GO-Ag found to be similar to GO with slight attenuation of C=O (from 1711 to 1719 cm^{-1}) and C=C peaks (from 1613 to1570 cm^{-1}), which depicts the partial reduction of GO and interaction of Ag NPs with oxygen moieties of GO.

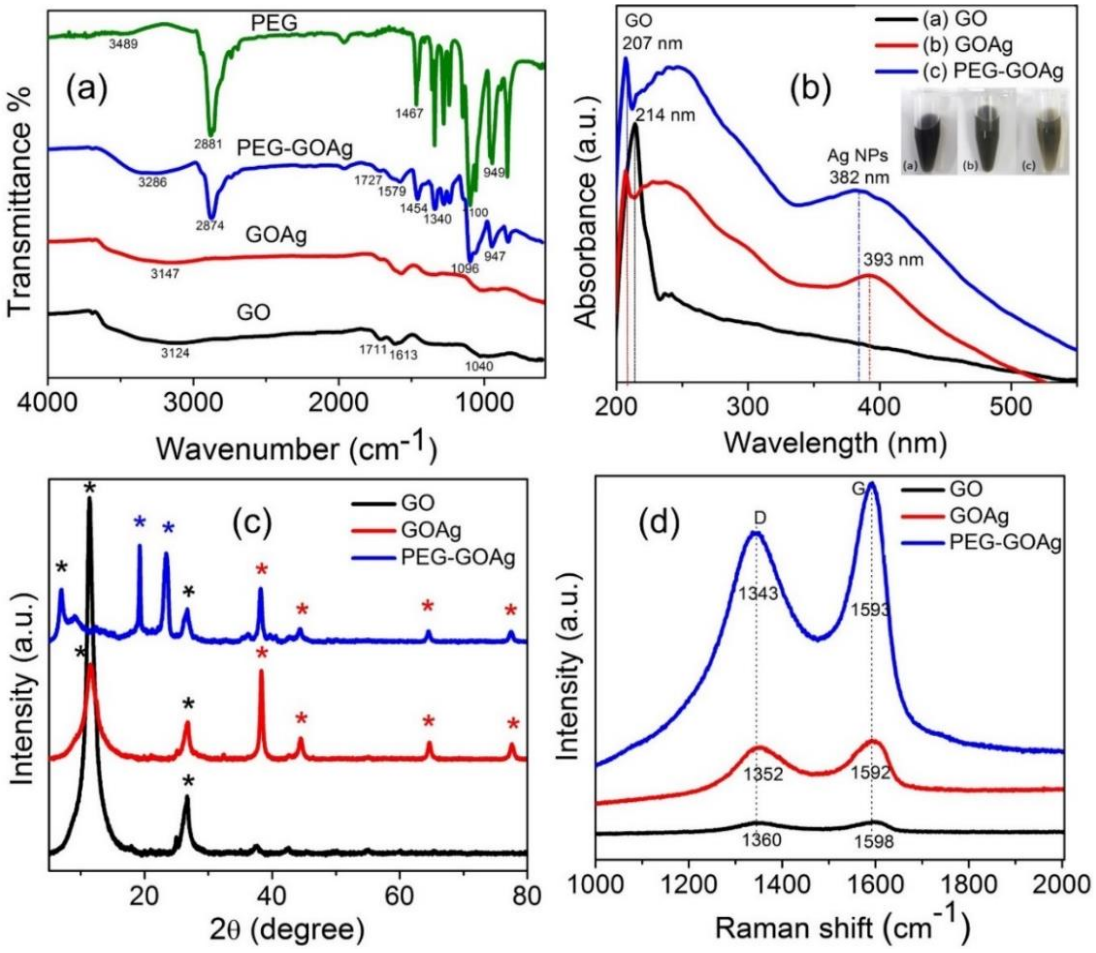

Figure 3.19. Characterization of as-synthesized GO, GO-Ag and PEG functionalized GO-Ag by; (a) FTIR spectra, (b) UV-vis spectra, (c) XRD patterns and (d) Raman spectra

In the FTIR spectrum of PEG functionalized GO-Ag, the peaks at 2874-1340 cm^{-1} and 947-1096 cm^{-1} are assigned to stretching and bending vibrations of -CH_2- groups and C-O-C groups of PEG, respectively [20, 23], which suggested that methylene and carbonyl groups of PEG were present on surface of GO-Ag as a result of PEGylation reaction [20, 23]. The epoxide stretching vibration peak of C=O (1719 cm^{-1}), C=C (1570 cm^{-1}) and C-O (1040 cm^{-1}) shifted to 1727 cm^{-1}, 1579 cm^{-1} and 1096 cm^{-1}, respectively. This observation indicated favorable H-bonding interaction taking place between epoxy groups of GO and PEG in PEG functionalized GO-Ag (**Figure 3.19 (a)**). Appearance of a broad hump in the range of 3100 to 3300 cm^{-1} with slight difference in all spectral pattern depicts the O-H stretching vibrations of GO. Further, the O-H stretching vibration of PEG-GO-Ag shifted towards lower wavenumber compared with pristine PEG. This red shift from 3489 to 3286 cm^{-1} suggested the H-bonding interaction between PEG and GO molecules in GO-Ag [167]. The presence of all these peaks confirms the functionalization of PEG molecules on the surface of GO-Ag.

3.2.1.3. UV Analysis of PEG-GO-Ag Nano-additive

Successful functionalization of PEG on GO sheets with Ag NPs was confirmed by employing UV-visible spectroscopy (**Figure 3.19 (b)**). The UV-vis spectra of GO exhibited an intense peak at 214 nm and a shoulder peak at 236 nm which corresponded to π-π^* transition of C=C and n-π^* transitions of C=O groups, respectively. In case of GO-Ag nanofiller, appearance of a clear peak at 393 nm corresponds to the surface plasmon resonance of Ag NPs [168, 169]. PEG-GO-Ag nanofillers showed a blue shift in π-π^* absorption of GO from 214 to 207 nm and increased absorption as compared with GO-Ag. The UV-vis spectrum of PEG functionalized GO-Ag nanofiller showed slight shift of Ag NPs absorption band from 393 nm towards lower wavelength at 382 nm, which suggested decrease in agglomeration of GOAg solution due to the intercalation of PEG chains within GO sheets (**Figure 3.19 (b)** inset).

3.2.1.4.XRD Analysis of PEG-GO-Ag Nano-additive

The XRD patterns of GO, GO-Ag and PEG functionalized GO-Ag are shown in **Figure 3.19 (c)**. Appearance of a sharp and intense diffraction peak at 2θ =11.56° in the XRD pattern of GO depicts the successful oxidation of graphite to graphene oxide and its highly crystalline nature (**Figure 3.19 (c)**). In case of GOAg nanofiller, presence Ag NPs on GO sheet can be clearly noticed by the appearance of diffraction peaks at 2θ = 38.47°, 44.51°, 64.54 ° and 77.71°, respectively **(Figure 3.19 (c))** [170, 171]. The intensity of the GO peaks 2θ =11.56° was found to decrease sharply by interaction of oxygen moieties of GO with Ag NPs in GO-Ag nanofiller. PEG modified GO-Ag nanofiller showed diffraction peaks of PEG at 2θ =19.09° and 2θ = 23.43°. Surface modification of GO-Ag by PEG showed shift in the 2θ position of characteristic diffraction peak of GO (2θ =11.56°) towards lower angle at 2θ =6.92°, which indicates the increase in interlayer spacing of GO due to interaction of PEG with GO nanosheets. This observation indicated the strong intercalation of oxygenated functional groups of PEG between GO sheets, which assisted the uniform dispersion of PEG-GOAg nanofiller as corroborated in SEM images (**Figure. 3.17 (c-d)**).

3.2.1.5. Raman Analysis of PEG-GO-Ag Nano-additive

As synthesized GO, GO-Ag and PEG-GO-Ag nano-additives were further characterized by Raman spectroscopy (**Figure 3.19 (d)**). In the Raman spectra of GO-Ag, the appearance of two peaks at about 1352 cm^{-1} and 1592 cm^{-1} were corresponding to the D and G bands, respectively (**Figure 3.19 (d)**). D and G bands resulted from the vibrations of sp^3 and sp^2 carbon atoms of GO sheets [172]. After PEG functionalization on GO-Ag, intensities of D and G bands increased drastically, and this implies charge transfer mechanism of PEG chains on GO-Ag nanofiller surface, which inferred successful functionalization of PEG on GO-Ag surface.

3.2.2. Characterization of Membranes

3.2.2.1. SEM Analysis of Membranes

The surface morphologies of Pristine-P (a), 1 GOAg-P (b), 0.2 PEG-GOAg-P (c), 0.6 PEG-GOAg-P (d), 1 PEG-GOAg-P (e) and 1.4 PEG-GOAg-P (f) membranes are shown in Figure 3.20 (a-f), respectively. The SEM images of GO-Ag embedded membranes showed multilayered GO stacked on membrane surface (**Figure 3.20 (b)**) as compared with smooth surface of pristine polymer membrane (**Figure 3.20 (a)**). The presence of a large number of oxygenated functionalities of PEG and its solvating capacity exfoliated Ag decorated GO nanosheets as observed in **Figure 3.20 (c-f)**. This process essentially reduced the physico-chemical interactions between exfoliated PEG functionalized GOAg membrane surface and the various organic substances that allow to minimize the irreversible fouling of membrane. PEG-GOAg 1 wt.% membrane exhibited high porosity and surface roughness as compared to Pristine-P and GOAg 1 wt.% membranes (**Figure 3.20 (e)**). Improved porosity depicts that the high hydrophilicity of PEG-GOAg facilitate the better diffusion of solvent during resin infiltration. Effect of varying wt.% of PEG-GOAg (0.2, 0.6,1 and 1.4 wt.%) on the porosity and surface roughness of membranes can be clearly evident from SEM micrographs (**Figure 3.20 (c-f)**), which supports the aggregation of nanofiller at higher loading (1.4 wt.%), resulting in decreased porosity and low hydrophilicity.

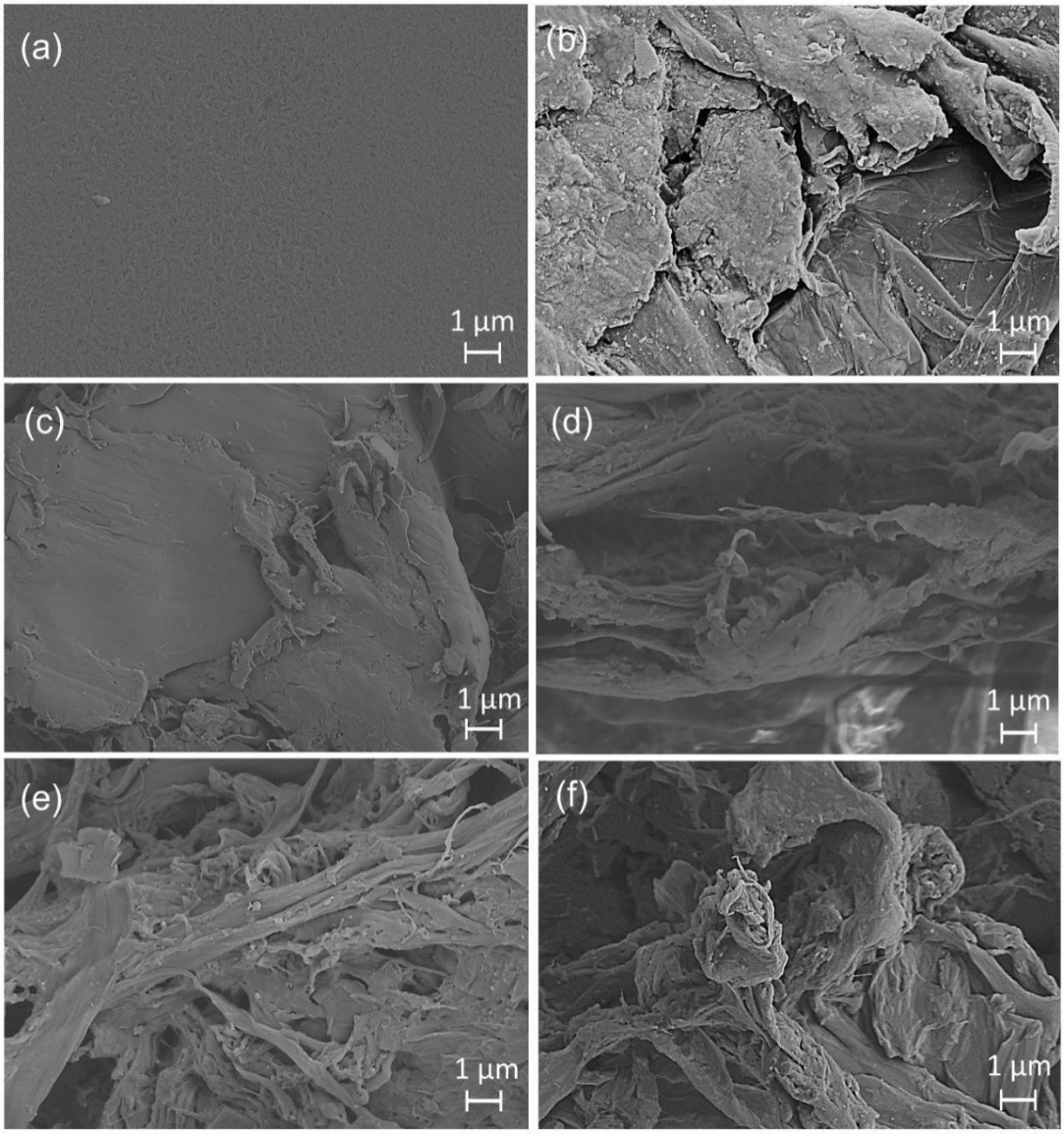

Figure 3.20. SEM images of membranes (a) Pristine-P, (b) 1 GOAg-P, (c) 0.2 PEG-GOAg-P, (d) 0.6 PEG-GOAg-P, (e) 1 PEG-GOAg-P and (f) 1.4 PEG-GOAg-P

The cross-sectional SEM image of pure PVDF-*co*-HFP membrane showed small finger like projections, which was consistent with previously reported literature [173] (**Figure 3.21 (a)**). While, the cross-sectional images of 1 GOAg-P membrane contain aggregated GO layers on the polymer support. Whereas, the cross-sectional images of PEG-GOAg membranes contain exfoliated GO layers intercalated and stacked on the polymer support

(**Figure 3.21 (c-d-e-f)**). Surface intercalation of nanofiller increases rapidly upto 1 wt.% filler content, which results in highly asymmetric and inhomogeneous structures. Interestingly, 1 PEG-GOAg-P (**Figure. 3.21 e (i-ii)**) showed appearance of finger-like micro cavities and high porous structure than 1 GOAg-P (**Figure 3.21 (b)**).

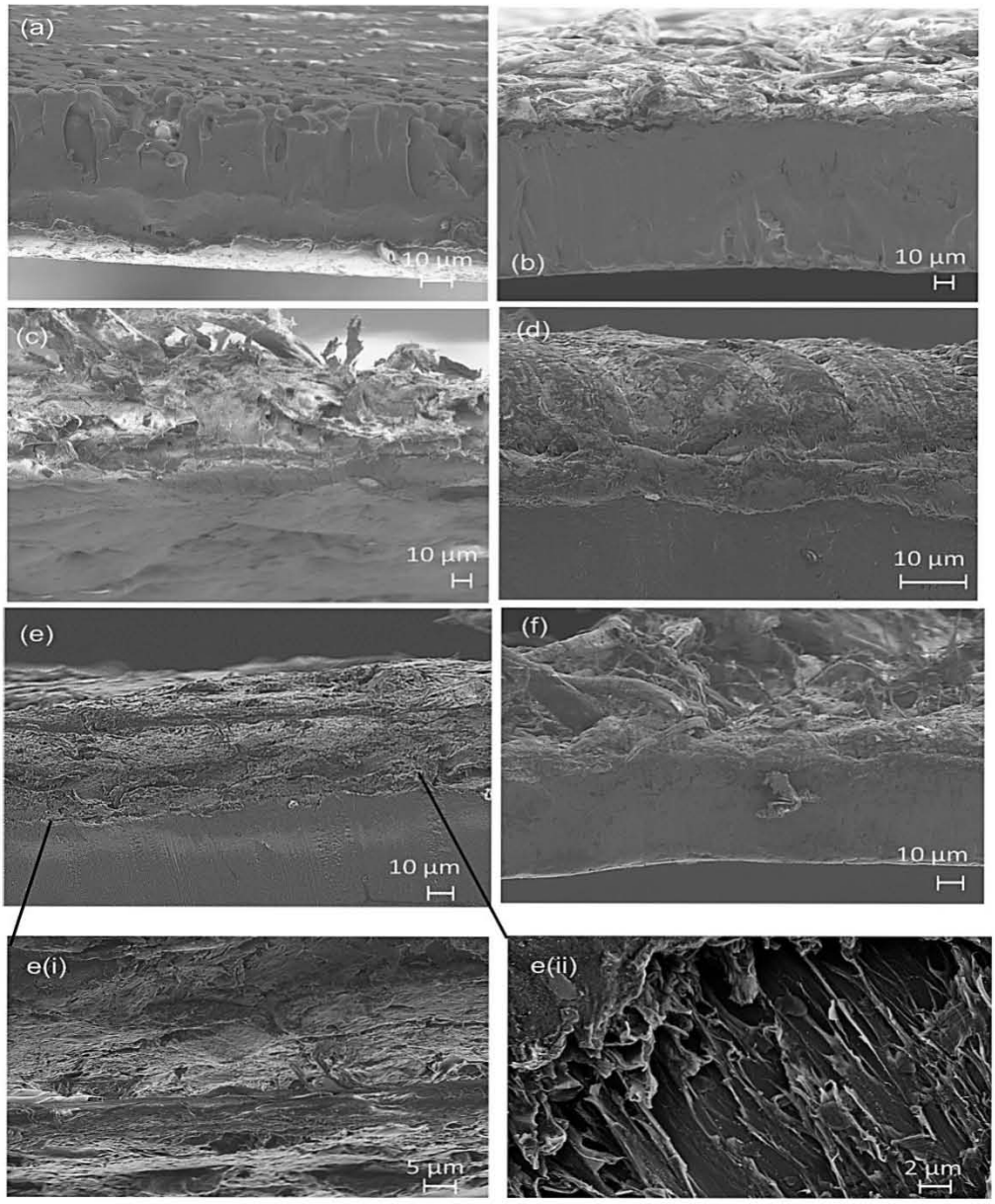

Figure 3.21. Cross-sectional scanning electron microscopic images of membranes (a) Pristine-P, (b) 1 GOAg-P, (c) 0.2 PEG-GOAg-P, (d) 0.6 PEG-GOAg-P, (e) 1 PEG-GOAg-P and (f) 1.4 PEG-GOAg-P

3.2.2.2. FTIR Analysis of Membranes

Intercalation of PEG-GOAg on PVDF-*co*-HFP resin was further confirmed by FTIR spectra (**Figure 3.22**). In case of pure PVDF-*co*-HFP membrane, the peaks at 833 cm^{-1} and 1174 cm^{-1} correspond to CF_3 stretching, while peak at 1400 cm^{-1} was attributed C-F stretching. The peak of C-C skeletal vibration of PVDF-*co*-HFP appeared at about 1067 cm^{-1} in all membranes [174]. The peak of α-phase of PVDF-*co*-HFP at 761 cm^{-1} and 612 cm^{-1} disappeared in PEG-GOAg membranes. The C-O-C stretching vibration of GO was found to be intense at 1229 cm^{-1} in PEG-GOAg-P as compared with 1 GOAg-P suggesting the enrichment of oxygenated functionalities on PEG functionalized membrane and thus contributing to hydrophilic nature of PEG-GOAg-P.

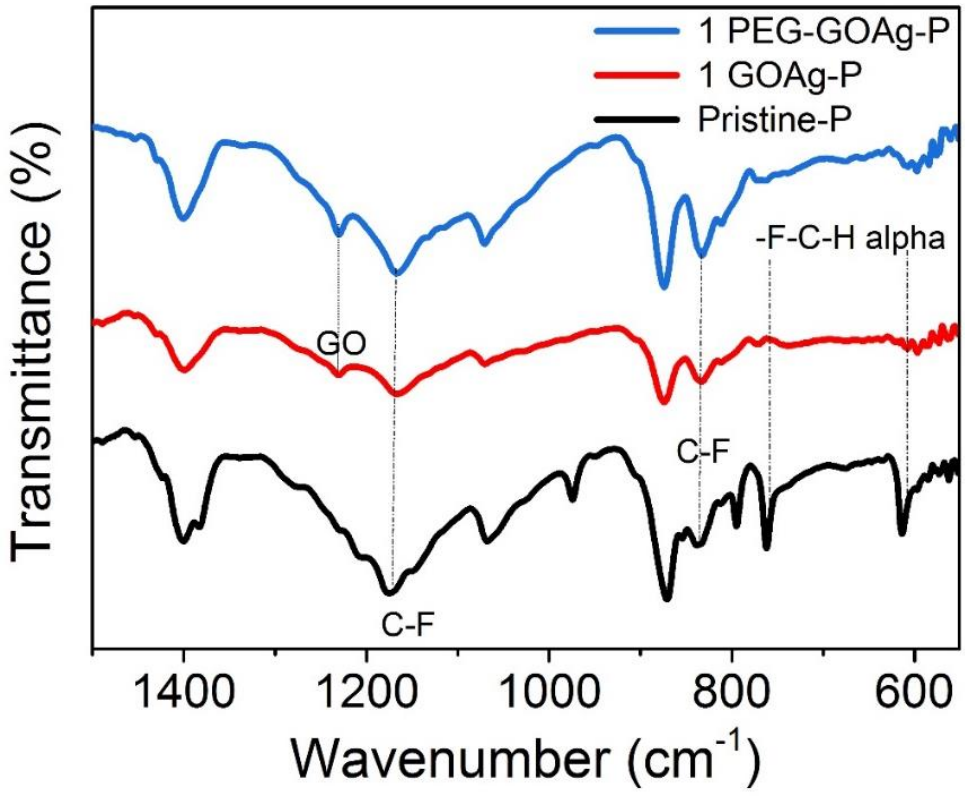

Figure 3.22. FTIR spectra of Pristine-P, 1 GOAg-P and 1 PEG-GOAg-P membranes

3.2.2.3. Porosity and Water Contact Angles of Membranes

Porosity of all the membranes was studied by employing gravimetric method. Porosities of the prepared GO-Ag and PEG-GO-Ag 1 wt.% membranes were 82.7 and 88.2%, respectively, while that of pristine PVDF-co-HFP membrane was 70.60% (**Figure 3.23 (a)**). Porosity of the as-synthesized membranes increased initially upon addition of GOAg and PEG-GOAg upto 1 wt.% and decreased gradually with high nano-additive content. The above result clearly indicated that the presence of hydrophilic PEG-GO-Ag nanofiller elevated the porosity of polymeric membranes and also exhibits the strong intercalation of nanofillers between polymer chains as evidenced in SEM images (**Figure 3.21 (a-f)**).

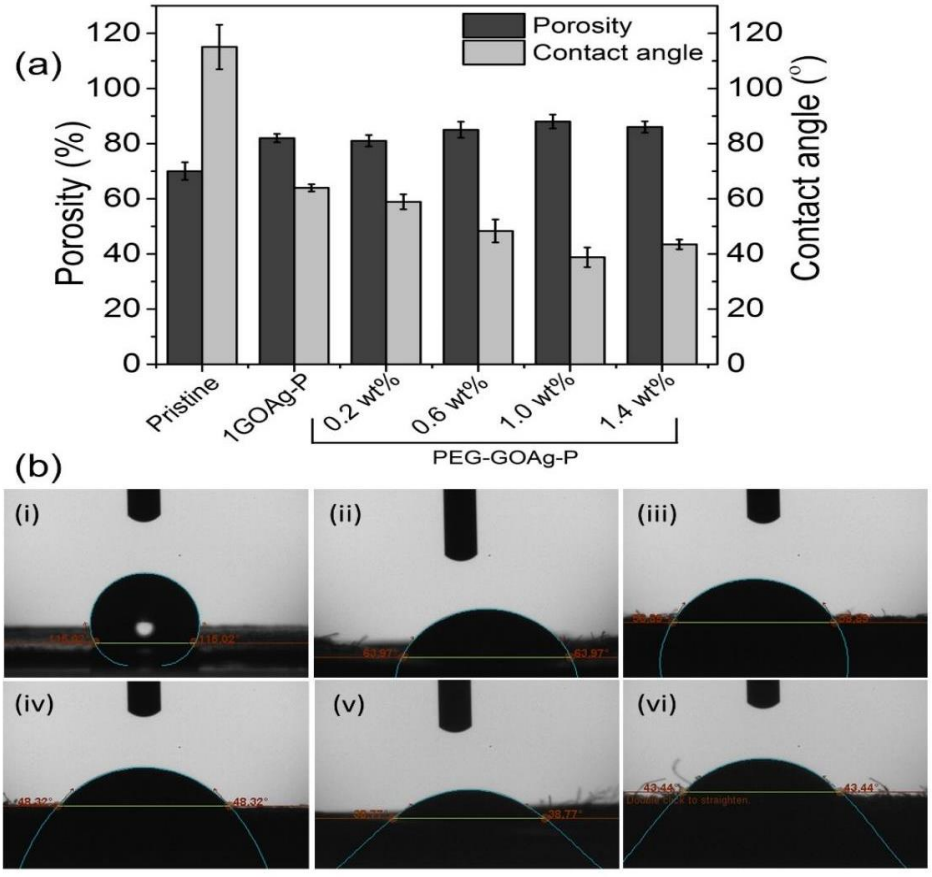

Figure 3.23. (a) The plot of porosity and contact angle of all membranes. **(b)** Images of contact angles of as-synthesized membranes Pristine-P (i), 1 GOAg-P (ii), 0.2 PEG-GOAg-P (iii), 0.6 PEG-GOAg-P (iv), 1 PEG-GOAg-P (v) and 1.4 PEG-GOAg-P (vi)

Hydrophilicity is a significant property of membranes as it affects the water flux and antifouling ability. Surface hydrophilicity of the fabricated membranes was calculated by measuring the contact angle of a water droplet on the membrane surface. **Figure 3.23 (b)** shows the contact angles of as-synthesized membranes (i) Pristine-P, (ii) 1 GOAg-P, (iii) 0.2 PEG-GOAg-P, (iv) 0.6 PEG-GOAg-P, (v) 1 PEG-GOAg-P and (vi) 1.4 PEG-GOAg-P. The contact angle of pristine membrane was 115.02˚, which depicts its hydrophobic nature and contact angle of PEG-GOAg active layer membranes was found to be reduced as compared to pristine PVDF-co-HFP membrane. Functional groups of nano-additive of GOAg and PEG-GOAg play a crucial role in increasing the surface hydrophilicity of PVDF-co-HFP membranes. By adding 1 wt.% of GOAg, the contact angle decreased up to 63.97˚ (**Figure 3.23 (b) (i-ii)**). Furthermore, the homogeneous dispersion of PEG-GOAg facilitated oxygenated functionalities on the membrane surface, which results in further reduction in the contact angle (**Figure 3.23 (b) (iii-vi)**). Addition of 1 wt.% of PEG-GO-Ag decreased the contact angle of the membrane to the lowest value of 38.77˚. However, PEG-GO-Ag nano-additive above 1 wt.% concentration (1.4 wt.%) exhibited decrease in the hydrophilicity of the membrane (43.44˚), which can be attributed to the aggregation of nano-additives at highest wt.%. Therefore, high oxygen moieties of 1 PEG-GOAg-P renders the excellent hydrophilicity to the membrane surface and potentially aids in elevating the flux recovery and antifouling of PEG-GOAg modified membrane.

3.2.2.4. Thermal Stability of Membranes

Thermal stability of the GO-Ag and PEG-GO-Ag nano-additives was measured by thermogravimetric analysis (**Figure 3.24 (a)**). GO-Ag exhibited a minor weight loss at 94 ºC due to the evaporation of adsorbed water molecules and a major weight loss at 232 ºC was observed, which can be attributed to the decomposition of oxygenated functionalities of GO. In case of PEG-GO-Ag nano-additive, improved thermal loss was observed with a slight weight loss at 216 ºC, and a rapid weight loss was observed at 392 ºC, which indicates the disintegration of PEG chains. Thermal stability of PEG-GO-Ag is significantly improved as compared with GO-Ag due to intercalation of PEG chains on GO nanosheets. However, at high temperature, residual weight of PEG-GO-Ag was much lower as

compared to GO-Ag, which depicts the strong degradation of PEG at higher temperature [175].

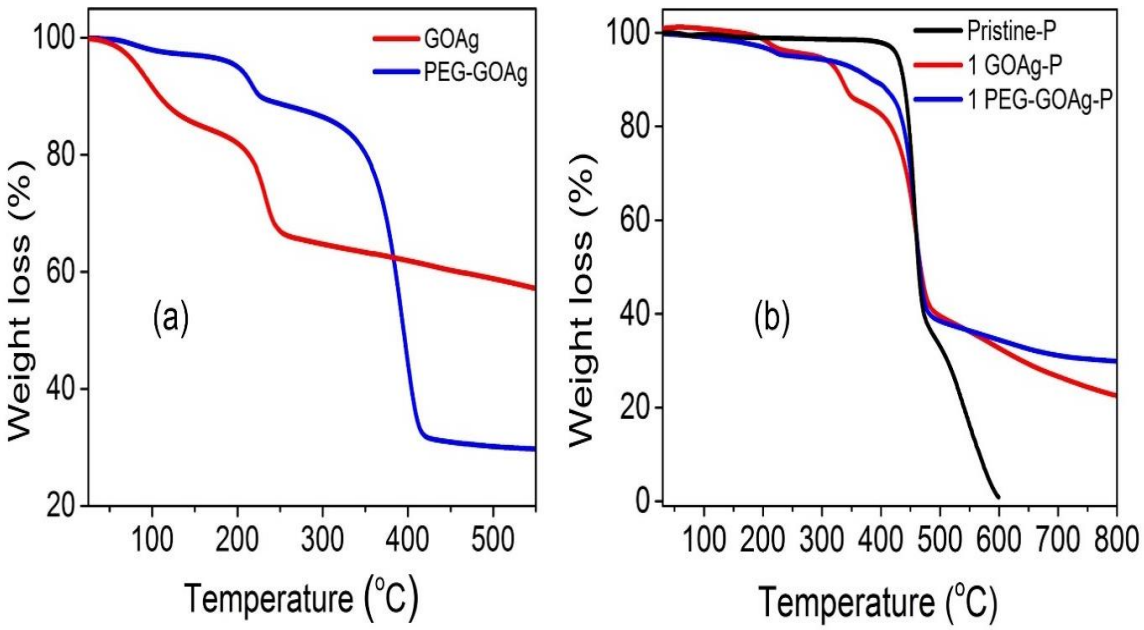

Figure 3.24. TGA curves of (a) nano-additives GO-Ag and PEG-GO-Ag and (b) Pristine-P, 1 GOAg-P, and 1 PEG-GOAg-P membranes

Figure 3.24 (b) shows the thermogravimetric curves of Pristine-P, 1 GOAg-P, and 1 PEG-GOAg-P membranes. TGA plot of 1 GOAg-P membrane exhibited 2% weight loss below 200 ºC which is possibly due to the evaporation of adsorbed water molecules. Whereas, TGA of 1 PEG-GOAg-P membrane exhibited much higher initial weight loss (4%), which corresponds to the high hydrophilic nature of PEG and possibly allow entrapping of more water molecules. However, no initial weight loss was observed in case of Pristine-P membrane. For GOAg membrane, 14% weight loss occured below 360 ºC, which depicts the degradation of GO molecules that further undergo major weight loss (60%) at 461ºC. While PEG-GO-Ag membrane exhibited a major weight loss (60 %) at 480 ºC showing its thermal stabilility relative to other two membranes

3.2.3. Membrane Performance Study

3.2.3.1.Water Flux and BSA Rejection of Membranes

The water flux performance of PEG functionalized GO-Ag active polymeric membrane was studied and shown in **Figure 3.25**. PEG cross-linked 2D carbon-silver NPs based polymeric membrane exhibited increase in water permeation flux as compared to Pristine-P membrane. The water flux of 1 PEG-GOAg-P membrane was found to be maximum about 906 $Lm^{-2}\ h^{-1}$ (enhanced by 319 %) as compared with Pristine-P membrane. Chains in PEG molecule with flexible C-O-C bonds favored the strong hydrogen interaction between its ethyl groups and -COOH and –OH functional groups of GO nanosheets, therefore 1 wt.% PEG-GOAg-P membrane showed enhanced capacity to permeate the water molecules resulting in its increased water flux performance.

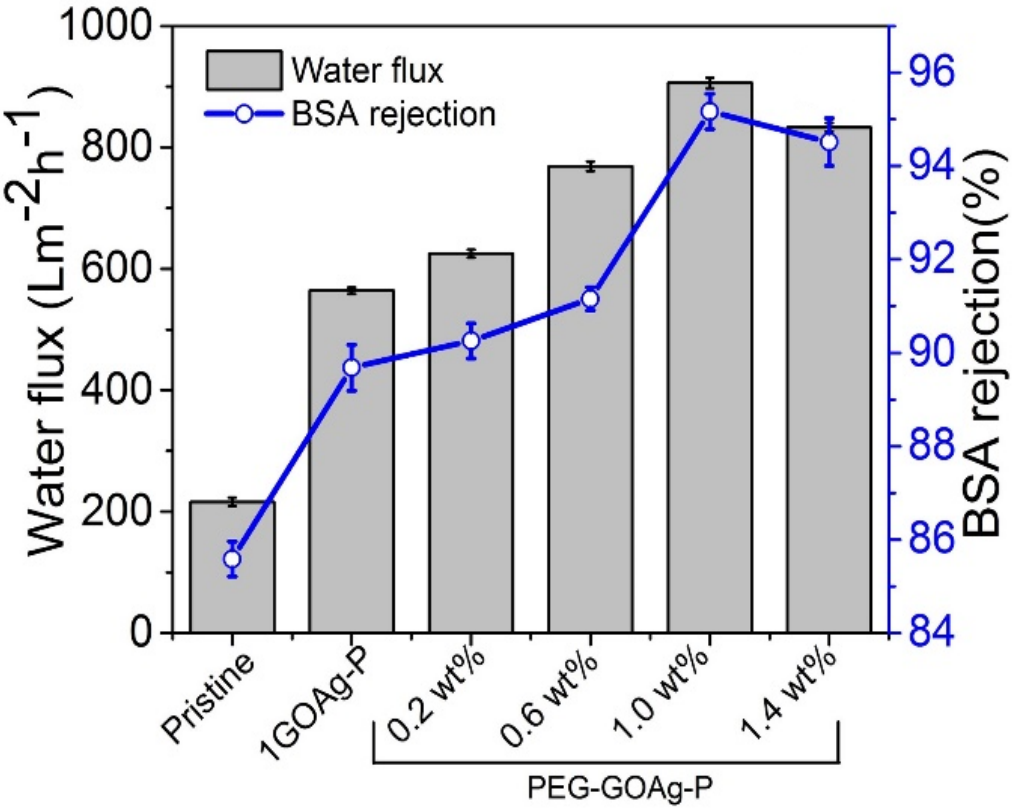

Figure 3.25. Pure water flux and BSA rejection of Pristine-P and PEG-GOAg based membranes

The water flux was moderately decreased with PEG-GO-Ag concentration greater than 1wt.% on support polymer membrane (*i.e.*1.4 wt.% PEG-GOAg-P), which is an indication of non-uniform distribution of additive at high concentration and therefore causing pore blocking on membrane surface. This observation was evident through higher contact angle value of 1.4 wt.% PEG-GOAg-P than with 1 wt.% PEG-GOAg-P membrane as well. BSA rejection capacity of 1wt.% PEG-GO-Ag was increased from 85.5 to 95.1% as compared with Pristine-P membranes (**Figure 3.25**). Increased rejection of BSA molecules corresponds to the high hydrophilic nature of PEG-GOAg-P, which prevented contact with BSA molecules. BSA rejection performance of 1 GOAg-P membrane (89.68%) was higher than that of Pristine-P (85%) and lesser as compared with PEG-GOAg membranes because of low hydrophilicity of GO-Ag without PEG.

3.2.3.2. Cyclic Filtration of Membranes

The fouling resistance of membranes can be determined by measuring permeation flux performance of pure water and BSA solution for repetitive filtration cycles, respectively. The results of recycling flux measurement of membranes are shown in **Figure 3.26**. In the first cycle, PEG functionalized membranes exhibited rapid increase in the pure water flux as compared with Pristine-P (**Figure 3.26**). However, the permeation flux of functionalized membranes found to be decreased against BSA protein in PBS solution. After washing, the water permeation of 1 PEG-GOAg showed maximum recovery of water flux as compared to Pristine-P and 1 GOAg-P, respectively. It is known that permeation of organic molecules, such as proteins (BSA) decreases as compared with pure water at initial cycles due to low physico-chemical interaction of protein with membrane. However, as filtration proceeds in a successive repetitive cycles, attachment and/or adsorption of particles/protein molecules tend to be greater on the porous membrane, which makes it extremely difficult to completely remove them by back flush or shear stress [176].

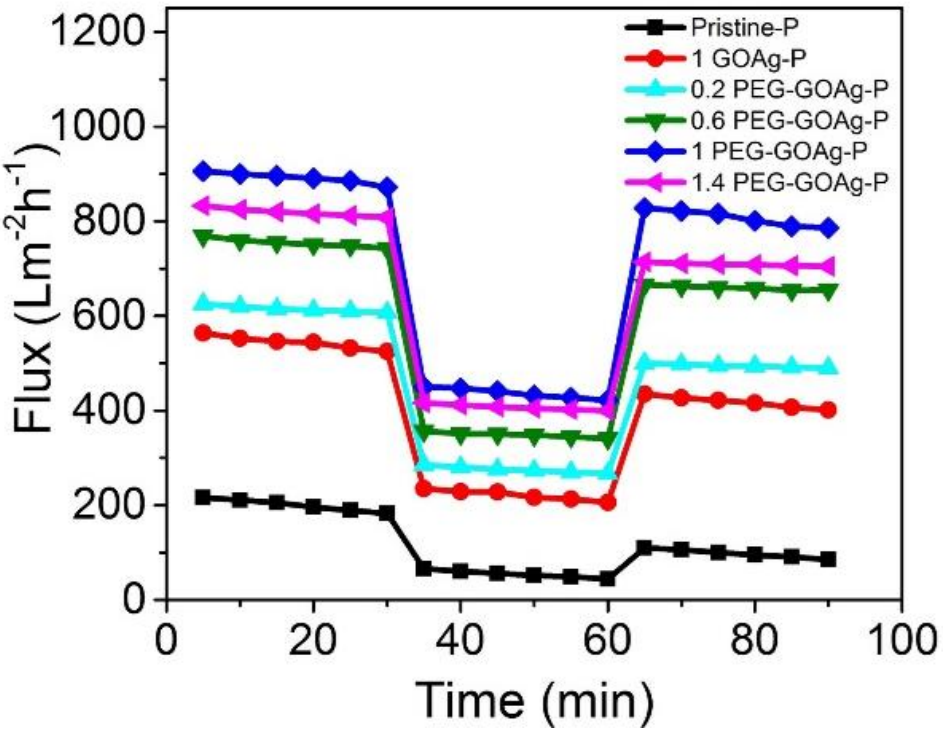

Figure 3.26. Flux recovery cycle of Pristine-P and all functionalized membranes

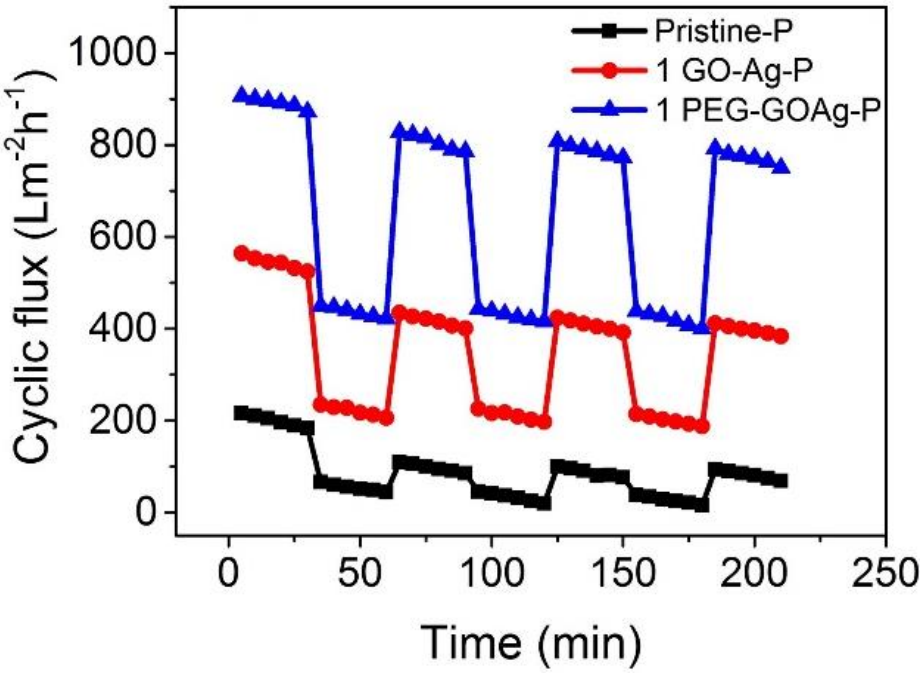

Figure 3.27. Cyclic Filtration of Pristine-P and Functionalized Membranes

Figure 3.27 showed the reusability of fabricated membranes by repetitive cycles of water and BSA filtration. Therefore, it is challenging to retain initial water flux after usage of membrane for several cycles and optimize the process in terms of quality and fabrication cost of membrane. GO-Ag-P and PEG-GOAg-P membranes retained higher water permeation flux as compared with Pristine-P membrane. The lower water flux values of Pristine-P membrane are attributed to hydrophobicity of Pristine-P and leads to irreversible fouling performance. While, in case of GO-Ag and PEG functionalized GO-Ag membranes, the enhanced hydrophilicity was provided by oxygen functionalities and strong hydrogen interaction existing between ethyl groups of PEG molecular chains and oxygen-containing groups of GO, respectively. This hydrophilic nature of membrane surfaces contributed to enhanced antifouling performance of the membrane, because organic molecules, such as BSA proteins are hydrophobic in nature and could minimize adsorption [177].

The water filtration process depends on different surface properties parameters, such as hydrophilic or hydrophobic interaction and charge because it contains organic soluble molecules or colloids. Therefore, in the water filtration process, the fouling of membrane is contributed by several parameters that include concentration polarization (CP) phenomena, cake or gel formation and adsorption of organic molecules/substances [176]. Membrane fouling is generally categorized as reversible and irreversible fouling. The CP affecting reversible fouling due to accumulation of particles/foulant molecules at interface of membrane. Reversible fouling of the membrane can be caused by formation of cake or gel layers, that is formed when the concentration of deposited protein layers reaches a threshold on the membrane surface that can be removed by back flush or shear stress. Further, adsorption of organic molecules/substances due to strong physico-chemical interactions between the different organic molecules and the membrane can lead to irreversible fouling through blocking of pores of membrane. This phenomenon is mainly contributing to the total fouling and crucial for permeation/separation performance of membrane [176].

3.2.3.3. Antifouling Properties and FRR% of Membranes

Antifouling properties of all membranes were assessed by calculating the total fouling ratio (R_t), reversible fouling ratio (R_r), irreversible fouling ratio (R_{ir}) and flux recovery ratio (FRR) (**Figure 3.28**). The total fouling and irreversible fouling ratios of PEG functionalized membranes were found to be lowest (R_t = 50.3% and R_{ir} = 8.6% for 1 PEG-GOAg-P) as compared with Pristine-P because of the antifouling properties of combined organic–inorganic hybrid PEG-GO-Ag nano-additives. The highest antifouling nature of 1 PEG-GOAg membrane can be accredited to the better hydrophilicity of PEG-GO-Ag. The adhesion forces between foulants like BSA and membrane surface can be categorized as: electrostatic forces, van der Waals forces, hydrogen bonding and hydrophobic forces [178-180]. BSA molecules are negatively charged at pH 7, increasing the negative charges on membrane surface results in strong electrostatic repulsion of these negatively charged BSA molecules on the membrane surface. PEG-GO-Ag modified membranes exhibited high FRR and low irreversible fouling, indicating that the PEGylated-GO-Ag has more negative charges as compared to GO-Ag due to the presence of additional oxygen atoms. Increased electrostatic interaction and improved H-bonding of PEGylated-GO-Ag results in high water flux with improved antifouling properties.

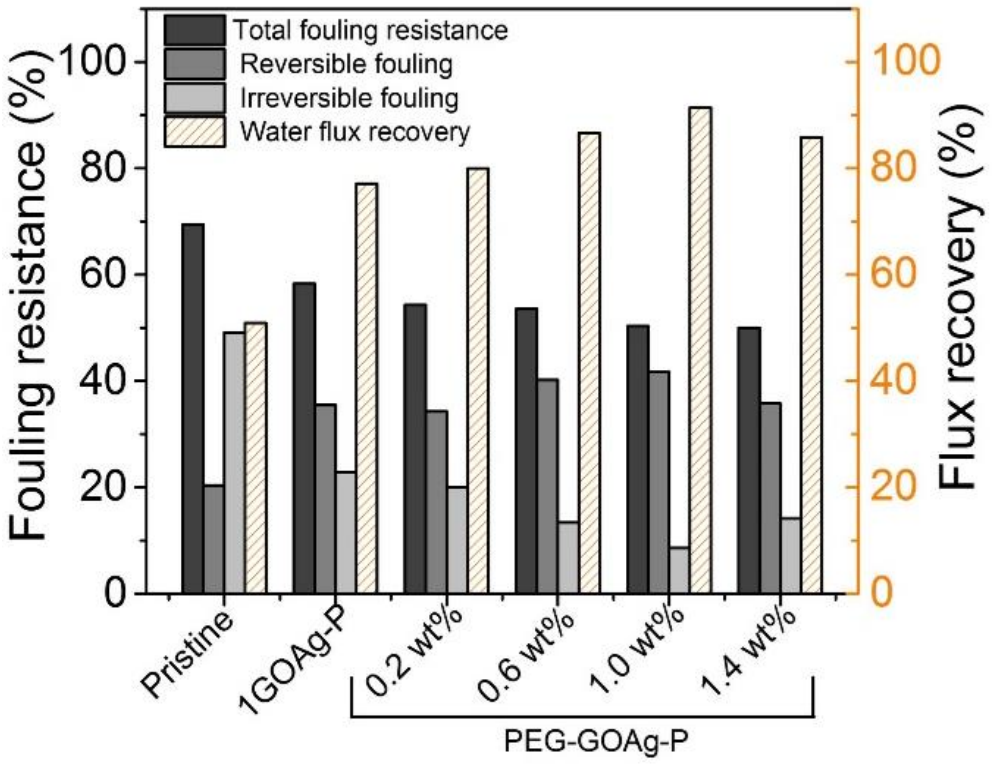

Figure 3.28. Antifouling performance and Flux recovery ratio of Pristine-P and functionalized membranes

The FRR performance of as-synthesized Pristine-P, 1 GOAg-P, 0.2 PEG-GOAg-P, 0.6 PEG-GOAg-P, 1 PEG-GOAg-P and 1.4 PEG-GOAg-P were found to be 50.8%, 77.1%, 79.9%, 86.6%, 91.3%, and 85.8%, respectively (**Figure 3.28**). The FRR performance was better with PEG-GO-Ag functionalized membranes as compared with Pristine-P and GO-Ag-P membranes. The 1 PEG-GOAg-P membrane exhibited relatively enhanced FRR, which was inherent to synergistic effects of oxygen-functionalities of both components PEG and GO-Ag leading to efficient retention of a thick layer of water molecules on the membrane surface. So the present study could offer a great potential to optimize quality and cost in fabrication of high-performance polymeric membranes with increased hydrophilicity, permeability, antifouling property and high thermal stability for wide range of industrial applications.

3.3. GO/Fe_3O_4 and Ag-GO/Fe_3O_4 based Active Layer PVDF-*co*-HFP Membranes for Water Treatment

3.3.1. Characterization of Magnetic Nanoparticles

3.3.1.1. XRD Analysis of GO, GO/Fe_3O_4 and Ag-GO/Fe_3O_4

XRD patterns of GO, GO/Fe_3O_4 and Ag-GO/Fe_3O_4 nanocomposites are shown in **Figure 3.29**. The appearance of strong characteristic peak at 12θ° corresponds to the GO nanocomposite. XRD pattern of GO/Fe_3O_4 confirms the presence of magnetic iron oxide nanoparticles from the existence of diffractions peaks at 30 θ°, 35 θ°, 44 θ°, 57 θ° and 63 θ°. XRD of Ag-GO/Fe_3O_4 nanocomposite displays strong diffraction peaks at 38 θ°, 44 θ°, 64 θ° and 77 θ° which supports the successful functionalization of GO/Fe_3O_4 with Ag nanoparticles. These results are supported from the literature [181, 182].

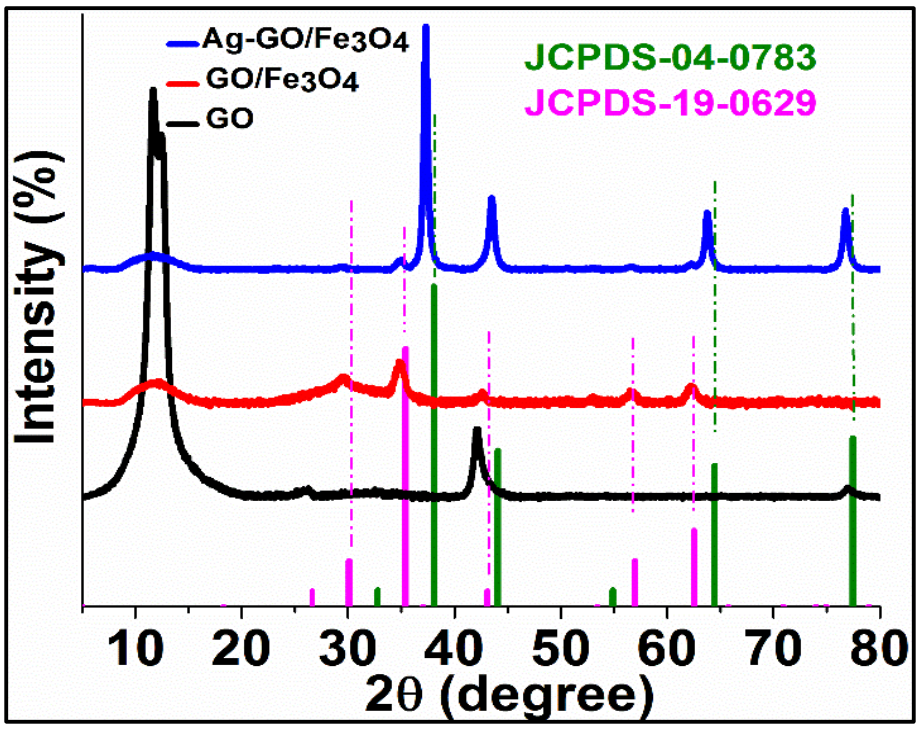

Figure 3.29. XRD of GO, GO/Fe_3O_4 and Ag-GO/Fe_3O_4

3.3.1.2. FTIR Analysis of GO, GO/Fe_3O_4 and Ag-GO/Fe_3O_4

Functional groups of the fabricated nanocomposites were further investigated by using FTIR spectroscopy as shown in **Figure 3.30**. Along with the appearance of characteristic GO bands at 1050, 1646 and 3302 cm^{-1} the presence of a clear and intense band at 552 cm^{-1} was observed in FTIR spectra of Fe_3O_4, GO/Fe_3O_4 and Ag-GO/Fe_3O_4 which corresponds to the Fe-O stretching vibration. This Fe-O band was attributed to the successful functionalization of GO with Fe_3O_4. A broad band 3302 cm^{-1} corresponds to the O-H stretching vibration [182].

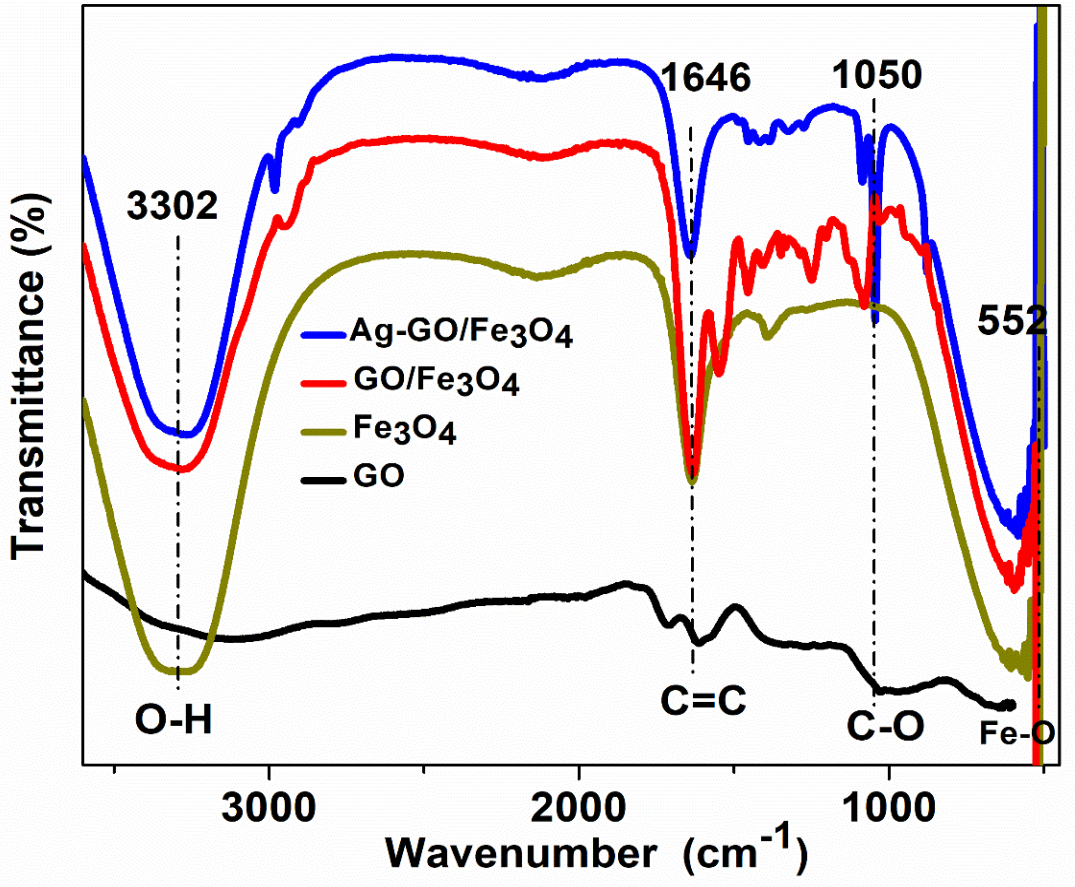

Figure 3.30. FTIR of GO, Fe_3O_4, GO/Fe_3O_4 and Ag-GO/Fe_3O_4

3.3.1.3. SEM Analysis of GO, GO/Fe_3O_4 and Ag-GO/Fe_3O_4

Structural morphology of the prepared nanocomposites was explored by employing SEM. **Figure 3.31** represents the SEM micrographs and EDX analysis of GO, GO/Fe_3O_4 and Ag-GO/Fe_3O_4. In case of GO smooth silk like layered pattern was observed which is the characteristic of GO. While in case of GO/Fe_3O_4 bright dotted patterns covering the GO sheets were clearly visible. Because of high magnetic properties the Fe_3O_4 nanoparticles tends to form small clusters on the surface of GO sheets. SEM study revealed the successful functionalization of GO with magnetic nanoparticles covering the surface of GO uniformly. The SEM analysis of silver functionalized magnetic GO also showed the small clusters of magnetic nanoparticles decorating the GO sheets. Furthermore, the EDX analysis was studied to check the elemental analysis of prepared samples. EDX confirms the presence of C, O, Fe and Ag in the respective nanocomposite samples.

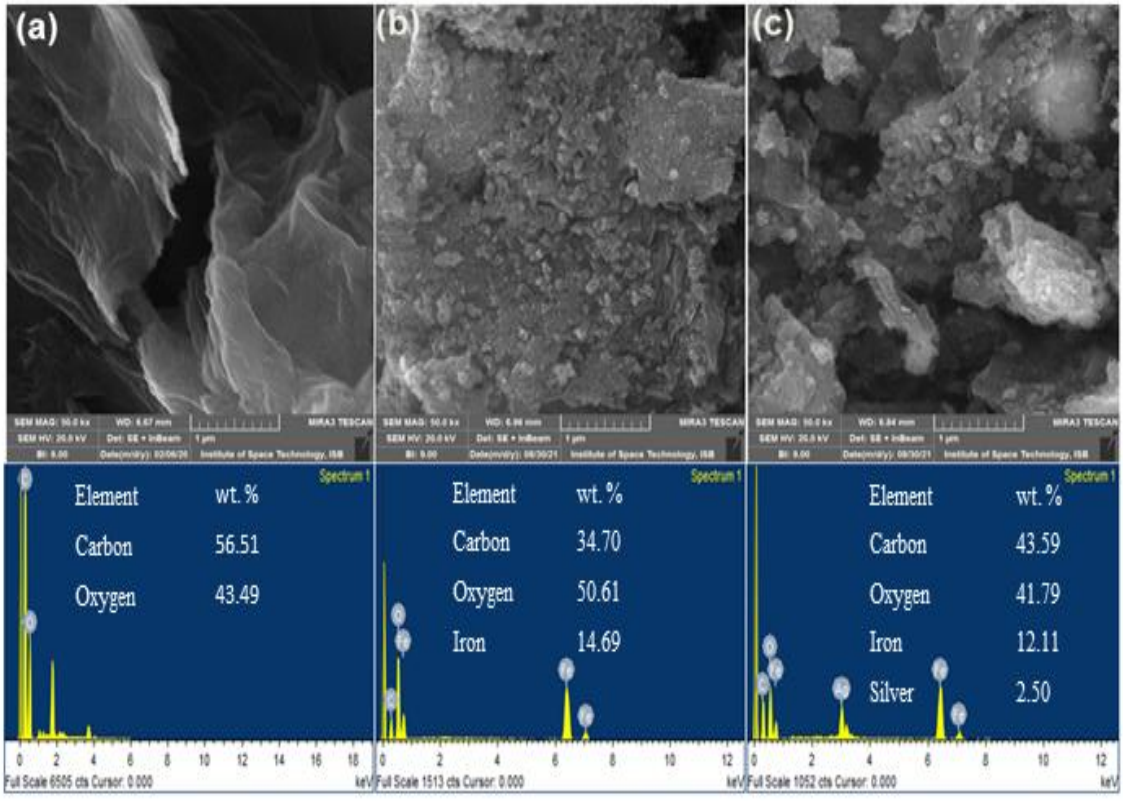

Figure 3.31. SEM analysis of GO, GO/Fe_3O_4 and Ag-GO/Fe_3O_4

3.3.2. Characterization of Magnetic Membranes

3.3.2.1. FTIR analysis of GO/Fe_3O_4 and Ag-GO/Fe_3O_4 based membranes

The functionalities of PVDF-*co*-HFP membranes with and without magnetic nanoparticles were analyzed by FTIR technique. **Figure 3.32** represents the FTIR spectra of pristine PVDF-*co*-HFP membrane and membranes incorporated with GO/Fe_3O_4 and Ag-GO/Fe_3O_4. The FTIR spectra of PVDF-*co*-HFP depicts clear bands at 1402 cm^{-1}, 973 cm^{-1}, and 790 cm^{-1} which identifies the α-phase of PVDF-*co*-HFP. While the bands at 1271 cm^{-1} and 834 cm^{-1} corresponds to the β-phase of PVDF-*co*-HFP. A clear reduction in α-phase was observed by addition of GO/Fe_3O_4 and Ag-GO/Fe_3O_4 nanofillers which suggests the favorable interaction of carbonyl group (C=O) of GO with CF_2 segments of PVDF-*co*-HFP [183]. In the FTIR spectra of GO/Fe_3O_4 and Ag-GO/Fe_3O_4 the appearance of a clear peak at 554 cm^{-1} confirms the presence of Fe-O functional group. So the FTIR analysis proved the successful fabrication of magnetic graphene oxide based PVDF-*co*-HFP membrane.

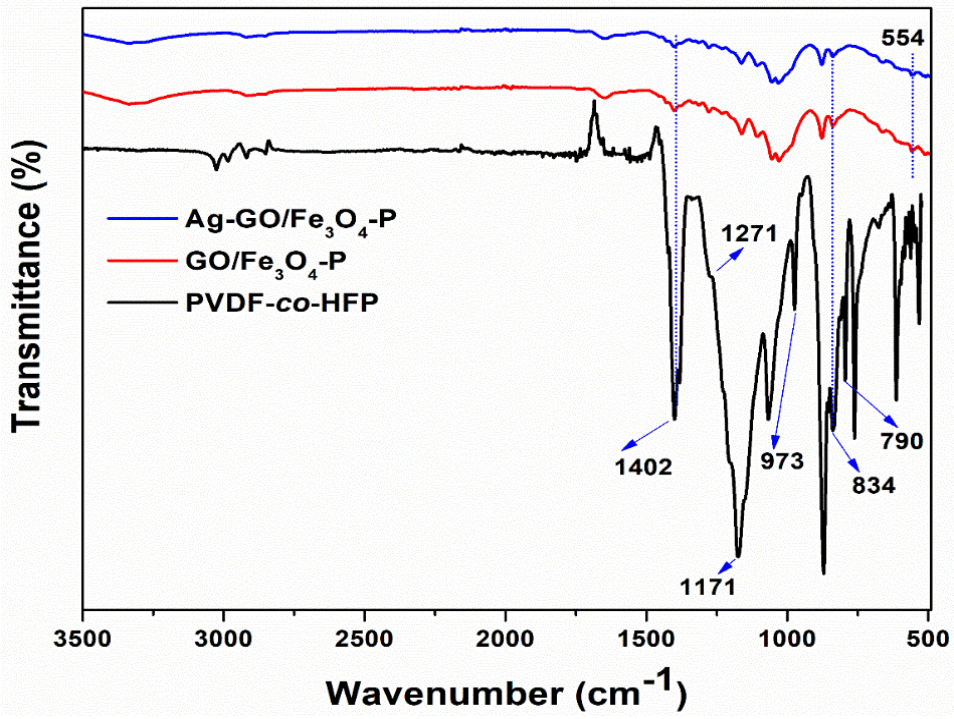

Figure 3.32. FTIR spectra of pristine PVDF-*co*-HFP membrane and membranes incorporated with GO/Fe_3O_4 and Ag-GO/Fe_3O_4

Magnetic behavior of GO/Fe_3O_4 (a,b) and Ag-GO/Fe_3O_4 (c) based PVDF-*co*-HFP membranes was checked by using a magnetic rod. By moving the magnetic rod near the membrane coupons, the synthesized membranes were highly attracted towards the magnetic rod as shown in **Figure 3.33**. These images support the resin infiltration approach to fabricate magnetic membranes without using any external magnets.

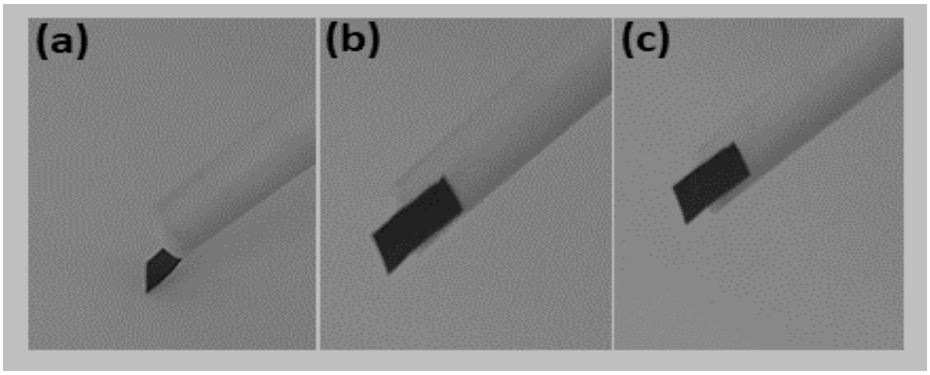

Figure 3.33. Magnetic behavior of (a,b) GO/Fe_3O_4 and (c) Ag-GO/Fe_3O_4 based PVDF-*co*-HFP membranes

3.3.2.2. SEM Analysis of GO/Fe_3O_4 and Ag-GO/Fe_3O_4 based Membranes

Cross-sectional morphology of membranes has large impact on its transport properties. **Figure 3.34** shows the cross-sectional images of bare PVDF-*co*-HFP membranes and GO/Fe_3O_4 and Ag-GO/Fe_3O_4 based membranes. SEM of bare PVDF-*co*-HFP membrane constrains a dense, compact and non-porous lamellar structure. while in case of magnetic GO based nanocomposite membrane the micro-porous GO/Fe_3O_4 based loose laminar layered pattern was observed. Appearance of micro cavities within the layered structure of GO sheets indicate the increased porosity and hydrophilicity of nanocomposites based PVDF-*co*-HFP membranes. Ag-GO/Fe_3O_4 based membranes also exhibit the highly permeable layered structure with finger like projections within the membrane cross-section. In contrast to the cross-sectional SEM of pure PVDF-*co*-HFP membrane both GO/Fe_3O_4 and Ag-GO/Fe_3O_4 nanofiller based membranes exhibit highly exfoliated membranes cross-sectional structure forming channels within the GO layers. These channels facilitate the water transport through membrane. These micro-structures can be

attributed to the hydrophilicity and uniform dispersibility of GO/Fe_3O_4 and Ag-GO/Fe_3O_4 nanofillers.

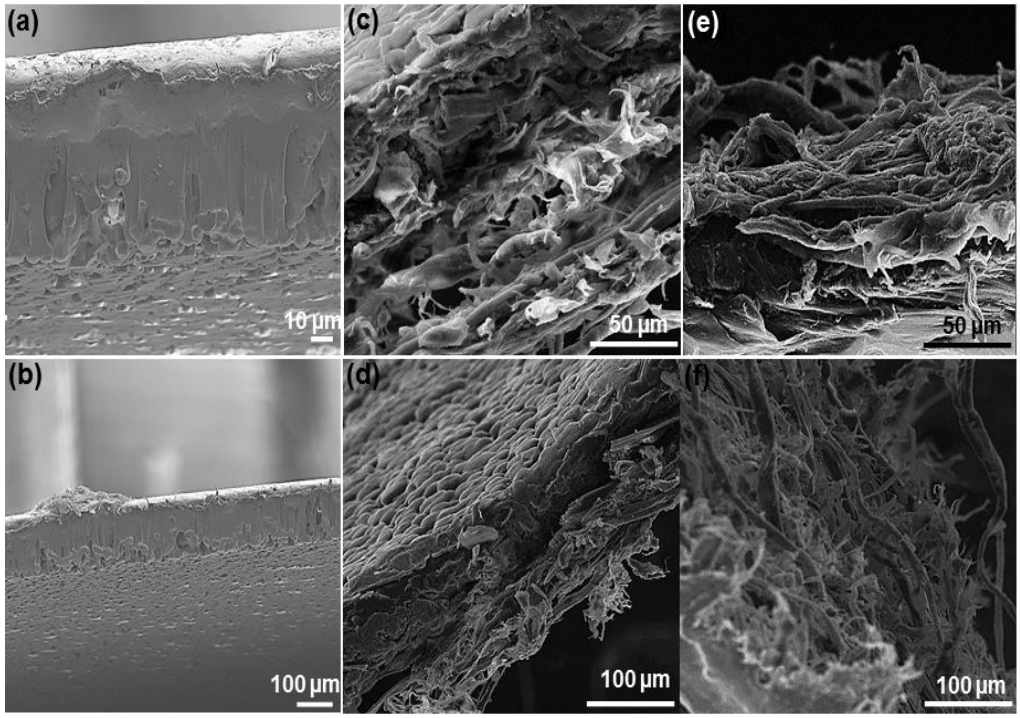

Figure 3.34. Cross-sectional SEM images of (a,b) PVDF-*co*-HFP (c,d) GO/Fe_3O_4 /PVDF-*co*-HFP and (e,f) Ag-GO/Fe_3O_4/PVDF-*co*-HFP membranes

3.3.2.3. Thermo-gravimetric Analysis of Ag-GO/Fe_3O_4 based Membrane

Thermal stability of membranes is highly considerable for their applicability towards high temperature conditions. TGA analysis of PVDF-*co*-HFP membrane and Ag-GO/Fe_3O_4 based PVDF-*co*-HFP membrane was studied upto 600°C and shown in **Figure 3.35**. In case of pristine PVDF-*co*-HFP membrane a major weight loss was observed at 420°C which increases upto 526°C by incorporation of Ag-GO/Fe_3O_4 nanocomposite. The Ag-GO/Fe_3O_4/PVDF-*co*-HFP membranes exhibit high thermal stability because of synergetic stable performance of GO and Fe_3O_4. This increased stability of magnetic graphene oxide based nanocomposite membrane was supported by already reported results [184].

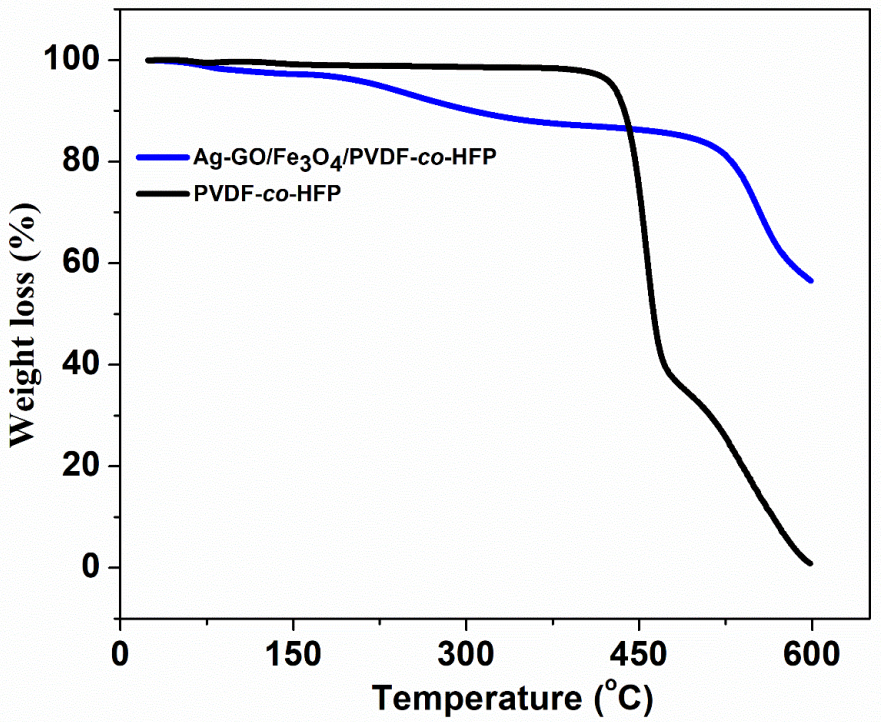

Figure 3.35. Thermogravimetric analysis of Ag-GO/Fe_3O_4 based membrane

3.3.3. Membranes Performance Study

3.3.3.1. Contact Angle and Porosity of GO/Fe_3O_4 and Ag-GO/Fe_3O_4 based membranes

In contrast to the pristine PVDF-*co*-HFP membrane the hydrophilicity of GO/Fe_3O_4 and Ag-GO/Fe_3O_4 based membranes increased drastically as shown in **Figure 3.36**. Water contact angle of PVDF-*co*-HFP membrane was noticed to be 115˚ which depicts the hydrophobic nature of polymer membrane. By incorporation of GO/Fe_3O_4 nanofiller the water contact angle decreased to the 51˚. Furthermore, the silver functionalized magnetic graphene oxide nanofiller (Ag-GO/Fe_3O_4) reduces the water contact angle to the lowest value i.e. 46˚. So the GO/Fe_3O_4 nanofiller has positive impact in enhancing the hydrophilicity of polymer membranes [135].

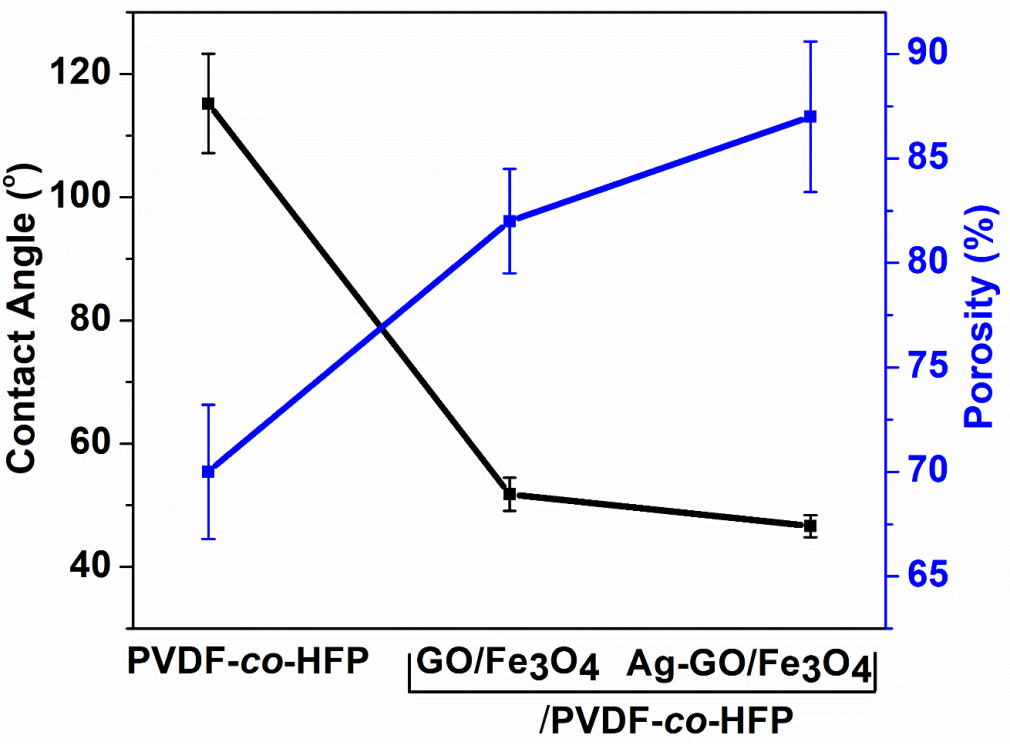

Figure 3.36. Contact angle and porosity of GO/Fe_3O_4 and $Ag\text{-}GO/Fe_3O_4$ based membranes

Besides this, the porosity of the PVDF-*co*-HFP membranes also increases from 70% to 82% and 87% respectively by addition of GO/Fe_3O_4 and $Ag\text{-}GO/Fe_3O_4$ nanofiller. These results showed that both GO/Fe_3O_4 and $Ag\text{-}GO/Fe_3O_4$ have excellent hydrophilic characters to upgrade the membranes permeability and transport properties.

3.3.3.2. Water and BSA Flux of GO/Fe3O4 and Ag-GO/Fe3O4 based Membranes

To check the permeability of fabricated membranes, pure water and BSA solution were used as feed and permeate fluxes were measured one by one. Water flux of PVDF-*co*-HFP membrane was 216 $Lm^{-2}h^{-1}$ which suggests the strong hydrophobic character of pristine polymer. However, the permeability of PVDF-*co*-HFP membranes enhanced appreciably by adding hydrophilic GO/Fe_3O_4 and $Ag\text{-}GO/Fe_3O_4$ nanofillers. The graphene oxide and magnetic nanoparticles helps in creating the microporous structures within the membrane cross-section as shown in **Figure 3.34**. These structures acts as transport channels to permeate water molecules through the stacked layers of GO/Fe_3O_4. The water flux of

GO/Fe_3O_4 based membrane was 756 $Lm^{-2}h^{-1}$ while that of Ag-GO/Fe_3O_4 based membrane was 801 $Lm^{-2}h^{-1}$ respectively. BSA flux of nanofiller based membranes was also increased in comparison to the pure PVDF-*co*-HFP membrane. The BSA flux of pure PVDF-*co*-HFP membrane was 66 which increases to 356 $Lm^{-2}h^{-1}$ and 392 $Lm^{-2}h^{-1}$. The lower BSA flux value as compared to the elevated water flux was associated with adsorption of BSA molecules either on the membrane surface or within the cross-section. Figure represents the water flux and BSA flux of fabricated membranes.

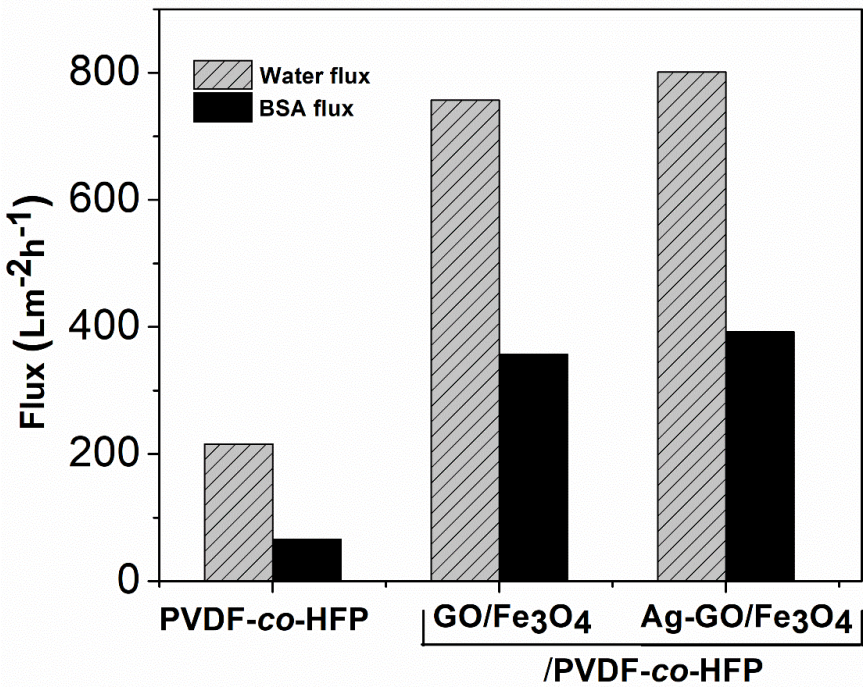

Figure 3.37. Water flux and BSA flux of GO/Fe_3O_4 and Ag-GO/Fe_3O_4 based membranes

3.3.3.3. BSA Rejection of GO/Fe_3O_4 and Ag-GO/Fe_3O_4 based Membranes

BSA was used as a model foulant to study the protein adsorption by GO/Fe_3O_4 and Ag-GO/Fe_3O_4. BSA rejection of PVDF-*co*-HFP membrane and nanofillers based membranes is shown in **Figure 3.38**. In case of pure PVDF-*co*-HFP membrane the BSA rejection was 85.5% which increases to 96% and 98% by assimilation of GO/Fe_3O_4 and Ag-GO/Fe_3O_4 respectively. The wrapping of Fe_3O_4 nanoparticles with GO sheets increases the specific surface area of GO/Fe_3O_4 nanofiller. The increased surface area along with abundant

oxygenated functionalities on the GO surface boosts the adsorption capacity of GO/Fe_3O_4 [135].

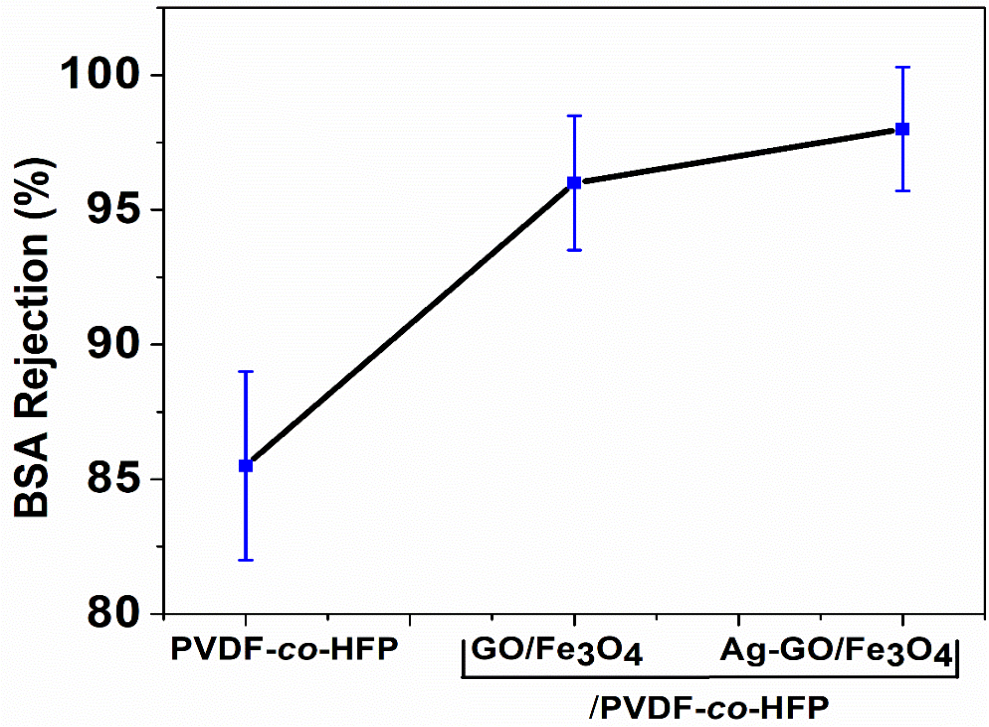

Figure 3.38. BSA Rejection of GO/Fe_3O_4 and Ag-GO/Fe_3O_4 based membranes

3.3.3.4. Antifouling Properties of GO/Fe_3O_4 and Ag-GO/Fe_3O_4 based Membranes

Fouling of polymer membranes is a major concern in waste water treatment. Fouling is directly associated with hydrophobic character of applied membrane. **Figure 3.39** shows the total fouling, reversible fouling and irreversible fouling of pristine PVDF-*co*-HFP membrane and nanofiller based polymer membranes. As confirmed from the water contact angle results (**Figure 3.36**) the PVDF-*co*-HFP membrane comprises a highly hydrophobic character leading to the highest total fouling ratio (69.4%) and highest irreversible (49.1%) fouling as well. The GO/Fe_3O_4 and Ag-GO/Fe_3O_4 nanofillers decreases the total fouling ratio to 52.8% and 51.0%. The reversible fouling ratio was highest for Ag-GO/Fe_3O_4 (43.4%) based membranes which indicate the highly antifouling nature of Ag-GO/Fe_3O_4 nanofiller. From the above discussions, it is obvious that magnetic graphene oxide plays a crucial role in controlling the permeability and fouling of polymer membranes.

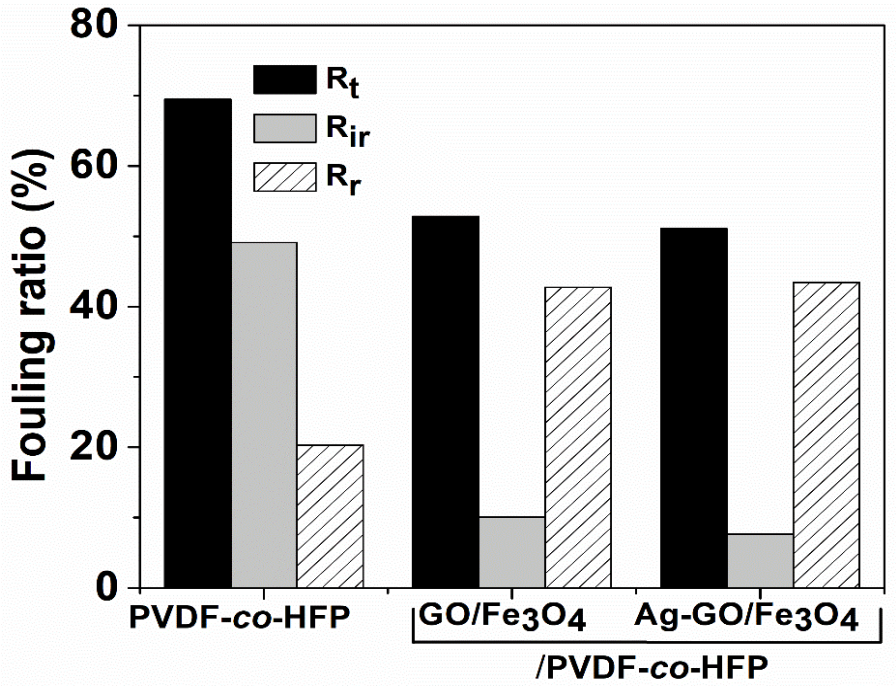

Figure 3.39. Antifouling properties of GO/Fe_3O_4 and Ag-GO/Fe_3O_4 based membranes

3.3.3.5. Flux Recovery Ratio of GO/Fe_3O_4 and Ag-GO/Fe_3O_4 based Membranes

Flux recovery ratio is an important parameter while analyzing the reusability of fabricated membranes. The fabricated membranes used to measure the water and BSA fluxes were washed with pure water to remove the physically adsorbed foulant molecules, followed by measuring the water and BSA flux again. By comparing the fluxes of two consecutive filtration cycles it was noticed that the PVDF-*co*-HFP membrane exhibit the lowest flux recovery ratio (50.8%) (**Figure 3.40**). This poor flux recovery was due to the hydrophobic character of PVDF-*co*-HFP membrane which resulted in increased fouling of membrane surface. This surface fouling leads to pore blockage, hence reduces the permeability of membrane. However, by using the highly hydrophilic and antifouling GO/Fe_3O_4 and Ag-GO/Fe_3O_4 nanofillers the flux recovery ratio improves upto 89.9% and 92.3%. This increased flux recovery proclaimed the reusability and better life span of fabricated nanocomposite membranes.

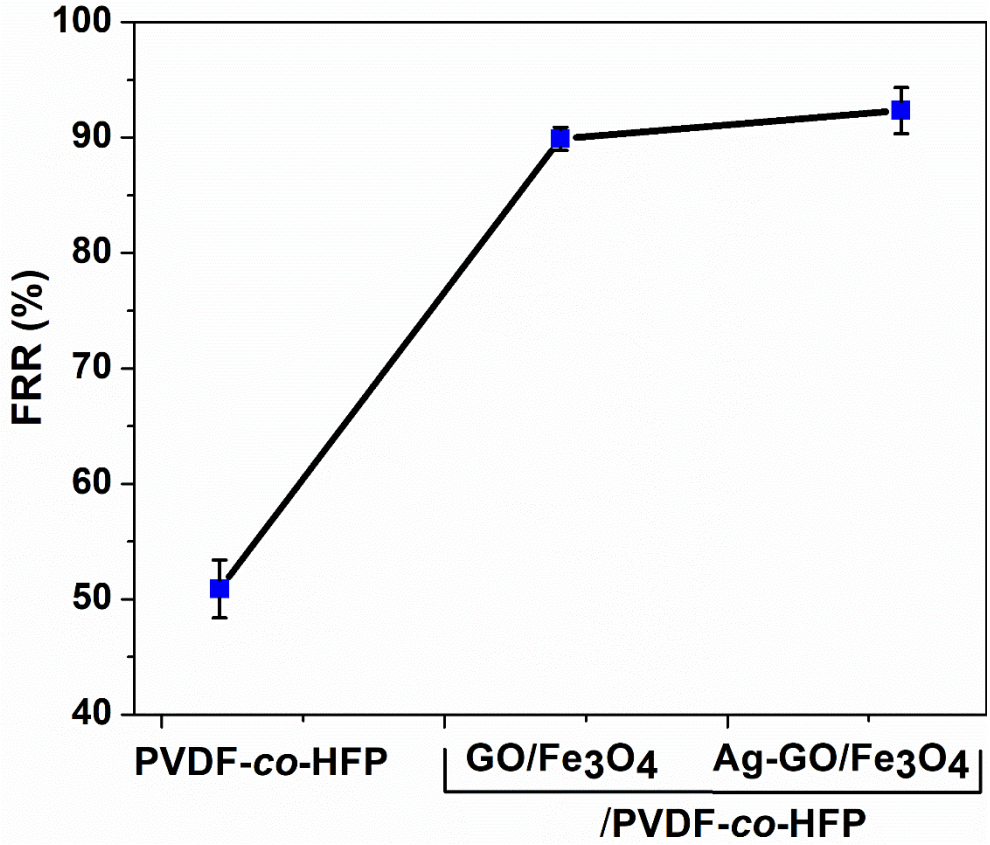

Figure 3.40. Flux recovery ratio (FRR%) of GO/Fe_3O_4 and $Ag\text{-}GO/Fe_3O_4$ based membranes

3.4. Comparison with Literature

Table 3.1. compares the performance of fabricated membranes with some other membranes from literature. Comparison was made interms of water flux, rejection and flux recovery ratio of membranes by the addition of different modifiers. Ahmed et al. [185] reported the synthesis of pluronic F127/polyacrylonitrile/ bentonite-PVC membrane for ultrafiltration. The fabricated membrane possesses excellent features interms of ultralow water contact angle, increased antifouling property with > 97% oil removal efficiency. Alardhi et al. [186] proclaimed the use of PVC hollow fiber membranes for the rejection of methyl green from simulated waste water with a removal efficiency of 59.46% and permeate flux of 32.71 $L/h.m^2$. Karim et al. [187] designed an ultrafiltration membrane based on $Ag\text{-}TiO_2$ and α-aminophosphonate modified montmorillonite (MMT). The composite membrane comprises excellent permeate flux 400 $Lm^{-2}h^{-1}$ and reduced protein

fouling. Abdel-Wahed et al. [188] demonstrate the use of ZnO-TiO_2 based ceramic glass material as photocatalyst for decontamination of textile waste water. ZnO-TiO_2 photocatalyst exhibit maximum efficiency of 53% for removal of humic acid. Ali et al. [189] deliberate the use of activated carbon and zirconium oxide (ZrO_2) for the photodegradation of 4-octylphenol. Table 3.1 depicts the outstanding permeate flux of modified GO based nanocomposite membranes as compared to many other membranes. This comparison supports the use of GO-Ag, PEG/GO-Ag, GO/Fe_3O_4 and Ag-GO/Fe_3O_4 nanofillers as a surface modifier, as well as a highly hydrophilic and antifouling adsorbent to treat the biofouling of polymer membranes.

Table No 3.1. Comparison of our work with already reported literature

Polymer	Modifier	Casting Method	Water Flux ($Lm^{-2}h^{-1}$)	FRR (%)	Rejection (%)	Ref.
PVC	GO-nanodimond	Phase inversion	440	83.0	95 (BSA)	[90]
PVC	Graphene-quantum dots	Phase inversion	19.4	~ 80	98 (BSA)	[190]
PVC	PEGMA	Phase separation	472.14	> 65	95.72 (Salt)	[191]
PVDF	S-GO	Phase separation	740	88.7	98 (BSA)	[161]
PES	C-GO/Fe_3O_4	spinning	110	97.8	99.5 (HSA)	[192]
PES	GO/Fe_3O_4	Phase separation	252	87.9	92.0 (BSA)	[135]
PVC	Cellulose acetate	Phase inversion	85	78	78.4 (BSA)	[193]
P-sulfone	GO-Titania	Phase separation	13.05	-	91.27 (NH_3)	[194]
P-sulfone	GO-gum Arabica	Phase inversion	63.55	88	95 (HA)	[195]
PVC	AgNPs/ Silica	Wet spinning	418	99.8	94 COD	[196]
PVC	Halloysite nanotubes	Phase separation	212.2	92.1	93 BSA	[197]
PVC	ZnO	Phase inversion	66.7	87	73.6 (COD)	[198]

PVC	Pluronic F127/Bentonite	Phase inversion	607.8	71.65	92.8 (OIL)	[199]
PES	$Cu@Fe_3O_4$	Phase separation	43.3	80.1	90 (BSA)	[200]
PVC	GO-Ag	Resin infiltration	613	85.64	92.1 (BSA)	This work
PVDF-*co*-HFP	PEG/GO-Ag	Resin infiltration	906	91.3	95.1 (BSA)	This work
PVDF-*co*-HFP	GO/Fe_3O_4	Resin infiltration	756	89.94	96 (BSA)	This work
PVDF-*co*-HFP	$Ag\text{-}GO/Fe_3O_4$	Resin infiltration	801	92.38	98 (BSA)	This work

3.5. Membrane Cost Analysis and Comparison

Polymer membranes undergo complex fouling due to accumulation of organic and inorganic foulants either on the membrane surface or within the cross-sectional microporous structures. This fouling results in the formation of a cake/gel layer, deteriorating the water quality and resulting in poor water flux. So, the fouling leads to quick replacement of membrane filters. This continued replacement of membrane filters affects the cost of filtration system. The present work is focused on controlling the fouling of polymer membranes by using modified GO (GO-Ag, PEG-GO-Ag, GO/Fe_3O_4 and $Ag\text{-}GO/Fe_3O_4$) based nanocomposites.

Polymer membranes cost is dependent on the

- Cost of precursors
- Cost of synthesis reactions
- Cost of membrane preparation
- Cost of physiochemical characterization
- Cost of operating
- Cost of maintenance (cleaning or replacement (fouling/accident))
- Cost of Labor

The costs of commercially available membrane filters of polycarbonate (PC), polyether sulfone (PES), polytetrafluoroethylene (PTFE) and polyvinylidene fluoride (PVDF) are shown in **Table 3.2**. The cost of the membrane precursors and synthesis steps mainly control the cost of the product. We have used graphite powder as main precursor to synthesize GO which is relatively cheaper than polymers. Besides this, as we use nanocomposite to form a layer pattern, very little quantity of polymer is used in this project as compare to the pristine polymer membranes. Both the low cost precursors, easy fabrication strategies and high antifouling features, along with excellent flux recovery and reusability makes the present work highly economical and affordable.

Table 3.2. Cost comparison of different polymer membranes 50 pieces /pack

Membrane	Pore size	Thickness	Price (Rupees)
PC	0.2µm	25mm	106,268 Rs.
PES	0.2µm	25mm	57908 Rs.
PTFE	0.2µm	25mm	69613 Rs.
PVDF	0.2µm	25mm	57600 Rs.

Although the cost of membrane filters varies, depending on manufacturing conditions. Generally, the cost of high quality graphite powder/100mg is 7000 Rupees. The quantity of GO product depends on the extent of oxidation. In the present study, for each gram of graphite powder used almost 0.98g of GO was obtained, which suggest negligible loss of main precursor. So this study can be helpful in synthesizing the cost effective GO based polymer nanofiller composite membranes.

CONCLUSION

Membrane fouling is a pervasive problem effecting the economy and efficiency of polymer based membrane separation technology. Herein, we synthesized highly hydrophilic and antifouling nanofillers to compensate the hydrophobicity and fouling of polymer membranes. Graphene oxide (GO) was synthesized (from graphite powder by Hummer's method) and modified with silver nanoparticles (AgNPs), polyethylene glycol (PEG) and magnetic iron oxide (Fe_3O_4). Six series of polymer nanocomposite membranes PVC/GO, PVC/GOAg, PVDF-*co*-HFP/GO-Ag, and PVDF-*co*-HFP/PEG-GO-Ag, PVDF-*co*-HFP/GO/Fe_3O_4 and PVDF-*co*-HFP/Ag-GO/Fe_3O_4 were fabricated by incorporating the modified GO based nanofillers. Fourier transform infrared spectroscopy (FTIR), X-ray diffraction (XRD), Raman spectroscopy, scanning electron microscopy (SEM), transmission electron microscopy (TEM) and electron dispersive X-ray (EDX) analysis were used to explore the structural and chemical features of nanocomposites and their perspective membranes. The incorporation of GO-Ag nanofiller (0.5 wt.%) enhances the water flux and BSA rejection of PVC membrane from 192 $Lm^{-2}h^{-1}$ to 613 $Lm^{-2}h^{-1}$and 81.5% to 92.1%. The irreversible fouling ratio of PVC membrane was decreased from 54.6% to 14.4%. Similarly, the PEG/GO-Ag nanofiller (1.0 wt.%) raises the water flux of PVDF-*co*-HFP membrane from 216 $Lm^{-2}h^{-1}$ to 906 $Lm^{-2}h^{-1}$ by lowering the water contact angle from 115°.02 to 38°.77. Water flux and BSA rejection of PVDF-*co*-HFP membrane was improved upto 801 $Lm^{-2}h^{-1}$ and 98% by using Ag-GO/Fe_3O_4 nanofiller. Flux recovery ratio (FRR) for PVC/GO-Ag (0.5 wt.%) membrane was 85% while that of PVDF-*co*-HFP/PEG-GO-Ag (1.0 wt.%) membrane was 91% and PVDF-*co*-HFP/Ag-GO/Fe_3O_4 (1.0 wt.%) was 92% respectively. Besides this, the reversible fouling ratio of all the nanofiller based membranes increased drastically favoring the high antifouling property of fabricated membranes. The GO-Ag nanofiller was tested to be effective against *Escherichia coli*. The present study also constrains an easy and effective strategy to synthesize the GO/Fe_3O_4 and Ag-GO/Fe_3O_4 nanofillers based magnetically active membranes without using any external magnetic field. TGA stipulate the high thermal stability of all the nanocomposite based membranes. Inspired from the high permeability, increased BSA rejection, antifouling properties and thermal stability the modified GO nanofillers GO-Ag, PEG-GO-Ag,

GO/Fe_3O_4 and Ag-GO/Fe_3O_4 could offer a great potential in combating the clean water scarcity by optimizing the quality of high performance membrane filters.

FUTURE PROSPECTS

Because of high hydrophilicity, excellent antifouling property and enhanced thermal stability the GO-Ag, PEG/GO-Ag, GO/Fe_3O_4 and Ag-GO/Fe_3O_4 nanocomposite can help in tailoring the hydrophobic challenges of polymeric membranes. Although all nanocomposite based membranes possessed enhanced performance interms of water flux and BSA rejection, there is a need to improve the BSA rejection without compromising water flux. The synthesized membranes can be used for waste water treatment, heavy metal adsorption etc. The modified GO nanofiller have vast majority of applications in target drug delivery, bone regeneration, artificial muscle formation and coating of medical equipment's etc. However, these membranes still need a lot of modifications and tests to be used in food packaging and other real life applications. Resin infiltration method can be used to fabricate high performance magnetic membranes without using any magnetic field to move the nanoparticles to the membrane surface. Besides these, high thermal stability of synthesized nanocomposite membranes suggests their flame retardancy applications. So the present study is a gateway to explore the GO based membranes to tackle the environmental challenges.

6. REFERENCES

1. Association, A. P. H., Standard methods for the examination of water and wastewater. *American Public Health Association*.: **1926,** 6.

2. Tan, F.; Liu, M.; Li, K.; Wang, Y.; Wang, J.; Guo, X.; Zhang, G.; Song, C., Facile synthesis of size-controlled MIL-100 (Fe) with excellent adsorption capacity for methylene blue. *J. Chem. Eng.* **2015,** *281*, 360-367.

3. Boczkaj, G.; Fernandes, A., Wastewater treatment by means of advanced oxidation processes at basic pH conditions: A review. *J. Chem. Eng.* **2017,** *320*, 608-633.

4. Nasrollahi, N.; Ghalamchi, L.; Vatanpour, V.; Khataee, A.; Yousefpoor, M., Novel polymeric additives in the preparation and modification of polymeric membranes: A comprehensive review. *J. Ind. Eng. Chem.* **2022,** *109*, 100-124.

5. Wu, Y.; Chen, M.; Lee, H.-J.; A. Ganzoury, M.; Zhang, N.; de Lannoy, C.-F., Nanocomposite Polymeric Membranes for Organic Micropollutant Removal: A Critical Review. *ACS ES&T Engineering* **2022,** *2* (9), 1574-1598.

6. Isloor, A. M.; Ganesh, B.; Isloor, S. M.; Ismail, A.; Nagaraj, H.; Pattabi, M., Studies on copper coated polysulfone/modified poly isobutylene alt-maleic anhydride blend membrane and its antibiofouling property. *Desalination* **2013,** *308*, 82-88.

7. Méricq, J.-P.; Mendret, J.; Brosillon, S.; Faur, C., High performance PVDF-TiO2 membranes for water treatment. *Chem. Eng. Sci.* **2015,** *123*, 283-291.

8. Vatsha, B.; Ngila, J. C.; Moutloali, R. M., Preparation of antifouling polyvinylpyrrolidone (PVP 40K) modified polyethersulfone (PES) ultrafiltration (UF) membrane for water purification. *Phys. Chem. Earth.* **2014,** *67*, 125-131.

9. Kim, H. Y.; Cho, Y.; Kang, S. W., Porous cellulose acetate membranes prepared by water pressure-assisted process for water-treatment. *J. Ind. Eng. Chem.* **2019,** *78*, 421-424.

10 Tarboush, B. J. A.; Rana, D.; Matsuura, T.; Arafat, H.; Narbaitz, R., Preparation of thin-film-composite polyamide membranes for desalination using novel hydrophilic surface modifying macromolecules. *J. Membr. Sci.* **2008,** *325* (1), 166-175.

11. Ahmad, T.; Guria, C., Progress in the modification of polyvinyl chloride (PVC) membranes: A performance review for wastewater treatment. *J. Water Process Eng.* **2022,** *45*, 102466.

12. Rana, D.; Matsuura, T., Surface modifications for antifouling membranes. *Chem. Rev.* **2010,** *110* (4), 2448-2471.

13. Kochkodan, V.; Johnson, D. J.; Hilal, N., Polymeric membranes: Surface modification for minimizing (bio) colloidal fouling. *Adv. Colloid Interface Sci.* **2014,** *206*, 116-140.

14. Bellona, C.; Drewes, J. E.; Xu, P.; Amy, G., Factors affecting the rejection of organic solutes during NF/RO treatment—a literature review. *Water Res.* **2004,** *38* (12), 2795-2809.

15. Ulbricht, M., Advanced functional polymer membranes. *J. Polym.* **2006,** *47* (7), 2217-2262.

16. Baek, Y.; Yu, J.; Kim, S.-H.; Lee, S.; Yoon, J., Effect of surface properties of reverse osmosis membranes on biofouling occurrence under filtration conditions. *J. Membr. Sci.* **2011,** *382* (1-2), 91-99.

17. Baker, R. W., Membrane Technology and Applications, John Wiley & Sons. *Ltd., New York, NY* **2004**.

18. Escobar, I. C.; Hoek, E. M.; Gabelich, C. J.; DiGiano, F. A., Committee report: recent advances and research needs in membrane fouling. *J. AWWA.* **2005,** *97* (8), 79.

19. Matin, A.; Khan, Z.; Zaidi, S.; Boyce, M., Biofouling in reverse osmosis membranes for seawater desalination: phenomena and prevention. *Desalination* **2011,** *281*, 1-16.

20. Cadotte, J. E.; Petersen, R.; Larson, R.; Erickson, E., A new thin-film composite seawater reverse osmosis membrane. *Desalination* **1980,** *32*, 25-31.

21. Jeong, B.-H.; Hoek, E. M.; Yan, Y.; Subramani, A.; Huang, X.; Hurwitz, G.; Ghosh, A. K.; Jawor, A., Interfacial polymerization of thin film nanocomposites: a new concept for reverse osmosis membranes. *J. Membr. Sci.* **2007,** *294* (1-2), 1-7.

22. Vijay, Y.; Acharya, N.; Wate, S.; Avasthi, D., Characterization of track etched membranes by gas permeation. *Int. J. Hydrogen. Energy.* **2004,** *29* (5), 515-519.

23. Bryak, M.; Gancarz, I., Plasma modification of polymer membranes. *J. Membr. Modif: Techn. Appl.*, CRC Press New York: 2012; pp 179-214.

24. Khulbe, K.; Feng, C.; Matsuura, T., The art of surface modification of synthetic polymeric membranes. *J. Appl. Polym. Sci.* **2010,** *115* (2), 855-895.

25. Ighalo, J. O.; Yap, P.-S.; Iwuozor, K. O.; Aniagor, C. O.; Liu, T.; Dulta, K.; Iwuchukwu, F. U.; Rangabhashiyam, S., Adsorption of persistent organic pollutants (POPs) from the aqueous environment by nano-adsorbents: A review. *Environ. Res. J.* **2022,** *212*, 113123.

26. Ajala, O. J.; Tijani, J. O.; Bankole, M. T.; Abdulkareem, A. S., A critical review on graphene oxide nanostructured material: Properties, Synthesis, characterization and application in water and wastewater treatment. *J. Environ. Nanotechnol.* **2022,** *18*, 100673.

27. Cheng, P.; Liu, Y.; Yi, Z.; Wang, X.; Li, M.; Liu, Q.; Liu, K.; Wang, D., In situ prepared nanosized Pt-Ag/PDA/PVA-co-PE nanofibrous membrane for highly-efficient catalytic reduction of p-nitrophenol. *Compos. Commun.* **2018,** *9*, 11-16.

28. Subair, R.; Tripathi, B. P.; Formanek, P.; Simon, F.; Uhlmann, P.; Stamm, M., Polydopamine modified membranes with in situ synthesized gold nanoparticles for catalytic and environmental applications. *J. Chem. Eng.* **2016,** *295*, 358-369.

29. Liu, S.; Chen, J.; Sun, J., Preparation and Properties of Nano Platinum/Carbon Nanotubes/Bacterial Cellulose Conductive Hydrogel Electrode Films. *IJBLS* **2023,** *2* (3), 87-91.

30. De Faria, A. F.; Perreault, F.; Shaulsky, E.; Arias Chavez, L. H.; Elimelech, M., Antimicrobial electrospun biopolymer nanofiber mats functionalized with graphene oxide–silver nanocomposites. *ACS. Appl. Mater. Interfaces* **2015,** *7* (23), 12751-12759.

31. Mahmoudi, E.; Ng, L. Y.; Ba-Abbad, M. M.; Mohammad, A., Novel nanohybrid polysulfone membrane embedded with silver nanoparticles on graphene oxide nanoplates. *J. Chem. Eng.* **2015,** *277*, 1-10.

32. Guo, Z.; Lei, K.; Li, Y.; Ng, H. W.; Prikhodko, S.; Hahn, H. T., Fabrication and characterization of iron oxide nanoparticles reinforced vinyl-ester resin nanocomposites. *Compos. Sci. Techn.* **2008,** *68* (6), 1513-1520.

33. Ahmed, F.; Umar, A.; Kumar, S.; Shaalan, N. M.; Arshi, N.; Alam, M. G.; Hasan, P.; Ramay, S. M.; Khan, R.; Aljaafari, A., Manganese dioxide nanoparticles/reduced graphene oxide nanocomposites for hybrid capacitive desalination. *Adv. Compos. Hybrid Mater.***2023,** *6* (1), 19.

34. Guo, Z.; Pereira, T.; Choi, O.; Wang, Y.; Hahn, H. T., Surface functionalized alumina nanoparticle filled polymeric nanocomposites with enhanced mechanical properties. *J. Mater. Chem.* **2006,** *16* (27), 2800-2808.

35. Irshad, M. A.; Nawaz, R.; ur Rehman, M. Z.; Adrees, M.; Rizwan, M.; Ali, S.; Ahmad, S.; Tasleem, S., Synthesis, characterization and advanced sustainable applications of titanium dioxide nanoparticles: A review. *Ecotoxicol. Environ Safety* **2021,** *212*, 111978.

36. Park, J. E.; Shin, J.-H.; Oh, W.; Choi, S.-J.; Kim, J.; Kim, C.; Jeon, J., Removal of hexavalent chromium (VI) from wastewater using chitosan-coated iron oxide nanocomposite membranes. *Toxics* **2022,** *10* (2), 98.

37. Jahankhah, S.; Sabzehmeidani, M. M.; Ghaedi, M.; Dashtian, K.; Abbasi-Asl, H., Fabrication polyvinyl chloride mixed matrix membrane via embedding Fe_3O_4/polydopamine/Ag nanocomposite for water treatment. *Mater. Sci. Eng. B* **2022,** *285*, 115935.

38. Naseem, S.; Wu, C.-M.; Motora, K. G., Novel multifunctional RbxWO3@ Fe3O4 immobilized Janus membranes for desalination and synergic-photocatalytic water purification. *Desalination* **2021,** *517*, 115256.

39. Jamkhande, P. G.; Ghule, N. W.; Bamer, A. H.; Kalaskar, M. G., Metal nanoparticles synthesis: An overview on methods of preparation, advantages and disadvantages, and applications. *J. Drug Deliv. Sci. Tech.* **2019,** *53*, 101174.

40. Iravani, S., Green synthesis of metal nanoparticles using plants. *Green Chemistry* **2011,** *13* (10), 2638-2650.

41. Kumar, V.; Alam, M. N.; Manikkavel, A.; Song, M.; Lee, D.-J.; Park, S.-S., Silicone rubber composites reinforced by carbon nanofillers and their hybrids for various applications: A review. *Polymers* **2021,** *13* (14), 2322.

42. Hong, P. N.; Minh, D. N.; Van Hung, N.; Minh, P. N.; Khoi, P. H., Carbon nanotube and graphene aerogels—The world's 3D lightest materials for environment applications: A review. *Int. J. Mater. Sci. Appl* **2017,** *6*, 277.

43. Bhakta, A. K.; Kumari, S.; Hussain, S.; Martis, P.; Mascarenhas, R. J.; Delhalle, J.; Mekhalif, Z., Synthesis and characterization of maghemite nanocrystals decorated multi-wall carbon nanotubes for methylene blue dye removal. *J. Mater. Sci.* **2019,** *54* (1), 200-216.

44. Zheng, S.; Hao, L.; Zhang, L.; Wang, K.; Zheng, W.; Wang, X.; Zhou, X.; Li, W.; Zhang, L., Tea polyphenols functionalized and reduced graphene oxide-ZnO composites for selective Pb^{2+} removal and enhanced antibacterial activity. *J. Biomed. Nanotechnol.* **2018,** *14* (7), 1263-1276.

45. Yang, F.; Huo, D.; Zhang, J.; Lin, T.; Zhang, J.; Tan, S.; Yang, L., Fabrication of graphene oxide/copper synergistic antibacterial coating for medical titanium substrate. *J. Colloid. Interf. Sci.* **2023,** *638*, 1-13.

46. Hamouda, H. I.; Selim, M. S.; Higazy, S. A.; Shabana, S.; Hao, Z.; Liu, C., Novel nanoblades of graphene oxide decorated with zinc oxide nanocomposite as a powerful anti-microbial active weapon. *Synth. Met.* **2023,** *296*, 117349.

47. Hussain, N.; Bilal, M.; Iqbal, H. M., Carbon-based nanomaterials with multipurpose attributes for water treatment: Greening the 21st-century nanostructure materials deployment. *Biomater. Polym. Hori.* **2022,** *1* (1), 48-58.

48. Kausar, A.; Ilyas, H.; Siddiq, M., Current research status and application of polymer/carbon nanofiller buckypaper: A review. *Polym. Plast. Techn. Eng.***2017,** *56* (16), 1780-1800.

49. Hosseinzadeh, A.; Bozorg, A.; Ranjbar, P. R., Magnetic graphene oxide functionalized with crystalline nanocellulose and zwitterionic polymers to achieve UF nanocomposite membranes of advanced performance. J. Environ. Chem. Eng. **2023,** *11* (1), 109198.

50. Zhong, D.; Zhang, J.; Lv, L.; Lv, Y.; Jiang, Y., Magnetically Ultrastabilized Graphene Oxide-Based Membrane Filter for Point-of-Use Water Treatment. *ACS ES&T Engineering* **2022,** *2* (5), 769-779.

51. Rastgar, M.; Shakeri, A.; Bozorg, A.; Salehi, H.; Saadattalab, V., Highly-efficient forward osmosis membrane tailored by magnetically responsive graphene oxide/Fe3O4 nanohybrid. *Appl. Surf. Sci.* **2018,** *441*, 923-935.

52. Zhu, Y.; Murali, S.; Cai, W.; Li, X.; Suk, J. W.; Potts, J. R.; Ruoff, R. S., Graphene and graphene oxide: synthesis, properties, and applications. *Adv. Mater.* **2010,** *22* (35), 3906-3924.

53. Lerf, A.; He, H.; Forster, M.; Klinowski, J., Structure of graphite oxide revisited. *The J. Phys. Chem. B* **1998,** *102* (23), 4477-4482.

54. Kudin, K. N.; Ozbas, B.; Schniepp, H. C.; Prud'Homme, R. K.; Aksay, I. A.; Car, R., Raman spectra of graphite oxide and functionalized graphene sheets. *Nano Lett.* **2008,** *8* (1), 36-41.

55. Ammar, A.; Al-Enizi, A. M.; AlMaadeed, M. A.; Karim, A., Influence of graphene oxide on mechanical, morphological, barrier, and electrical properties of polymer membranes. *Arab. J. chem.* **2016,** *9* (2), 274-286.

56. Liu, L.; Wang, L.; Gao, J.; Zhao, J.; Gao, X.; Chen, Z., Amorphous structural models for graphene oxides. *Carbon* **2012,** *50* (4), 1690-1698.

57. Mao, S.; Pu, H.; Chen, J., Graphene oxide and its reduction: modeling and experimental progress. *RSC. Adv.* **2012,** *2* (7), 2643-2662.

58. Saxena, S.; Tyson, T. A.; Shukla, S.; Negusse, E.; Chen, H.; Bai, J., Investigation of structural and electronic properties of graphene oxide. *Appl. Phys. Lett.* **2011,** *99* (1).

59. Nakajima, T.; Matsuo, Y., Formation process and structure of graphite oxide. *Carbon* **1994,** *32* (3), 469-475.

60. Lerf, A.; He, H.; Riedl, T.; Forster, M.; Klinowski, J., 13C and 1H MAS NMR studies of graphite oxide and its chemically modified derivatives. *Solid State Ion.* **1997,** *101*, 857-862.

61. Szabó, T.; Berkesi, O.; Forgó, P.; Josepovits, K.; Sanakis, Y.; Petridis, D.; Dékány, I., Evolution of surface functional groups in a series of progressively oxidized graphite oxides. *Chem. Mater.* **2006,** *18* (11), 2740-2749.

62. Brodie, B. C., XIII. On the atomic weight of graphite. *Philos. Trans. R. Soc. L.* **1859,** (149), 249-259.

63. Chen, J.; Li, Y.; Huang, L.; Li, C.; Shi, G., High-yield preparation of graphene oxide from small graphite flakes via an improved Hummers method with a simple purification process. *Carbon* **2015,** *81*, 826-834.

64. Sai, P. S. T.; Sharma, K.; Devarayapalli, K.; Rao, J. R., GO-TiO2 nano composites for silicon PV cell application. Philos. Trans. R. Soc. L **2015,** *2* (9), 4557-4562.

65. Marcano, D. C.; Kosynkin, D. V.; Berlin, J. M.; Sinitskii, A.; Sun, Z.; Slesarev, A.; Alemany, L. B.; Lu, W.; Tour, J. M., Improved synthesis of graphene oxide. *ACS Nano.* **2010,** *4* (8), 4806-4814.

66.Tang, L.; Li, X.; Ji, R.; Teng, K. S.; Tai, G.; Ye, J.; Wei, C.; Lau, S. P., Bottom-up synthesis of large-scale graphene oxide nanosheets. *J. Mater. Chem.***2012,** *22* (12), 5676-5683.

67. Sreeprasad, T. S.; Maliyekkal, S. M.; Lisha, K. P.; Pradeep, T., Reduced graphene oxide–metal/metal oxide composites: facile synthesis and application in water purification. *J. Hazard. Mater.* **2011,** *186* (1), 921-931.

68. Mohan, D.; Pittman Jr, C. U., Arsenic removal from water/wastewater using adsorbents—a critical review. *J. Hazard. Mater.* **2007,** *142* (1-2), 1-53.

69. Zhang, K.; Dwivedi, V.; Chi, C.; Wu, J., Graphene oxide/ferric hydroxide composites for efficient arsenate removal from drinking water. *J. Hazard. Mater.* **2010,** *182* (1-3), 162-168.

70. Chandra, V.; Park, J.; Chun, Y.; Lee, J. W.; Hwang, I.-C.; Kim, K. S., Water-dispersible magnetite-reduced graphene oxide composites for arsenic removal. *ACS nano* **2010,** *4* (7), 3979-3986.

71. Yang, S.-T.; Chang, Y.; Wang, H.; Liu, G. Chen, S.; Wang, Y.; Liu, Y.; Cao, A., Folding/aggregation of graphene oxide and its application in Cu^{2+} removal. *J. Colloid. Interf. Sci.* **2010,** *351* (1), 122-127.

72. Kausar, A.; Ilyas, H.; Siddiq, M., Aptitude of graphene oxide–silver in advance polymer nanocomposite: a review. *Polym. Plast. Techn. Eng.* **2018,** *57* (4), 283-301.

73. Dinh, N. X.; Chi, D. T.; Lan, N. T.; Lan, H.; Van Tuan, H.; Van Quy, N.; Phan, V. N.; Huy, T. Q.; Le, A.-T., Water-dispersible silver nanoparticles-decorated carbon nanomaterials: synthesis and enhanced antibacterial activity. *Appl. Phys. A.* **2015,** *119*, 85-95.

74. Bao, Q.; Zhang, D.; Qi, P., Synthesis and characterization of silver nanoparticle and graphene oxide nanosheet composites as a bactericidal agent for water disinfection. *J. Colloid. Interf. Sci.* **2011,** *360* (2), 463-470.

75. Chung, Y. T.; Mahmoudi, E.; Mohammad, A. W.; Benamor, A.; Johnson, D.; Hilal, N., Development of polysulfone-nanohybrid membranes using ZnO-GO composite for enhanced antifouling and antibacterial control. *Desalination* **2017,** *402*, 123-132.

76. Yu, L.; Zhang, Y.; Zhang, B.; Liu, J.; Zhang, H.; Song, C., Preparation and characterization of HPEI-GO/PES ultrafiltration membrane with antifouling and antibacterial properties. *J. Membr. Sci.* **2013,** *447*, 452-462.

77. Liu, L.; Bai, H.; Liu, J.; Sun, D. D., Multifunctional graphene oxide-TiO2-Ag nanocomposites for high performance water disinfection and decontamination under solar irradiation. *J. Hazard. Mater.* **2013,** *261*, 214-223.

78. Hosseini, M.; Azamat, J.; Erfan-Niya, H., Improving the performance of water desalination through ultra-permeable functionalized nanoporous graphene oxide membrane. *Appl. Surf. Sci.* **2018,** *427*, 1000-1008.

79. Liu, K.-K.; Jiang, Q.; Tadepalli, S.; Raliya, R.; Biswas, P.; Naik, R. R.; Singamaneni, S., Wood–graphene oxide composite for highly efficient solar steam generation and desalination. *ACS. Appl. Mater. Interfaces* **2017,** *9*, 7675-7681.

80. Yang, E.; Kim, C.-M.; Song, J.-h.; Ki, H.; Ham, M.-H.; Kim, I. S., Enhanced desalination performance of forward osmosis membranes based on reduced graphene oxide laminates coated with hydrophilic polydopamine. *Carbon* **2017,** *117*, 293-300.

81. Finnerty, C.; Zhang, L.; Sedlak, D. L.; Nelson, K. L.; Mi, B., Synthetic graphene oxide leaf for solar desalination with zero liquid discharge. Environ. Sci. Technol. **2017,** *51*, 11701-11709.

82. Hegab, H. M.; ElMekawy, A.; Barclay, T. G.; Michelmore, A.; Zou, L.; Losic, D.; Saint, C. P.; Ginic-Markovic, M., A novel fabrication approach for multifunctional

graphene-based thin film nano-composite membranes with enhanced desalination and antibacterial characteristics. *Sci. Rep.* **2017,** *7* (1), 7490.

83. Liang, B.; Zhan, W.; Qi, G.; Lin, S.; Nan, Q.; Liu, Y.; Cao, B.; Pan, K., High performance graphene oxide/polyacrylonitrile composite pervaporation membranes for desalination applications. *J. Mater. Chem. A.* **2015,** *3* (9), 5140-5147.

84. Abraham, J.; Vasu, K. S.; Williams, C. D.; Gopinadhan, K.; Su, Y.; Cherian, C. T.; Dix, J.; Prestat, E.; Haigh, S. J.; Grigorieva, I. V., Tunable sieving of ions using graphene oxide membranes. *Nat. Nanotechnol.* **2017,** *12* (6), 546-550.

85. Zahirifar, J.; Karimi-Sabet, J.; Moosavian, S. M. A.; Hadi, A.; Khadiv-Parsi, P., Fabrication of a novel octadecylamine functionalized graphene oxide/PVDF dual-layer flat sheet membrane for desalination via air gap membrane distillation. *Desalination.* **2018,** *428*, 227-239.

86. Tang, X.-Z.; Li, X.; Cao, Z.; Yang, J.; Wang, H.; Pu, X.; Yu, Z.-Z., Synthesis of graphene decorated with silver nanoparticles by simultaneous reduction of graphene oxide and silver ions with glucose. *Carbon* **2013,** *59*, 93-99.

87. Cobos Zamarreño, M.; De la Pinta Aresti, I.; Quindós Andrés, G.; Fernández Fernández, M. J.; Fernández Fernández, M. D., Synthesis, Physical, Mechanical and Antibacterial Properties of Nanocomposites Based on Poly (vinyl alcohol)/Graphene Oxide–Silver Nanoparticles. *J. Chem*. **2020**. *67*, 81-90.

88. Tran Thi, V. H.; Pham, T. N.; Pham, T. T.; Le, M. C., Synergistic adsorption and photocatalytic activity under visible irradiation using Ag-ZnO/GO nanoparticles derived at low temperature. *J. Chem.* **2019,** *19*, 2979517.

89. Xu, H.; Ding, M.; Chen, W.; Li, Y.; Wang, K., Nitrogen–doped GO/TiO2 nanocomposite ultrafiltration membranes for improved photocatalytic performance. *Sep Purif Technol.* **2018,** *195*, 70-82.

90. Khakpour, S.; Jafarzadeh, Y.; Yegani, R., Incorporation of graphene oxide/nanodiamond nanocomposite into PVC ultrafiltration membranes. *Chem. Eng. Res. Des.* **2019,** *152*, 60-70.

91. Yu, Y.; Yang, Y.; Yu, L.; Koh, K. Y.; Chen, J. P., Modification of polyvinylidene fluoride membrane by silver nanoparticles-graphene oxide hybrid nanosheet for effective membrane biofouling mitigation. *Chemosphere* **2021,** *268*, 129187.

92. Cobos, M.; De-La-Pinta, I.; Quindós, G.; Fernández, M. J.; Fernández, M. D., Synthesis, physical, mechanical and antibacterial properties of nanocomposites based on poly (vinyl alcohol)/graphene oxide–silver nanoparticles. *Polymers* **2020,** *12* (3), 723.

93. Wen, Y.; Yuan, J.; Ma, X.; Wang, S.; Liu, Y., Polymeric nanocomposite membranes for water treatment: a review. *Environ. Chem. Lett.* **2019,** *17*, 1539-1551.

94. Zodrow, K.; Brunet, L.; Mahendra, S.; Li, D.; Zhang, A.; Li, Q.; Alvarez, P. J., Polysulfone ultrafiltration membranes impregnated with silver nanoparticles show improved biofouling resistance and virus removal. *Water Res.* **2009,** *43* (3), 715-723.

95. Vilar, G.; Fernández-Rosas, E.; Puntes, V.; Jamier, V.; Aubouy, L.; Vázquez-Campos, S. In Monitoring migration and transformation of nanomaterials in polymeric composites during accelerated aging. *J. physc*: conference series, IOP Publishing: 2013; p 012044.

96. Li, X.; Fang, X.; Pang, R.; Li, J.; Sun, X.; Shen, J.; Han, W.; Wang, L., Self-assembly of TiO2 nanoparticles around the pores of PES ultrafiltration membrane for mitigating organic fouling. *J. Membr. Sci.* **2014,** *467*, 226-235.

97. Kamal, A.; Ashmawy, M.; Algazzar, A. M.; Elsheikh, A. H., Fabrication techniques of polymeric nanocomposites: A comprehensive review*: J. Mech. Eng. Sci.* **2022,** *236* (9), 4843-4861.

98. Danda, G.; Drndić, M., Two-dimensional nanopores and nanoporous membranes for ion and molecule transport. *Curr Opin Biotechnol.* **2019,** *55*, 124-133.

99. Priya, A.; Gnanasekaran, L.; Kumar, P. S.; Jalil, A.; Hoang, T. K.; Rajendran, S.; Soto-Moscoso, M.; Balakrishnan, D., Recent trends and advancements in nanoporous membranes for water purification. *Chemosphere* **2022,** *303*, 135205.

100. Lalia, B. S.; Guillen-Burrieza, E.; Arafat, H. A.; Hashaikeh, R., Fabrication and characterization of polyvinylidenefluoride-co-hexafluoropropylene (PVDF-HFP) electrospun membranes for direct contact membrane distillation. *J. Membr. Sci.* **2013,** *428*, 104-115.

101. Lalia, B. S.; Kochkodan, V.; Hashaikeh, R.; Hilal, N., A review on membrane fabrication: Structure, properties and performance relationship. *Desalination* **2013,** *326*, 77-95.

102. Ilyas, H.; Haleem, A.; Iqbal, M.; Siddiq, M., Influence of GO-Ag nano-filler on the antibacterial, antifouling and hydrophilic characteristics of polyvinyl chloride membrane. *J. Water Process Eng.* **2021,** *44*, 102336.

103. Esfahani, M. R.; Aktij, S. A.; Dabaghian, Z.; Firouzjaei, M. D.; Rahimpour, A.; Eke, J.; Escobar, I. C.; Abolhassani, M.; Greenlee, L. F.; Esfahani, A. R., Nanocomposite membranes for water separation and purification: Fabrication, modification, and applications. *Sep Purif Technol.* **2019,** *213*, 465-499.

104. Khan, Z. U.; Khan, W. U.; Ullah, B.; Ali, W.; Ahmad, B.; Yap, P.-S., Graphene oxide/PVC composite papers functionalized with p-Phenylenediamine as high-performance sorbent for the removal of heavy metal ions. *J. Environ. Chem. Eng*. **2021,** *9* (5), 105916.

105. Li, W.-R.; Xie, X.-B.; Shi, Q.-S.; Zeng, H.-Y.; Ou-Yang, Y.-S.; Chen, Y.-B., Antibacterial activity and mechanism of silver nanoparticles on Escherichia coli. *Appl. Microbiol. Biotechol.* **2010,** *85*, 1115-1122.

106. Suhalim, N. S.; Kasim, N.; Mahmoudi, E.; Shamsudin, I. J.; Jamari, N. L.-A.; Mohamed Zuki, F., Impact of Silver-Decorated Graphene Oxide (Ag-GO) towards Improving the Characteristics of Nanohybrid Polysulfone Membranes. *Membr. J.* **2023,** *13*, 602.

107. de Faria, A. F.; de Moraes, A. C. M.; Andrade, P. F.; da Silva, D. S.; do Carmo Gonçalves, M.; Alves, O. L., Cellulose acetate membrane embedded with graphene oxide-silver nanocomposites and its ability to suppress microbial proliferation. *Cellulose.* **2017,** *24*, 781-796.

108. Soroush, A. Development of Antimicrobial Thin-Film Composite Forward Osmosis Membranes by Using Silver Nanoparticles and Graphene Oxide Nanosheets. *Concordia University*, *Doctoral dissertation*. 2015.

109. Vatanpour, V.; Keskin, B.; Mehrabani, S. A. N.; Karimi, H.; Arabi, N.; Behroozi, A. H.; Shokrollahi-far, A.; Gul, B. Y.; Koyuncu, I., Investigation of boron nitride/silver/graphene oxide nanocomposite on separation and antibacterial improvement of polyethersulfone membranes in wastewater treatment. *J. Environ. Chem. Eng*. **2022,** *10*, 107035.

110. Ko, K.; Yu, Y.; Kim, M.-J.; Kweon, J.; Chung, H., Improvement in fouling resistance of silver-graphene oxide coated polyvinylidene fluoride membrane prepared by pressurized filtration. *Sep Purif Technol.* **2018,** *194*, 161-169.

111. Jose, J. K.; Mishra, B.; Kootery, K. P.; Cherian, C. T.; Tripathi, B. P.; Sarojini, S.; Balachandran, M., Fabrication of silver nanoparticle decorated graphene oxide membranes for water purification, antifouling and antibacterial applications. *Mater. Sci. Eng. B* **2023,** *297*, 116789.

112. Isawi, H., Synthesis of graphene oxide-silver (GO-Ag) nanocomposite TFC RO membrane to enhance morphology and separation performances for groundwater desalination, (case study Marsa Alam area-Red Sea). *Chem. Eng. Process.* **2023,** *187*, 109343.

113. Sun, X.-F.; Qin, J.; Xia, P.-F.; Guo, B.-B.; Yang, C.-M.; Song, C.; Wang, S.-G., Graphene oxide–silver nanoparticle membrane for biofouling control and water purification. *J. Chem. Eng.* **2015,** *281*, 53-59.

114. Mahmoudi, E.; ANG, W. L.; Panomsuwan, G.; Jongprateep, O.; Mohammad, A. W.; Ng, L. Y.; Ba-Abbad, M. M., Influence of graphite feedstock on the characteristics of

silver-decorated graphene oxide and antimicrobial property. *J. Met. Mater. Miner.* **2021,** *31* (4), 143-150.

115. Alkhouzaam, A.; Qiblawey, H., Functional GO-based membranes for water treatment and desalination: Fabrication methods, performance and advantages. A review. *Chemosphere* **2021,** *274*, 129853.

116. Zhao, G.; Hu, R.; He, Y.; Zhu, H., Physically coating nanofiltration membranes with graphene oxide quantum dots for simultaneously improved water permeability and salt/dye rejection. *Adv. Mater. Interfaces* **2019,** *6* (5), 1801742.

117. Abdelamir, A. I.; Al-Bermany, E.; Sh Hashim, F. Enhance the optical properties of the synthesis PEG/graphene-based nanocomposite films using GO nanosheets, *In J. of Phys*: *Conference Series, IOP Publishing*: 2019; 022029.

118. Mansourpanah, Y.; Shahebrahimi, H.; Kolvari, E., PEG-modified GO nanosheets, a desired additive to increase the rejection and antifouling characteristics of polyamide thin layer membranes. *Chem. Eng. Res. Des.* **2015,** *104*, 530-540.

119. Wu, L.-g.; Yang, C.-h.; Wang, T.; Zhang, X.-y., Enhanced the performance of graphene oxide/polyimide hybrid membrane for CO2 separation by surface modification of graphene oxide using polyethylene glycol. *Appl. Surf. Sci.* **2018,** *440*, 1063-1072.

120. Chen, J.-J.; Li, Y.; Zheng, X.-M.; He, F.-A.; Lam, K.-H., Enhancement in electroactive crystalline phase and dielectric performance of novel PEG-graphene/PVDF composites. *Appl. Surf. Sci.* **2018,** *448*, 320-330.

121. Jatoi, A. H.; Kim, K. H.; Khan, M. A.; Memon, F. H.; Iqbal, M.; Janwery, D.; Phulpoto, S. N.; Samantasinghar, A.; Choi, K. H.; Thebo, K. H., Functionalized graphene oxide-based lamellar membranes for organic solvent nanofiltration applications. *RSC Adv.* **2023,** *13* (19), 12695-12702.

122. Jihad, M. A.; Noori, F. T.; Jabir, M. S.; Albukhaty, S.; AlMalki, F. A.; Alyamani, A. A., Polyethylene glycol functionalized graphene oxide nanoparticles loaded with nigella

sativa extract: a smart antibacterial therapeutic drug delivery system. *Molecules* **2021,** *26* (11), 3067.

123. Yuan, P.; Zhang, P.; Liang, T.; Zhai, S., Effects of surface functionalization on thermal and mechanical properties of graphene/polyethylene glycol composite phase change materials. *Appl. Surf. Sci.* **2019,** *485*, 402-412.

124. Veerapandian, M.; Seo, Y.-T.; Yun, K.; Lee, M.-H., Graphene oxide functionalized with silver@ silica–polyethylene glycol hybrid nanoparticles for direct electrochemical detection of quercetin. *Biosens. Bioelectron.* **2014,** *58*, 200-204.

125. Kumar, A.; Kebaili, I.; Boukhris, I.; Vaish, R.; Kumar, A.; Park, H. K. B.; Joo, Y. H.; Sung, T. H., Cotton functionalized with polyethylene glycol and graphene oxide for dual thermoregulating and UV-protection applications. *Sci. Rep.* **2023,** *13* (1), 5923.

126. Orecchioni, M.; Cabizza, R.; Bianco, A.; Delogu, L. G., Graphene as cancer theranostic tool: progress and future challenges. *Theranostics* **2015,** *5* (7), 710.

127. Rout, D. R.; Jena, H. M., Polyethylene glycol functionalized reduced graphene oxide coupled with zinc oxide composite adsorbent for removal of phenolic wastewater. *Environ. Res. J.* **2022,** *214*, 114044.

128. Jeshvaghani, P. A.; Pourmadadi, M.; Yazdian, F.; Rashedi, H.; Khoshmaram, K.; Nigjeh, M. N., Synthesis and characterization of a novel, pH-responsive sustained release nanocarrier using polyethylene glycol, graphene oxide, and natural silk fibroin protein by a green nano emulsification method to enhance cancer treatment. *Int. J. Biol. Macromol.* **2023,** *226*, 1100-1115.

129. Mohammadi, S.; Babaei, A., Poly (vinyl alcohol)/chitosan/polyethylene glycol-assembled graphene oxide bio-nanocomposites as a prosperous candidate for biomedical applications and drug/food packaging industry. *Int. J. Biol. Macromol.* **2022,** *201*, 528-538.

130. Lingamdinne, L. P.; Koduru, J. R.; Karri, R. R., A comprehensive review of applications of magnetic graphene oxide based nanocomposites for sustainable water purification. *J. Environ. Manag.* **2019,** *231*, 622-634.

131. Wang, D.; Liu, L.; Jiang, X.; Yu, J.; Chen, X., Adsorption and removal of malachite green from aqueous solution using magnetic β-cyclodextrin-graphene oxide nanocomposites as adsorbents. *Colloids Surf A.* **2015,** *466*, 166-173.

132. Hosseinzadeh, A.; Ranjbar, P. R.; Bozorg, A., pH-responsive P (AA-b-SBMA)-grafted magnetic GO high-performance ultrafiltration membrane with improved antifouling tendency and cleaning efficiency. *Desalination* **2024**, 117299.

133. Abdi, G.; Alizadeh, A.; Zinadini, S.; Moradi, G., Removal of dye and heavy metal ion using a novel synthetic polyethersulfone nanofiltration membrane modified by magnetic graphene oxide/metformin hybrid. *J. Membr. Sci.* **2018,** *552*, 326-335.

134. Xu, Z.; Wu, T.; Shi, J.; Wang, W.; Teng, K.; Qian, X.; Shan, M.; Deng, H.; Tian, X.; Li, C., Manipulating migration behavior of magnetic graphene oxide via magnetic field induced casting and phase separation toward high-performance hybrid ultrafiltration membranes. *ACS. Appl. Mater. Interfaces* **2016,** *8*, 18418-18429.

135. Mirzaei, M.; Mohammadi, T.; Kasiri, N.; Tofighy, M. A., Fabrication of magnetic field induced mixed matrix membranes containing GO/Fe_3O_4 nanohybrids with enhanced antifouling properties for wastewater treatment applications. J. Environ. Chem. Eng. **2021,** *9*, 105675.

136. Chai, P.; Mahmoudi, E.; Mohammad, A.; Choy, P. Iron oxide decorated graphene oxide embedded polysulfone mixed-matrix membrane: Comparison of different types mixed-matrix membranes on antifouling and performance. *In IOP Conference Series: Earth. Environ. Sci. IOP Publishing*: 2020; 012174.

137. Zhang, X.; Gao, J.; Wei, T.; Wu, D.; Shen, J.; Wei, Y.; Wang, C., Polymer brush grafted immobilized metal ion affinity adsorbent based on polydopamine/polyethyleneimine-coated magnetic graphene oxide for selective enrichment of cytokinins in plants. *Microchim. Acta* **2023,** *190*, 191.

138. Tara, N.; Abomuti, M. A.; Alshareef, F.; Abdullah, O.; Allehyani, E. S.; Chaudhry, S. A.; Oh, S., Nigella sativa-Manganese Ferrite-Reduced Graphene Oxide-Based Nanomaterial: A Novel Adsorbent for Water Treatment. *Molecules* **2023,** *28*, 5007.

139. Alam, S. N.; Sharma, N.; Kumar, L., Synthesis of graphene oxide (GO) by modified hummers method and its thermal reduction to obtain reduced graphene oxide (rGO). *Graphene.* **2017,** *6*, 1-18.

140. Ilyas, H.; Shawuti, S.; Siddiq, M.; Niazi, J. H.; Qureshi, A., PEG functionalized graphene oxide-silver nano-additive for enhanced hydrophilicity, permeability and fouling resistance properties of PVDF-co-HFP membranes. *Colloids Surf A.* **2019,** *579*, 123646.

141. Huang, L.; Yang, H.; Zhang, Y.; Xiao, W., Study on synthesis and antibacterial properties of Ag NPs/GO nanocomposites. *J. Nanomaterials* **2016,** *2016*.

142. Li, C.; Xiang, M.; Ye, L., Intercalation behavior and orientation structure of graphene oxide/polyethylene glycol hybrid material. *RSC Adv.* **2016,** *6* (76), 72193-72200.

143. Kamakshi, T.; Sundari, G. S.; Erothu, H.; Rao, T., Synthesis and characterization of graphene based iron oxide (Fe3O4) nanocomposites. *Rasayan J. Chem.* **2018,** *11* (3), 1113-1119.

144. He, J.; Song, G.; Wang, X.; Zhou, L.; Li, J., Multifunctional magnetic Fe3O4/GO/Ag composite microspheres for SERS detection and catalytic degradation of methylene blue and ciprofloxacin. *Journal of Alloys and Compounds* **2022,** *893*, 162226.

145. Jalal Sadiq, A.; Shabeeb, K. M.; Khalil, B. I.; Alsalhy, Q. F., Effect of embedding MWCNT-g-GO with PVC on the performance of PVC membranes for oily wastewater treatment. *Chemical Engineering Communications* **2020,** *207* (6), 733-750.

146. Nawaz, H.; Umar, M.; Ullah, A.; Razzaq, H.; Zia, K. M.; Liu, X., Polyvinylidene fluoride nanocomposite super hydrophilic membrane integrated with Polyaniline-Graphene oxide nano fillers for treatment of textile effluents. *J. Hazard. Mater.* **2021,** *403*, 123587.

147. Ahmad, T.; Guria, C.; Mandal, A., Optimal synthesis, characterization and antifouling performance of Pluronic F127/bentonite-based super-hydrophilic polyvinyl chloride ultrafiltration membrane for enhanced oilfield produced water treatment. *J. Ind. Eng. Chem.* **2020,** *90*, 58-75.

148. Xu, Z.; Yan, X.; Du, Z.; Li, J.; Cheng, F., Effect of oxygenic groups on desalination performance improvement of graphene oxide-based membrane in membrane distillation. *Sep Purif Technol***2020,** *251*, 117304.

149. Dadvar, E.; Heidari, A., A Review on Separation Techniques of Graphene Oxide (GO)/Base on Hybrid Polymer Membranes for Eradication of Dyes and Oil Compounds: Recent Progress in Graphene Oxide (GO)/Base on Polymer Membranes–Related Nanotechnologies. *Clin Med Rev Case Rep* **2018,** *5*, 228.

150. Liu, Z.; He, W.; Zhang, Q.; Shapour, H.; Bakhtari, M. F., Preparation of a GO/MIL-101 (Fe) Composite for the Removal of Methyl Orange from Aqueous Solution. *ACS omega* **2021,** *6* (7), 4597-4608.

151. Abdelghany, A., Synthesis and structural-biological correlation of PVC\PVAc polymer blends. *Journal of materials Research and technology* **2019**, 3908-3916.

152. Hosseini, S.; Alibakhshi, H.; Jashni, E.; Parvizian, F.; Shen, J.; Taheri, M.; Ebrahimi, M.; Rafiei, N., A novel layer-by-layer heterogeneous cation exchange membrane for heavy metal ions removal from water. *J. Hazard. Mater.* **2020,** *381*, 120884.

153. Khan, Z. U.; Khan, W. U.; Ullah, B.; Ali, W.; Ahmad, B.; Yap, P.-S., Graphene oxide/PVC composite papers functionalized with p-Phenylenediamine as high-performance sorbent for the removal of heavy metal ions. J. Environ. Chem. Eng. **2021**, 105916.

154. Vadukumpully, S.; Paul, J.; Mahanta, N.; Valiyaveettil, S., Flexible conductive graphene/poly (vinyl chloride) composite thin films with high mechanical strength and thermal stability. *Carbon* **2011,** *49* (1), 198-205.

155. Sadiq, A. J.; Awad, E. S.; Shabeeb, K. M.; Khalil, B. I.; Al-Jubouri, S. M.; Sabirova, T.; Tretyakova, N.; Majdi, H. S.; Alsalhy, Q. F.; Braihi, A. J., Comparative study of embedded functionalised MWCNTs and GO in Ultrafiltration (UF) PVC membrane: interaction mechanisms and performance. *Inter. J. Environ. Analytic. Chem.* **2020**, 1-22.

156. Jia, P.; Hu, L.; Feng, G.; Bo, C.; Zhang, M.; Zhou, Y., PVC materials without migration obtained by chemical modification of azide-functionalized PVC and triethyl citrate plasticizer. *Mater. Chem. Phys.* **2017,** *190*, 25-30.

157. Xu, D.; Liang, H.; Zhu, X.; Yang, L.; Luo, X.; Guo, Y.; Liu, Y.; Bai, L.; Li, G.; Tang, X., Metal-polyphenol dual crosslinked graphene oxide membrane for desalination of textile wastewater. *Desalination.* **2020,** *487*, 114503.

158. Lou, L.; Kendall, R. J.; Smith, E.; Ramkumar, S. S., Functional PVDF/rGO/TiO2 nanofiber webs for the removal of oil from water. *Polymer.* **2020,** *186*, 122028.

159. Xu, W.; Li, S.; Ye, Z.; Zhang, J.; Deng, L.; Dong, A., Optimization of sulfonated polyethyleneimine zwitterionic coating mediated by polydopamine for poly (vinyl chloride) antifouling. *J. Appl. Polym. Sci.* **2021,** *138* (1), 49636.

160. Sari, A.; Al Maskari, N. S.; Saeedi, A.; Xie, Q., Impact of surface roughness on wettability of oil-brine-calcite system at sub-pore scale. *J. Molec. Liq.* **2020,** *299*, 112107.

161. Ayyaru, S.; Ahn, Y.-H., Application of sulfonic acid group functionalized graphene oxide to improve hydrophilicity, permeability, and antifouling of PVDF nanocomposite ultrafiltration membranes. *J. Membr. Sci.* **2017,** *525*, 210-219.

162. Deng, H.; Huang, J.; Qin, C.; Xu, T.; Ni, H.; Ye, P., Preparation of high-performance nanocomposite membranes with hydroxylated graphene and graphene oxide. *J. Water Process Eng.* **2021,** *40*, 101945.

163. Li, J.; Liu, X.; Lu, J.; Wang, Y.; Li, G.; Zhao, F., Anti-bacterial properties of ultrafiltration membrane modified by graphene oxide with nano-silver particles. *J. Colloid. Interf. Sci.* **2016,** *484*, 107-115.

164. Pounraj, S.; Somu, P.; Paul, S., Chitosan and graphene oxide hybrid nanocomposite film doped with silver nanoparticles efficiently prevents biofouling. *Appl. Surf. Sci.* **2018,** *452*, 487-497.

165. de Faria, A. F.; de Moraes, A. C. M.; Andrade, P. F.; da Silva, D. S.; do Carmo Gonçalves, M.; Alves, O. L., Cellulose acetate membrane embedded with graphene oxide-

silver nanocomposites and its ability to suppress microbial proliferation. *Cellulose* **2017,** *24* (2), 781-796.

166. de Moraes, A. C. M.; Lima, B. A.; de Faria, A. F.; Brocchi, M.; Alves, O. L., Graphene oxide-silver nanocomposite as a promising biocidal agent against methicillin-resistant Staphylococcus aureus. *Int J Nanomed* **2015,** *10*, 6847-6861.

167. Li, C. J.; Xiang, M.; Ye, L., Intercalation behavior and orientation structure of graphene oxide/polyethylene glycol hybrid material. *Rsc Adv* **2016,** *6* (76), 72193-72200.

168. Solomon, S. D.; Bahadory, M.; Jeyarajasingam, A. V.; Rutkowsky, S. A.; Boritz, C.; Mulfinger, L., Synthesis and study of silver nanoparticles. *J Chem Educ* **2007,** *84* (2), 322-325.

169. Vi, T. T. T.; Kumar, S. R.; Rout, B.; Liu, C. H.; Wong, C. B.; Chang, C. W.; Chen, C. H.; Chen, D. W.; Lue, S. J., The Preparation of Graphene Oxide-Silver Nanocomposites: The Effect of Silver Loads on Gram-Positive and Gram-Negative Antibacterial Activities. *Nanomaterials-Basel* **2018,** *8* 354-363.

170. Chen, J. L.; Zheng, X. L.; Wang, H.; Zheng, W. T., Graphene oxide-Ag nanocomposite: In situ photochemical synthesis and application as a surface-enhanced Raman scattering substrate. *Thin Solid Films* **2011,** *520*, 179-185.

171. Li, Y. L.; Zhao, X. J.; Zhang, P. P.; Ning, J.; Li, J. F.; Su, Z. Q.; Wei, G., A facile fabrication of large-scale reduced graphene oxide-silver nanoparticle hybrid film as a highly active surface-enhanced Raman scattering substrate. *J Mater Chem C* **2015,** *3* (16), 4126-4133.

172. Padaki, M.; Surya Murali, R.; Abdullah, M. S.; Misdan, N.; Moslehyani, A.; Kassim, M. A.; Hilal, N.; Ismail, A. F., Membrane technology enhancement in oil–water separation. A review. *Desalination* **2015,** *357*, 197-207.

173. Ai, J.; Yang, L.; Liao, G.; Xia, H.; Xiao, F., Applications of graphene oxide blended poly (vinylidene fluoride) membranes for the treatment of organic matters and its membrane fouling investigation. *Appl. Surf. Sci.* **2018,** *455*, 502-512.

174. Nunes-Pereira, J.; Ribeiro, S.; Ribeiro, C.; Gombek, C. J.; Gama, F.; Gomes, A.; Patterson, D.; Lanceros-Méndez, S., Poly (vinylidene fluoride) and copolymers as porous membranes for tissue engineering applications. *Polym. Test.* **2015,** *44*, 234-241.

175. Zahed, B.; Hosseini-Monfared, H., A comparative study of silver-graphene oxide nanocomposites as a recyclable catalyst for the aerobic oxidation of benzyl alcohol: Support effect. *Appl. Surf. Sci.* **2015,** *328*, 536-547.

176. Bessiere, Y.; Bacchin, P.; Jefferson, B., Dead-end filtration of natural organic matter: experimental evidence of critical conditions. *Desalination* **2005,** *175* (1), 29-36.

177. Zhang, J.; Xu, Z.; Mai, W.; Min, C.; Zhou, B.; Shan, M.; Li, Y.; Yang, C.; Wang, Z.; Qian, X., Improved hydrophilicity, permeability, antifouling and mechanical performance of PVDF composite ultrafiltration membranes tailored by oxidized low-dimensional carbon nanomaterials. *J. Mater. Chem. A* **2013,** *1* (9), 3101-3111.

178. Wang, P.; Ma, J.; Wang, Z.; Shi, F.; Liu, Q., Enhanced separation performance of PVDF/PVP-g-MMT nanocomposite ultrafiltration membrane based on the NVP-grafted polymerization modification of montmorillonite (MMT). *Langmuir* **2012,** *28* (10), 4776-4786.

179. Kim, D.-G.; Kang, H.; Han, S.; Lee, J.-C., The increase of antifouling properties of ultrafiltration membrane coated by star-shaped polymers. *J. Mater. Chem.***2012,** *22* (17), 8654-8661.

180. Vatanpour, V.; Madaeni, S. S.; Moradian, R.; Zinadini, S.; Astinchap, B., Fabrication and characterization of novel antifouling nanofiltration membrane prepared from oxidized multiwalled carbon nanotube/polyethersulfone nanocomposite. *J. Membr. Sci.* **2011,** *375*, 284-294.

181. Li, Y.; Lu, H.; Wang, Y.; Zhao, Y.; Li, X., Efficient removal of methyl blue from aqueous solution by using poly (4-vinylpyridine)–graphene oxide–Fe_3O_4 magnetic nanocomposites. *J. Mater. Sci.* **2019,** *54*, 7603-7616.

182. Huong, P. T. L.; Son, T. V.; Phan, V. N.; Tam, L. T.; Le, A.-T., Microstructure and Chemo-Physical characterizations of functional graphene oxide-iron oxide-silver ternary nanocomposite synthesized by one-pot hydrothermal method. *J. Nanosci. Nanotechnol.* **2018,** *18*, 5591-5599.

183. Labihi, S.; Chakhchaoui, N.; Eddiai, A.; El Achaby, M.; Meddad, M.; Cherkaoui, O.; Mazroui, M. h., Enhancement of piezoelectric β-polymorph formation and properties of graphene oxide and PZT-incorporated in PVDF-HFP matrix for energy harvesting applications. *Polym. Compos.* **2023,** *44*, 2296-2304.

184. Hatel, R.; Majdoub, S. E.; Bakour, A.; Khenfouch, M.; Baitoul, M. Graphene oxide/Fe3O4 nanorods composite: Structural and Raman investigation. *J. Phys. IOP Publishing*: **2018**, 012006.

185. Ahmad, T.; Guria, C.; Mandal, A., Optimal synthesis of high fouling-resistant PVC-based ultrafiltration membranes with tunable surface pore size distribution and ultralow water contact angle for the treatment of oily wastewater. *Sep Purif Technol* **2021,** *257*, 117829.

186. Alardhi, S. M.; Alrubaye, J. M.; Albayati, T. M. In Removal of Methyl Green Dye from simulated waste water using Hollow Fiber Ultrafiltration Membrane. *Mater. Sci. Eng*. **2020**, *54*, 052020.

187. Abdel-Karim, A.; El-Naggar, M. E.; Radwan, E.; Mohamed, I. M.; Azaam, M.; Kenawy, E.-R., High-performance mixed-matrix membranes enabled by organically/inorganic modified montmorillonite for the treatment of hazardous textile wastewater. *J. Chem. Eng.* **2021,** *405*, 126964.

188. Abdel-Wahed, M. S.; Abdel-Karim, A.; Margha, F. H.; Gad-Allah, T. A., UV sensitive ZnO and TiO2-ZnO nanocrystalline transparent glass-ceramic materials for photocatalytic decontamination of surface water and textile industry wastewater. *Environ. Prog. Sustain. Ener.* **2021**, 13653.

189. Ali, M. E.; Jamil, T. S.; Abdel-Karim, A.; El-Kady, A. A., Utilization of activated carbon for maximizing the efficiency of zirconium oxide for photodegradation of 4-octylphenol. *J. Environ. Health, Part A* **2019,** *54* (11), 1055-1065.

190. Vatanpour, V.; Khadem, S. S. M.; Masteri-Farahani, M.; Mosleh, N.; Ganjali, M. R.; Badiei, A.; Pourbashir, E.; Mashhadzadeh, A. H.; Munir, M. T.; Mahmodi, G., Anti-fouling and permeable polyvinyl chloride nanofiltration membranes embedded by hydrophilic graphene quantum dots for dye wastewater treatment. *J. Water Process Eng.* **2020,** *38*, 101652.

191.Wu, H.; Li, T.; Liu, B.; Chen, C.; Wang, S.; Crittenden, J. C., Blended PVC/PVC-g-PEGMA ultrafiltration membranes with enhanced performance and antifouling properties. *Appl. Surf. Sci.* **2018,** *455*, 987-996.

192. Modi, A.; Bellare, J., Efficient separation of biological macromolecular proteins by polyethersulfone hollow fiber ultrafiltration membranes modified with Fe3O4 nanoparticles-decorated carboxylated graphene oxide nanosheets. *Int. J. Biol. Macromol.* **2019,** *135*, 798-807.

193. Aji, M. M.; Narendren, S.; Purkait, M. K.; Katiyar, V., Utilization of waste polyvinyl chloride (PVC) for ultrafiltration membrane fabrication and its characterization. J. Environ. Chem. Eng. **2020,** *8* (2), 103650.

194. Kusworo, T. D.; Susanto, H.; Aryanti, N.; Rokhati, N.; Widiasa, I. N.; Al-Aziz, H.; Utomo, D. P.; Masithoh, D.; Kumoro, A. C., Preparation and characterization of photocatalytic PSf-TiO2/GO nanohybrid membrane for the degradation of organic contaminants in natural rubber wastewater. J. Environ. Chem. Eng. **2021,** *9*, 105066.

195. Chai, P.; Choy, P.; Teoh, W.; Mahmoudi, E.; Ang, W., Graphene oxide based mixed matrix membrane in the presence of eco-friendly natural additive gum Arabic. J. Environ. Chem. Eng. **2021,** *9* (4), 105638.

196. Behboudi, A.; Jafarzadeh, Y.; Yegani, R., Enhancement of antifouling and antibacterial properties of PVC hollow fiber ultrafiltration membranes using pristine and modified silver nanoparticles. J. Environ. Chem. Eng. **2018,** *6* (2), 1764-1773.

197. Mishra, G.; Mukhopadhyay, M., Enhanced antifouling performance of halloysite nanotubes (HNTs) blended poly (vinyl chloride) (PVC/HNTs) ultrafiltration membranes: For water treatment. *J. Ind. Eng. Chem.* **2018,** *63*, 366-379.

198. Alsalhy, Q. F.; Al-Ani, F. H.; Al-Najar, A. E.; Jabuk, S. I., A study of the effect of embedding ZnO-NPs on PVC membrane performance use in actual hospital wastewater treatment by membrane bioreactor. *Chem. Eng. Process.* **2018,** *130*, 262-274.

199. Ahmad, T.; Guria, C.; Mandal, A., Enhanced performance of salt-induced Pluronic F127 and bentonite blended polyvinyl chloride ultrafiltration membrane for the processing of oilfield produced water. *J. Water Process Eng.* **2020,** *34*, 101144.

200. Abdel-Karim, A.; Ismail, S. H.; Bayoumy, A. M.; Ibrahim, M.; Mohamed, G. G., Antifouling PES/Cu@ Fe_3O_4 mixed matrix membranes: Quantitative structure–activity relationship (QSAR) modeling and wastewater treatment potentiality. *J. Chem. Eng.* **2021,** *407*, 126501.

LIST OF PUBLICATIONS

From this work

Hafsa Ilyas, Abdul Haleem, Muzaffar Iqbal, & Muhammad Siddiq. Influence of GO-Ag nano-filler on the antibacterial, antifouling and hydrophilic characteristics of polyvinyl chloride membrane. *J. Water Process Eng.*, **2021**, *44*, 102336.

Hafsa Ilyas, Shalima Shawuti, Muhammad Siddiq, Niazi, J. H., & Anjum Qureshi. PEG functionalized graphene oxide-silver nano-additive for enhanced hydrophilicity, permeability and fouling resistance properties of PVDF-co-HFP membranes. *Colloids Surf A.*, **2019**, *579*, 123646.

Ayesha Kausar, **Hafsa Ilyas** & Muhammad Siddiq. Aptitude of graphene oxide–silver in advance polymer nanocomposite: a review. *Polym. Plastics Technol. Eng.*, **2018**, *57*(4), 283-301.

Ayesha Kausar, **Hafsa Ilyas** & Muhammad Siddiq. "Current research status and application of polymer/carbon nanofiller buckypaper: A review." *Polym. Plastics Technol. Eng.*, **2017**, 56, 1780-1800.

From other work

Pervaiz, S., Bibi, I., Hussain Shah, S. W., Wahab, Z. U., **Hafsa Ilyas**, Khan, A., & Zada, A. (2022). Oil mediated green synthesis of nano silver in the presence of surfactants for catalytic and food preservation application. *Zeitschrift für Physikalische Chemie*, **2022**, 236 (11-12), 1493-1513.